A microscopic treatment of correlated nucleons : collective properties in stable and exotic nuclei

Olivier Vasseur

université PARIS-SACLAY

NNT : 2019SACLS223

Thèse de doctorat

A microscopic treatment of correlated nucleons: Collective properties in stable and exotic nuclei

Thèse de doctorat de l'**Université Paris-Saclay**
préparée à l'**Université Paris-Sud**

Ecole doctorale **n°576 Particules, Hadrons, Énergie, Noyau, Instrumentation, Imagerie, Cosmos et Simulation (PHENIICS)**
Spécialité de doctorat : **Structure et réactions nucléaires**

Thèse présentée et soutenue à l'Institut de Physique Nucléaire (IPN) Orsay,
le **18 septembre 2019**, par

Olivier VASSEUR

devant le Jury composé de :

Gianluca COLÒ Professeur, Università Degli Studi di Milano	Rapporteur
Danilo GAMBACURTA Chercheur, Extreme Light Infrastructure – Nuclear Physics (ELI-NP), Horia Hulubei National Institute for Physics and Nuclear Engineering	Co-directeur de thèse
Marcella GRASSO Directeur de Recherche CNRS, Institut de Physique Nucléaire (IPN) Orsay (UMR 8608 - CNRS/IN2P3)	Directeur de thèse
Denis LACROIX Directeur de Recherche CNRS, Institut de Physique Nucléaire (IPN) Orsay (UMR 8608 - CNRS/IN2P3)	Président du jury
Frédéric NOWACKI Directeur de Recherche CNRS, Institut Pluridisciplinaire Hubert CURIEN (IPHC) Strasbourg (UMR 7178)	Rapporteur
Nathalie PILLET Ingénieur-Chercheur, Commissariat à l'Énergie Atomique et aux Énergies Alternatives (CEA), Direction des Applications Militaires (DAM) Île-de-France	Examinateur

To my mother Anna and my brother Quentin.
To my father Jean-Luc.

Contents

Acknowledgements vii

1 Introduction 1
- 1.1 General motivations and objectives . . . 1
- 1.2 Context . . . 3

2 Mean-field methods within energy-density-functional theories 11
- 2.1 Energy-density functionals . . . 11
- 2.2 The Hartree-Fock method . . . 13
  - 2.2.1 General assumptions and notation conventions . . . 13
  - 2.2.2 Derivation of the Hartree-Fock equations . . . 14
- 2.3 HF-based RPA . . . 17
  - 2.3.1 Derivation of the RPA equations . . . 17
  - 2.3.2 Unsufficiency and inconsistency of the standard RPA . . . 21

3 A beyond-mean-field approach as a starting point: Second RPA 23
- 3.1 Towards the second random-phase approximation . . . 23
- 3.2 The SRPA model . . . 24
  - 3.2.1 Derivation of the SRPA equations . . . 24
  - 3.2.2 Drawbacks of the SRPA model . . . 28

4 A correction of SRPA: Subtracted SRPA 33
- 4.1 Principle of the subtracted SRPA (SSRPA) . . . 33
  - 4.1.1 SRPA as an energy-dependent RPA-like problem . . . 33
  - 4.1.2 Benefits and practical use of the subtraction method . . . 35
- 4.2 Results: Assessment of the correction capabilities of SSRPA . . . 40
  - 4.2.1 Residual interaction in SSRPA calculations . . . 40
  - 4.2.2 Dipole response and polarizability in ^{48}Ca . . . 43
  - 4.2.3 Quadrupole response: systematics on selected nuclei . . . 51
  - 4.2.4 Beyond-mean-field effects on the effective masses . . . 58

5 Extensions of the model **67**
5.1 Treating nuclei with partially-filled orbitals: Equal-filling approximation . . . 67
5.1.1 Within the HF approximation . . . 68
5.1.2 With a superfluid ground state . . . 69
5.1.3 Results . . . 73
5.2 Going beyond the QBA . . . 77
5.2.1 An extension of RPA and SRPA with renormalization factors: Formalism . . . 80
5.2.2 An extension of RPA and SRPA with renormalization factors: Results . . . 84

6 General conclusions & perspectives **91**

7 Appendices **95**
Appendix 1. Computation of renormalized matrix elements . . . 95
Appendix 2. Expression for the occupation numbers . . . 102

Résumé en français **105**
1 Introduction . . . 105
2 Méthodes de champ moyen en théorie des fonctionnelles de la densité . . . 106
2.1 Fonctionnelles de la densité . . . 106
2.2 La méthode de Hartree-Fock . . . 107
2.3 RPA basée sur l'état de HF . . . 108
3 Une approche au-delà du champ moyen comme point de départ: SRPA . . . 110
3.1 Formalisme . . . 110
3.2 Inconvénients de la SRPA standard . . . 112
4 Une correction de la SRPA: SRPA avec soustraction . . . 112
4.1 Principe de la SRPA avec soustraction . . . 112
4.2 Résultats: Polarisabilité et réponse dipolaire de ^{48}Ca . . . 113
4.3 Résultats: Réponse quadrupolaire: systématiques sur une sélection de noyaux . . . 114
4.4 Résultats: Effets au-delà du champ moyen sur les masses effectives . . . 115
5 Extensions du modèle . . . 116
5.1 Noyaux à orbitales partiellement occupées et appariement 116
5.2 Extension au-delà de la QBA . . . 118

6 Conclusion générale et perspectives 119

List of Figures **133**

Index **135**

Acknowledgements

I first wish to thank my supervisor, Marcella Grasso, for her availability during my whole Ph.D. despite her heavy responsibilities, for her help in everyday work but also when I was preparing my conferences and schools, for her understanding and patience, and for putting effort in raising my motivation. I am also greatly indebted to her for helping me in writing and reviewing the present thesis manuscript.

Secondly, I am grateful to Danilo Gambacurta, my co-supervisor during these three years, without whom all this work would have been impossible. He provided me with the necessary help on both the computer side and the physics, kindly made himself available whenever needed, and also contributed to reviewing this manuscript.

I would like to thank Bruno Espagnon, Director of IPN Orsay at the time when I started my Ph.D., and Michel Guidal, Director during the second part of my Ph.D., for giving me the opportunity to carry out this thesis work at IPN.

Many thanks go to Michael Urban, head of the Theory Group during the two first years of my Ph.D., for his help in diverse administrative tasks, and also for advising me when preparing my missions abroad.

I am indebted to Jean-Philippe Lansberg, head of the Theory Group during the last year of my Ph.D., for the very kind, spontaneous and precious help he provided me with when I was organizing my mission to the ANPC conference in South Africa. In addition, I would like to thank him for being so active in improving the practical life in the group, from coffee machines to computing resources. For example, he was to my knowledge at the origin of the installation of Condor on the group's computers, which turned out to be very useful at the end of my Ph.D..

Warm thanks go to Antoine Boulet, my "thesis brother", who I also like to call the Capitaine Haddock, for his support during the hard times and for mitigating the good ones. We had many fruitful discussions, especially on psychoanalytical introspection ("Complexe de Dick"), and shared many jokes. Besides being a (self-acknowledged) specialist in the creation and

propagation of false but harmless gossips, he is talented when it comes to explaining physics in a simple way, which I found very helpful.

I would also like to thank Jérémy Bonnard, with whom I shared the office at IPN during the first two years. Aside from his very pleasant company in the office, he always answered my questions about physics.

I am addressing my special thanks to three persons, who I list here in alphabetical order. First, Yann Beaujeault-Taudiere carried out a full review of this manuscript, and provided very useful and accurate remarks. Second, David Durel was generous and thoughtful enough to regularly express his talent for cooking by sharing delicious cakes with the whole group. Third, David Regnier kindly advised me several times on various questions, both professional and personal, and often brought highly instructive discussions with good mood.

I wish to acknowledge the great help provided by Annie Talbot, secretary of the Theory Group in the first half of my Ph.D., Valérie Piazza, secretary during the second half, and Jean-Yves Zana from the Financial Service at IPN, in the preparation of my trips to schools and conferences.

I am also grateful to all the Ph.D. students with whom I shared very pleasant moments and who did not hesitate to help me with technical tasks.

Finally, I would like to express my gratitude to my mother Anna, my brother Quentin, and to my remaining family members and friends, who will recognize themselves, for their help and support throughout my whole Ph.D..

These acknowledgements are by no means exhaustive and I wish to thank all those who I may have omitted in these acknowledgements.

CHAPTER 1

Introduction

Contents

1.1 General motivations and objectives 1
1.2 Context 3

1.1 General motivations and objectives

The overall aim of the thesis work presented in this manuscript is the improvement of the microscopic description of nuclear collective properties. Ultimately, we wish to analyze in an accurate and predictive way the excitation spectra of stable and unstable nuclei. To that end, the approach which we adopt consists in coupling individual degrees of freedom and multiparticle-multihole configurations of the nucleons. This allows us to overcome the mean-field (MF) approximation, enriching in this way the description of the excited modes of nuclei. Such a mixing of configurations provides a much more complete and realistic description of the excitation spectra. This is done in practice using a second-random-phase-approximation(SRPA)-based model where the multiparticle-multihole configurations are 2 particle-2 hole (2p2h) configurations.

The general context in which this work was developed is described in the next section of this chapter (Sec. 1.2).

This work followed several steps, which we may attempt to summarize here by presenting the structure of the manuscript.

A model which is often used to describe collective excitations is the random-phase approximation (RPA), where the excited modes are superpositions of 1 particle-1 hole (1p1h) configurations only. Despite all its qualities and advantages, the RPA applied on top of the Hartree-Fock (HF) method is a theoretical approach which remains at the MF level.

Chapter 2 focuses on these MF methods that form the basis of the models later presented in this manuscript, and is therefore a prerequisite to the next developments. We first provide an overview of the energy-density-functional (EDF) framework, in which all our models are applied. We next derive the HF equations, and describe the main formal aspects of the RPA.

In order to go beyond this MF framework, we base our developments on the extension of the RPA to 2p2h configurations, known as the SRPA.

In Chap. 3, we present this model, which constitutes our starting point. After a brief historical overview of the SRPA applications, the main formal aspects are discussed, as well as the limitations that motivated the present work. In fact, the straightforward extension of the standard RPA to 2p2h configurations suffers from strong drawbacks which do not allow for a satisfactory description of the nuclear excitation spectra.

Chapter 4 is devoted to a way of addressing the drawbacks of the SRPA model, namely the subtraction method. We describe formally this method and its practical use in a first part, and then present all the applications that were carried out in this thesis work. This theoretical method is called the subtracted SRPA (SSRPA). In particular, SSRPA applications are carried out to analyze the dipole low-lying spectrum and the dipole giant resonance region in ^{48}Ca (the electric dipole polarizability is also analyzed), to study isoscalar quadrupole resonances in several nuclei, from medium-mass systems to heavy nuclei, and to estimate beyond-MF effects on the effective mass, based on calculations of giant quadrupole excitations. Comparisons with available experimental results are discussed.

The second main part of the manuscript, presented in Chap. 5, is dedicated to several extensions.

First, an extension of the SSRPA model is presented which allows us to deal with nuclei having a partially filled last orbital. This was a limitation of the previously available SSRPA model due to which several nuclei could not be treated, for instance most open-shell nuclei. The equal-filling approximation is employed to perform this extension. As a first step, this extension is used on top of a genuine HF ground state. Then, it is used on top of a correlated ground state. In particular, pairing correlations are introduced through occupation numbers obtained from a Bardeen-Cooper-Schrieffer (BCS) calculation and this allows us to make a first estimation of the effects of pairing correlations.

Low-lying 2^+ excitations in some Argon isotopes are analyzed and a comparison with experimental results is presented.

Secondly, we present an extension (already employed in the past years for metal clusters) to go beyond the quasiboson approximation (QBA) in RPA-type models. Factors containing the occupation numbers of a correlated ground state are introduced to renormalize matrix elements. The application of this approach to atomic nuclei is made here for the first time. The occupation numbers are computed using the X and Y RPA amplitudes. The correlations computed in this way have thus a relevant impact only in many-body systems where the Y amplitudes are not negligible. We discuss the effects of introducing such a correlated ground state in the SRPA model.

Finally, we summarize our results and conclusions in Chap. 6, and provide an outlook on further possible developments.

1.2 Context

When introducing nuclear physics, complexity is usually the characteristic feature which is foremost highlighted. This complexity can be glimpsed from different viewpoints.

From the conceptual one, nuclei are self-bound quantum many-body systems, composed of particles having a spin and an isospin, if one adopts the low-energy description of a nucleus, in which protons and neutrons are the relevant degrees of freedom. We place our study in this framework, and consider protons and neutrons as point-like and structureless particles. The degrees of freedom which are relevant at different energy scales are illustrated in Fig. 1.1.

From the observational point of view, nuclei feature very diverse phenomena, among which ground-state properties (mass, size, ...), excitation modes studied by spectroscopy, various decay modes, reaction processes (fusion, transfer, knock-out, ...) and exotic behaviors (clustering, halos, ...). Several nuclei are superfluid and this has an impact on their properties such as their binding energy (there is a contribution to the total energy coming from superfluidity) or their excitation spectra, in particular their low-lying modes. Such a superfluidity is characterized by the existence of Cooper pairs composed of nucleons.

Some fundamental questions arise from observations, such as

- How many nuclei exist?
- What is the heaviest possible element? How does stability behaves for super-heavy elements?

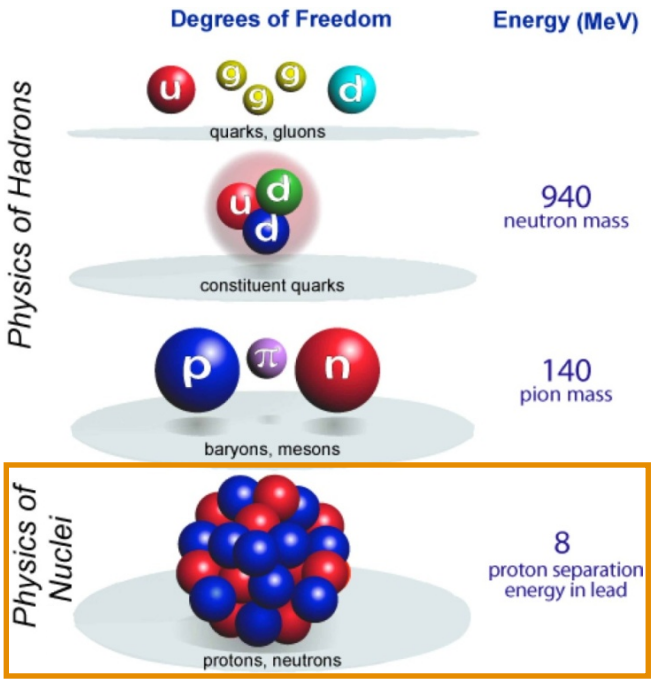

Figure 1.1: Illustration of the considered degrees of freedom at different energy scales.

- Are magic numbers the same for unstable nuclei?
- Are there more exotic decay modes than α, β, γ decays and fission?

In this thesis, we are mainly concerned with the many-body description of nuclei, which are studied as systems composed of A nucleons (Z protons and N neutrons).

Many-body techniques are of course not specific to nuclei, but form a set of very interdisciplinary theoretical tools. Examples of domains in which such tools find applications are atomic physics, condensed-matter physics and chemistry. Similar methods are applied, leading to the description of systems as diverse as Bose-Einstein condensates of ultra-cold trapped atoms or molecules. A pictorial representation of such a variety of many-body systems is shown on Fig. 1.2.

In particular, the interdisciplinary aspect of the work presented in this manuscript may be seen in that some formal developments on which it is based were first carried out in the study of metal clusters. For example, some applications of RPA renormalization schemes, which we discuss in Sec. 5.2, were done for these many-body systems, providing useful physical insights and tests.

Also, as will be explained later in this manuscript, several analogies ex-

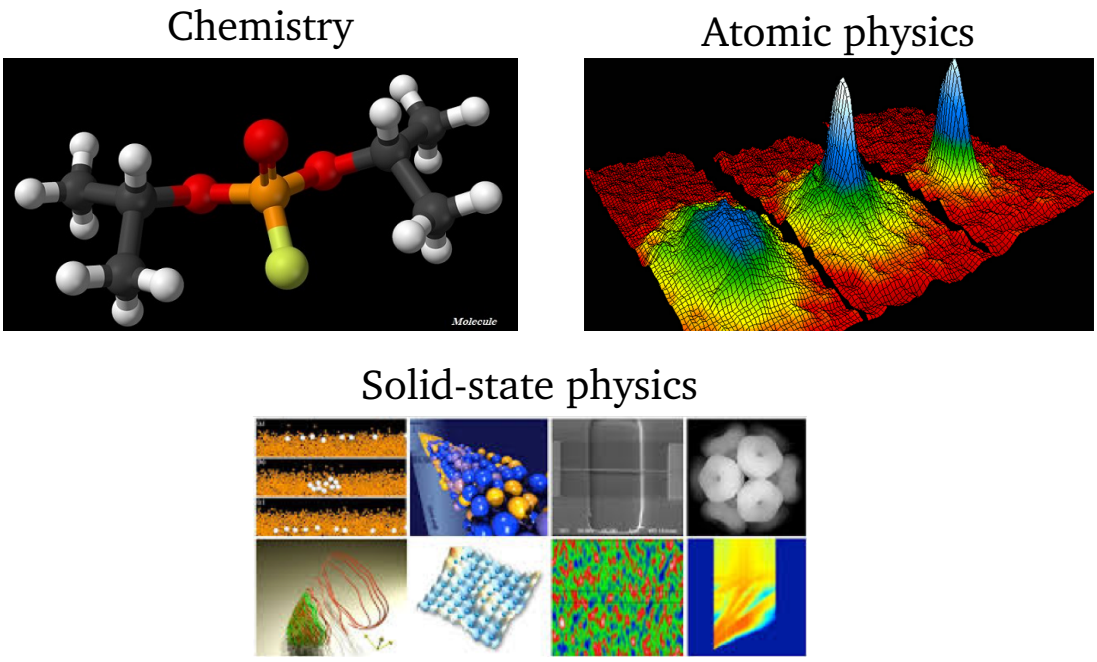

Figure 1.2: Examples of other domains where many-body techniques and models may be applied.

ist between what is developed for the nuclear many-body problem and the density functional theory, which is used in chemistry and solid-state physics.

Moreover, a very interesting interdisciplinary link exists with nuclear astrophysics and, in particular, with the physics of neutron stars. A schematic view of a neutron star is displayed on Fig. 1.3. Such a link with nuclear physics exists for several reasons. First, many-body models may be employed for the treatment of the internal and external crusts of neutron stars, where exotic nuclei and extremely neutron-rich nuclear systems are located.

Let us mention that nuclear physics is often approached through nuclear matter. Nuclear matter is an idealized infinite system whose properties may be related to properties of nuclei and whose study may thus help for a better understanding of nuclei as well as for checking the validity of the employed functionals and interactions. As an example of application, many properties of a neutron star are strongly related to the equation of state of neutron-rich and pure neutron matter.

A given choice for the functional (interaction) and for the approximation scheme (for example, MF approximation or second-order approximation) generates specific equations of state for matter. Examples of equations of state for infinite matter are illustrated on Fig. 1.4, from symmetric (lowest curve) to pure neutron (highest curves), for different values of the isospin

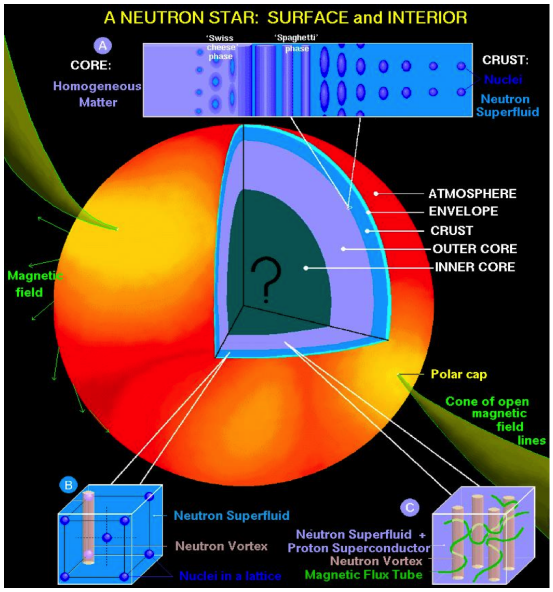

Figure 1.3: Schematic view of a neutron star.

asymmetry $\delta = \frac{N-Z}{A}$, from $\delta = 0$ (symmetric matter) to $\delta = 1$ (pure neutron matter). The two highest curves are two examples of equations of state for pure neutron matter.

In the recent years, *ab initio* models based on the use of chiral potentials have produced microscopic equations of state, especially for neutron matter (see for example Ref. [1]). However, uncertainty bands for these equations of state are still very large, except at extremely low densities. Furthermore, in most cases such models do not reproduce the empirical saturation point of symmetric matter (see, for example, Ref. [2]), with the exception of those specific cases where additional adjustments of parameters are carried out on selected properties of finite nuclei [3].

Several properties of nuclear matter are related to excitation spectra and collective excited modes of nuclei, which constitute the heart and the main topic of this thesis work. For example, the incompressibility modulus is related to isoscalar giant monopole resonances (breathing modes) and to isoscalar giant dipole resonances. The effective mass is related to isoscalar giant quadrupole resonances (axial breathing modes). The symmetry energy and its density dependence may be related for instance to giant dipole resonances and to the so-called pygmy dipole modes. Recent reviews may be found in Refs. [4–7].

The developments made in this thesis are based on the SRPA model (see

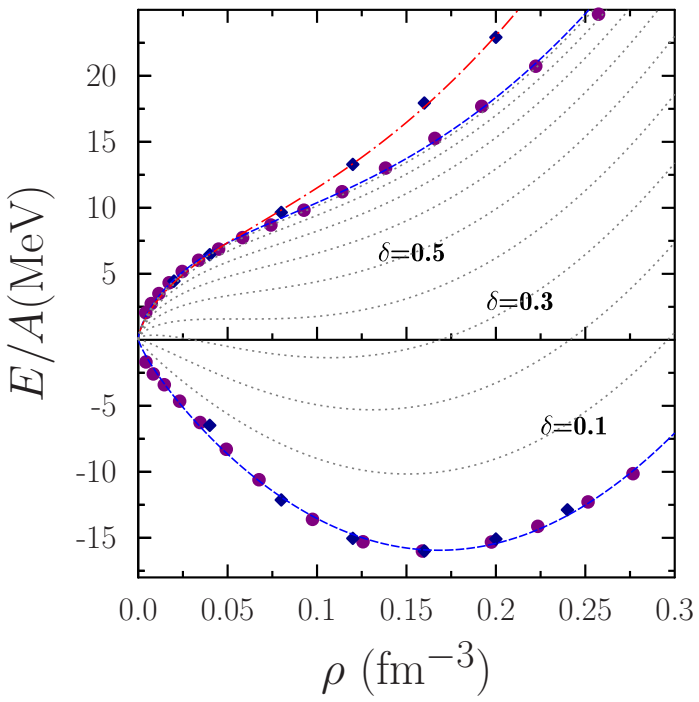

Figure 1.4: Examples of equations of state of infinite matter for different values of the isospin asymmetry δ.

Chap. 3). As we discuss in more detail in a dedicated section (Sec. 2.1), we use this many-body tool in the context of EDFs. In principle, this approach allows for a description of nuclei throughout the whole nuclear chart.

We stress that in all applications done in this thesis work, only even-even nuclei with assumed spherical symmetry are treated. With the aim of microscopically describing collective excitations of nuclei, the targeted phenomena are low-lying states and giant resonances.

Unlike giant resonances, low-lying states are those states usually located below 10-12 MeV in the excitation spectrum of a nucleus. They may be simpler excitations which involve a few nucleons (therefore they do not feature collectivity) or, in some cases, they may have a more collective nature, for instance in some pygmy dipole resonances.

The occurrence of collective excitations is a common characteristic of many-body systems. Giant resonances are a manifestation of this collectivity, where many particles moving coherently are involved, and can be schematically seen as macroscopic vibrations of the system. Because of their collective nature, they depend on global properties of the systems (size, number of particles) on the one hand, and can provide information on their bulk properties and dynamics on the other hand. They were extensively studied,

and detailed descriptions of their various aspects can be found in the literature [8–12]. They correspond to resonances which lie higher in excitation energy than low-lying states. These resonances are characterized by a width Γ and a centroid energy E_C. Different modes of giant resonances exist, some of which are schematically represented on Fig. 1.5.

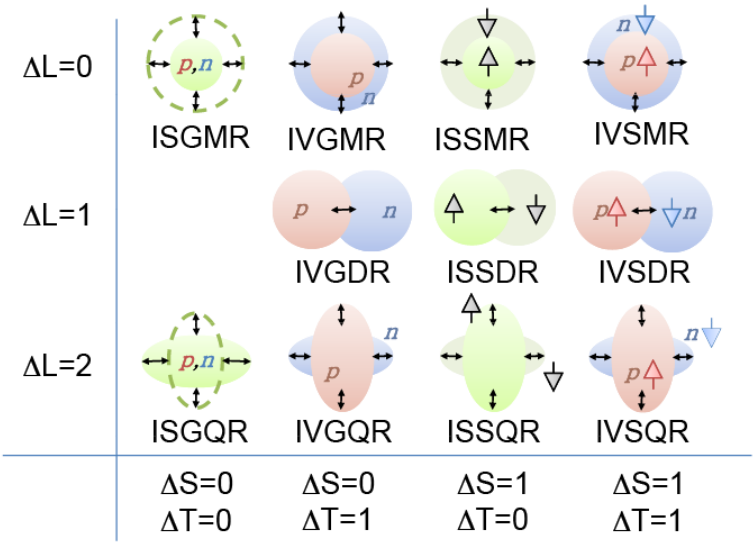

Figure 1.5: Schematic view of collective modes characterizing giant resonances. ΔL, ΔS and ΔT are respectively the change in multipolarity, total spin and total isospin occurring in the excitations. The not represented isoscalar giant dipole resonance (ISGDR) corresponds to a translation of the system as a whole, and is thus not an intrinsic excitation.

Phenomenologically, giant resonances can be observed as more-or-less broad resonances (for example by photon absorption or scattering of a particle), usually spreading over the region of transferred energy between 10 MeV and 30 MeV (for isoscalar excitations). The main difficulty when measuring giant resonances is the overlapping of resonances of various modes in the same excitation energy region. Specific probes have to be used in order to excite selectively the studied modes. In addition, spectra in these energy regions can be spoiled by a background contribution, which can be addressed by performing coincidence experiments.

The width of giant resonances can be explained by several damping mechanisms. It is convenient to conceptually separate these different mechanisms by associating each of them with one contribution to the total width of the resonance. Indeed, a giant resonance is composed of a collective state, which is a coherent superposition of several configurations that have a given multipolarity, spin and isospin — characterizing the giant resonance. The strength of this collective state can be spread and fragmented, so that the total result-

ing width can be expressed as follows:

$$\Gamma^{t} = \Gamma^{L} + \Gamma^{s} + \Gamma^{e} . \tag{1.1}$$

In this equation, the so-called Landau-damping width Γ^{L} represents the fragmentation of the strength due to the possible presence, in the energy region of the collective state, of elementary 1p1h states that have the same quantum numbers. In nuclei, this constitutes a single-particle contribution to the total width which may be accounted for by MF-based models.

The spreading width Γ^{s} is the most important term in the total width, and arises from couplings of different configurations, for example from the coupling of 1p1h configurations to higher-order ones (2p2h, 3 particle-3 hole, etc.). One can easily imagine that couplings of higher order than 2p2h are less important.

Now in the SRPA model, 1p1h and 2p2h configurations are coupled by construction. That is why the SRPA describes naturally the spreading and therefore allows for a much better description of the total width than the RPA, which only accounts for 1p1h configurations.

Lastly, the escape width Γ^{e} is induced by the coupling with the continuum. It is expected to be generally less important than the spreading width, but in some nuclei these two contributions can become comparable. In the studies presented in this thesis manuscript, the coupling to the states lying in the continuum is not treated and, consequently, the escape width cannot be described.

CHAPTER 2

Mean-field methods within energy-density-functional theories

Contents

2.1 Energy-density functionals **11**
2.2 The Hartree-Fock method **13**
2.2.1 General assumptions and notation conventions 13
2.2.2 Derivation of the Hartree-Fock equations 14
2.3 HF-based RPA **17**
2.3.1 Derivation of the RPA equations 17
2.3.2 Unsufficiency and inconsistency of the standard RPA 21

2.1 Energy-density functionals

Nuclear EDFs are generally derived from so-called effective phenomenological interactions. The latter are nuclear interactions containing several parameters to be adjusted on selected observables and on properties of nuclear matter, and are built with the aim of gathering as much physics of the nucleus as possible. Microscopic models which employ such effective phenomenological interactions lead in general to a satisfactory description of bulk properties of finite nuclei, such as masses and charge radii. These models place themselves in between *ab initio* models, which use microscopic nucleon-nucleon potentials as ansatz, and macroscopic models, such as the nuclear liquid-drop model, based on global properties of the nucleus.

Nuclear EDFs have been used since the 1970s, for a variety of applications, among which the study of binding energies, radii, shell-structure properties, deformation properties, low-energy excitations and giant resonances. The form of the functionals (and the number of parameters to adjust) depends on assumptions one makes on the nucleon-nucleon interaction, for

instance its zero or non-zero range. Different choices can be made, which lead to different EDFs. The two mostly used types of interactions are the phenomenological Skyrme [13–15] and Gogny [16, 17] interactions.

All the terms of Skyrme interactions have zero range, whereas the Gogny interaction contains both finite-range terms (Gaussians) and zero-range density-dependent and spin-orbit terms.

The first applications which were carried out in the 1970s were essentially MF calculations aimed at describing the ground state of even-even closed-shell nuclei. Ref. [18] summarizes some of these first applications which were performed at that time.

Also, it is interesting to remind that attempts to link these interactions to the bare nucleon-nucleon potential were discussed in those years. For example, for the case of the Skyrme interaction, one can mention the work of Negele and Vautherin [19, 20], where a procedure based on the density-matrix expansion was used.

Ref. [21] is a more recent review on EDF theories and their applications to the ground state of spherical and deformed nuclei as well as to excited states. It contains also the description of several beyond-MF models.

The nuclear EDF and the density-functional theories (DFTs) used in chemistry and in condensed matter physics show important analogies and, also, several differences. DFT was founded in a well-defined theoretical scheme based on the Hohenberg-Kohn theorems [22, 23]: in a many-body system put in an external potential, the density is determined in a unique way. The external potential energy is a functional of the density. The total energy is as well a functional of the density and the density which minimizes it leads to the exact ground-state energy.

These theorems were demonstrated for a many-body system localized by an external potential. This is not the case for finite nuclei which are self-bound systems. This represents the main important difference between the nuclear EDF and DFT theories (other differences exist but we will not mention them because this is not the focus of the present work).

Despite the differences, the MF equations which are solved for a nuclear system have strong analogies with the Kohn-Sham equations [24]. These equations follow from the Hohenberg-Kohn theorems.

We stress once again that, whereas DFT was constructed over the years based on a well-defined theoretical framework, the nuclear EDF was developed in a quite empirical way and was not based on founding theorems.

EDF functionals have been extensively used and have generally achieved

success in reproducing properties of nuclei throughout the whole nuclear chart. Several developments have been conducted to improve the functionals, like alternative expressions of the density-dependent terms, higher-order derivatives of the density, or steps towards derivations of functionals which are closer to the DFT. The reader can refer to Ref. [25] for a more in-depth discussion of these improvements.

Of notable importance for the present study are the various problems that may arise when beyond-MF models are employed with EDFs, such as the overcounting of correlations, instabilities or divergences, some of which are related to the density dependence or to the zero range of the interactions. This will be discussed for the particular case of SRPA in Subsec. 3.2.2.

Finally, it is worth mentioning that current studies are also focusing on more *ab initio* approaches to nuclear EDFs, especially in an attempt to link the functionals to *ab initio* models, inspired by effective-field theories (EFTs) [26–36].

2.2 The Hartree-Fock method

2.2.1 General assumptions and notation conventions

We first wish to point out the following assumptions, which will hold also in the next parts of the present work. We place our study at low-energy scales — a few MeV/nucleon. Given these energy scales, it is sensible to consider that nucleons are structureless particles. Therefore we will assume that nucleon degrees of freedom are the relevant ones.

The formalism we will rely on throughout most of the derivations is the second quantization (see for example Ref. [37]). The vacuum will be denoted by $|-\rangle$, unless otherwise stated.

In this formalism, the general Hamiltonian operator that we will consider has the following expression:

$$\hat{H} = \hat{T} + \hat{V} = \sum_{\mu,\mu'} T_{\mu\mu'} a^\dagger_\mu a_{\mu'} + \frac{1}{4} \sum_{\mu,\nu,\mu',\nu'} v_{\mu\nu\mu'\nu'} a^\dagger_\mu a^\dagger_\nu a_{\nu'} a_{\mu'}, \tag{2.1}$$

where $T_{\mu\mu'}$ is a matrix element of the kinetic energy operator in the single-particle space, and $v_{\mu\nu\mu'\nu'}$ is an antisymmetrized matrix element of the two-

body potential:

$$\begin{aligned} T_{\alpha\beta} &:= \langle\alpha|\,\hat{T}\,|\beta\rangle\,, \\ v_{\alpha\beta\gamma\delta} &:= \langle\alpha\beta|\,\hat{V}\,|\gamma\delta\rangle - \langle\alpha\beta|\,\hat{V}\,|\delta\gamma\rangle \;=\; -v_{\beta\alpha\gamma\delta} \;=\; -v_{\alpha\beta\delta\gamma}\,. \end{aligned}$$

Assuming a ground state where all the states of lowest energy are occupied by the nucleons, the unoccupied single-particle states are called particle states, and the occupied ones are called hole states. Unless otherwise stated, we will conventionally use the subscripts i, j, k, l to refer to hole states, and m, n, p, q to refer to particle states, whereas greek letters will be used when such a distinction is not made.

2.2.2 Derivation of the Hartree-Fock equations

We succinctly follow here the derivation presented in Ref. [38].

In our study, the HF method allows us to obtain a ground state on which practical RPA calculations are made, as explained in more detail in Sec. 2.3. As we show here, this determination implies a minimization of the energy of the system, which relies on a variational principle.

To begin with, let us therefore recall the variational principle on the energy of the system

$$E(\Psi) := \frac{\left\langle\Psi\left|\hat{H}\right|\Psi\right\rangle}{\langle\Psi|\Psi\rangle}\,. \tag{2.2}$$

This variation is performed by imposing that the derivatives of the energy (2.2) with respect to the states $|\Psi\rangle$ and $\langle\Psi| = (|\Psi\rangle)^\dagger$ be equal to 0, that is

$$\begin{cases} \dfrac{\partial E}{\partial\,|\Psi\rangle}(\Psi) \;=\; 0 \\ \dfrac{\partial E}{\partial\,\langle\Psi|}(\Psi) \;=\; 0\,. \end{cases} \tag{2.3}$$

In particular, the state that minimizes the energy obviously satisfies Eq. (2.3).

Let us consider that the Hamiltonian operator is a sum of single-particle components $\hat{h}(i)$, each governing the motion of the nucleon labeled i:

$$\hat{H} \;=\; \sum_{i=1}^{A} \hat{h}(i)\,. \tag{2.4}$$

This assumption implies that the nucleons are thought of as independent particles evolving in a one-body field created by the action of all the particles, hence the name “mean field”.

The HF method consists in the following: assuming a Hamiltonian of the form (2.4), find the state $|\Phi_0\rangle$ that minimizes the energy. Note that, because of the assumption (2.4), the state determined in this way is only an approximation of the exact ground state.

Now because of the antisymmetry of the wave functions, the eigenfunction of the MF Hamiltonian of Eq. (2.4) associated to the lowest eigenvalue, *i.e.* the HF ground state, is a Slater determinant and can be written as

$$|\Phi_0\rangle = \prod_{i=1}^{A} a_i^\dagger |-\rangle \, .$$

Furthermore, each Slater determinant $|\Phi\rangle$ is uniquely associated with a one-body density $\rho(\Phi)$ [38] whose matrix elements in the single-particle space are defined as follows:

$$\rho_{\alpha\beta}(\Phi) := \langle\Phi| a_\beta^\dagger a_\alpha |\Phi\rangle \, . \tag{2.5}$$

Using the general expression (2.1) of the Hamiltonian, and recalling that a Slater determinant is by definition normalized, the energy reads

$$\begin{aligned} E(\Phi) &= \left\langle \Phi \left| \hat{H} \right| \Phi \right\rangle & (2.6)\\ &= \sum_{\mu,\mu'} T_{\mu\mu'} \left\langle \Phi \left| a_\mu^\dagger a_{\mu'} \right| \Phi \right\rangle + \frac{1}{4} \sum_{\mu,\nu,\mu',\nu'} v_{\mu\nu\mu'\nu'} \left\langle \Phi \left| a_\mu^\dagger a_\nu^\dagger a_{\nu'} a_{\mu'} \right| \Phi \right\rangle \\ &= \sum_{\mu,\mu'} T_{\mu\mu'} \rho_{\mu'\mu}(\Phi) + \frac{1}{2} \sum_{\mu,\nu,\mu',\nu'} v_{\mu\nu\mu'\nu'} \rho_{\mu'\mu}(\Phi) \rho_{\nu'\nu}(\Phi) \, , & (2.7) \end{aligned}$$

where in the last step we used the antisymmetry property of the potential and the Wick theorem [39] to evaluate the four-operator expectation value. The energy can therefore be seen as a function $E(\rho(\Phi))$ of the one-body density, which we write $E[\rho]$ for simplicity. Then, the variational principle translates into

$$\delta E[\rho] = 0 \, . \tag{2.8}$$

On the one hand, one always has

$$\delta E[\rho] = \sum_{\alpha,\beta} h_{\alpha\beta} \delta\rho_{\beta\alpha} \, , \tag{2.9}$$

with $h_{\alpha\beta}$ being defined as the partial derivative of E with respect to the (β, α) element of ρ:

$$h_{\alpha\beta} := \frac{\partial E[\rho]}{\partial \rho_{\beta\alpha}} \, . \tag{2.10}$$

On the other hand, one can obtain an expression for the quantity $h_{\alpha\beta}$ by

taking the derivative of Eq. (2.7) with respect to $\rho_{\beta\alpha}$:

$$h_{\alpha\beta} = T_{\alpha\beta} + \sum_{\mu,\mu'} v_{\alpha\mu\beta\mu'}\rho_{\mu'\mu}(\Phi)\,. \tag{2.11}$$

A new operator $\hat{\Gamma}$ can be introduced, called the self-consistent field, such that

$$\hat{h} = \hat{T} + \hat{\Gamma}\,,$$

and

$$\Gamma_{\alpha\beta} := \sum_{\mu,\mu'} v_{\alpha\mu\beta\mu'}\rho_{\mu'\mu}(\Phi)\,. \tag{2.12}$$

The HF method then amounts to finding the one-body density that minimizes the energy: variations are carried out on the density and not on the Slater determinant. As shown for example in Ref. [38], Appendix D.2., a wave function is a Slater determinant if and only if the associated one-body density matrix is a projector in the single-particle space, that is

$$\rho^2 = \rho\,. \tag{2.13}$$

This must hold also for the varied density $\rho + \delta\rho$:

$$(\rho + \delta\rho)^2 = \rho + \delta\rho\,. \tag{2.14}$$

Up to first order in $\delta\rho$, Eq. (2.14) implies

$$\rho\delta\rho\rho = 0\,,$$

which means that, in the single-particle basis that diagonalizes ρ, the particle-particle and hole-hole elements of $\delta\rho$ vanish. As a consequence, Eq. (2.9) reads

$$\delta E[\rho] = \sum_{m,i}(h_{mi}\delta\rho_{im} + h_{im}\delta\rho_{mi})\,.$$

This last equation and the variational condition (2.8) lead to

$$h_{mi} = h_{im} = 0\,.$$

In addition, ρ is a projector, therefore its eigenvalues are 1 and 0 and the elements of h expressed in the single-particle basis in which ρ is diagonal read

$$h_{\alpha\beta} = T_{\alpha\beta} + \sum_{k=1}^{A} v_{\alpha k\beta k}\,. \tag{2.15}$$

Hence in particular

$$T_{mi} + \sum_{k=1}^{A} v_{mkik} = 0\,,$$

which can be written as

$$[h, \rho] = 0$$

and implies that h and ρ can be diagonalized in the same single-particle basis:

$$h_{\alpha\beta} = \epsilon^{\mathrm{HF}}_{\alpha} \delta_{\alpha\beta} \,. \tag{2.16}$$

This basis is called the HF basis, and is obtained from the basis in which the expression (2.11) is written by a unitary transformation D, such that

$$\rho_{\mu'\mu} = \sum_{k=1}^{A} D_{\mu' k} D^{*}_{\mu k} \,.$$

Hence the so-called Hartree-Fock equations are:

$$\sum_{\nu} \left(T_{\alpha\nu} + \sum_{k=1}^{A} \sum_{\mu,\mu'} v_{\alpha\mu\beta\mu'} D_{\mu' k} D^{*}_{\mu k} \right) D_{\nu\beta} = \epsilon^{\mathrm{HF}}_{\alpha} D_{\alpha\beta} \,. \tag{2.17}$$

2.3 HF-based RPA

2.3.1 Derivation of the RPA equations

Rowe showed [40] that if one denotes by $|0\rangle$ the exact ground state of a given many-body system, characterized by a Hamiltonian $\hat{H}$, then the excitations of this system are described by the following equations of motion [41]:

$$\forall R,\ \forall \lambda \in \mathscr{H},\ \left\langle 0 \middle| \left[R, [\hat{H}, Q^{\dagger}_{\lambda}] \right] \middle| 0 \right\rangle = \hbar\omega_{\lambda} \left\langle 0 \middle| \left[R, Q^{\dagger}_{\lambda} \right] \middle| 0 \right\rangle, \tag{2.18}$$

where R is any operator on the Hilbert space $\mathscr{H}$, $|\lambda\rangle$ an eigenstate of the Hamiltonian (excited state) associated with the eigenvalue ω_{λ} (excitation energy of the state $|\lambda\rangle$), and $Q^{\dagger}_{\lambda}$ the operator that creates the excited state $|\lambda\rangle$ when applied to the ground state. In other words, the operator $Q^{\dagger}_{\lambda}$ is defined for each excited state $|\lambda\rangle$ by

$$\begin{cases} Q^{\dagger}_{\lambda} |0\rangle = |\lambda\rangle & (2.19) \\ Q_{\lambda} |0\rangle = 0 \,, & (2.20) \end{cases}$$

and will be called here an excitation operator for the state $|\lambda\rangle$.

Given a Hamiltonian, the general aim here is to determine the excited states $|\lambda\rangle$ of the nucleus by solving Eq. (2.18). The starting point of the method is to assume — in other words, to choose — a particular form of the excitation operator $Q^{\dagger}_{\lambda}$. Only the following two constraints on the excitation operators have to be fulfilled:

1. They should verify the relation $\forall(\lambda,\mu),\ [Q_\lambda, Q_\mu^\dagger] = \delta_{\lambda\mu}\mathbb{1}$, because we require the set of eigenstates to be orthonormal;

2. They should verify Eqs. (2.19) and (2.20).

This step is where the RPA starts strictly speaking. In fact, in RPA, the excitation operator is chosen so that it accounts for superpositions of 1 particle-1 hole (1p1h) configurations only. It is therefore chosen as the following expression:

$$Q_\nu^\dagger := \sum_{m,i} \left(X_{mi}(\nu)\, \alpha_{mi}^\dagger - Y_{mi}(\nu)\, \alpha_{mi} \right), \tag{2.21}$$

where $\alpha_{mi}^\dagger$ are products of a creation and an annihilation operator:

$$\alpha_{mi}^\dagger := a_m^\dagger a_i\,. \tag{2.22}$$

The amplitudes "X" (forward amplitude) and "Y" (backward amplitude) of the excitation operator are to be determined by the method (see below).

The arbitrary operator R in Eq. (2.18) can thus be any linear combination of $\alpha_{mi}^\dagger$ and α_{mi}.
From the choice (2.21), the equations of motion (2.18) can be written as a matrix equation, known as the RPA equations:

$$\begin{pmatrix} A & B \\ B^* & A^* \end{pmatrix} \begin{pmatrix} X(\nu) \\ Y(\nu) \end{pmatrix} = \hbar\omega_\nu \begin{pmatrix} G & 0 \\ 0 & -G^* \end{pmatrix} \begin{pmatrix} X(\nu) \\ Y(\nu) \end{pmatrix}. \tag{2.23}$$

The forward and backward amplitudes $X(\nu)$ and $Y(\nu)$, along with the excitation energies $\hbar\omega_\lambda$, are the unknowns of the problem. By solving the RPA equations, one thus gets the knowledge of the excitation operator, which in turn provides the knowledge of the excited states according to Eq. (2.19).

The elements of these matrices are defined as follows:

$$A_{mi,nj} := \left\langle 0 \middle| \left[a_i^\dagger a_m, [\hat{H}, a_n^\dagger a_j] \right] \middle| 0 \right\rangle, \tag{2.24}$$

$$B_{mi,nj} := -\left\langle 0 \middle| \left[a_i^\dagger a_m, [\hat{H}, a_j^\dagger a_n] \right] \middle| 0 \right\rangle, \tag{2.25}$$

$$G_{mi,nj} := \left\langle 0 \middle| \left[a_i^\dagger a_m, a_n^\dagger a_j \right] \middle| 0 \right\rangle = \delta_{mn}\rho_{ji} - \delta_{ji}\rho_{mn} = G_{nj,mi}^*\,. \tag{2.26}$$

When the ground state $|0\rangle$ is replaced by the HF ground state in the above definitions, one obtains that A and G are hermitian, and B is symmetric. Provided these properties of A, B and G, the matrices

$$\mathscr{S} := \begin{pmatrix} A & B \\ B^* & A^* \end{pmatrix} \tag{2.27}$$

and

$$\mathscr{M} := \begin{pmatrix} G & 0 \\ 0 & -G^* \end{pmatrix}, \tag{2.28}$$

which are respectively known as the stability matrix and the metric matrix, are both hermitian. The RPA equations (2.23) are compactly written as

$$\mathscr{S}\mathscr{Z}(\nu) = \hbar\omega_\nu \mathscr{M}\mathscr{Z}(\nu), \tag{2.29}$$

where we define

$$\mathscr{Z}(\nu) := \begin{pmatrix} X(\nu) \\ Y(\nu) \end{pmatrix}. \tag{2.30}$$

Let us explain at this point the link between the stability condition of the collective modes and the stability matrix $\mathscr{S}$. A collective mode $|\nu\rangle$ is unstable if its energy $\hbar\omega_\nu$, as calculated by the resolution of Eq. (2.29), is non-real. The stability condition of the RPA solutions was discussed in detail in the past [40, 42–44]. The Thouless theorem [42] establishes the equivalence between the minimization of the expectation value of the Hamiltonian $\langle\psi|\hat{H}|\psi\rangle$ by a Slater determinant $|\psi\rangle$ and the stability of the solutions of these equations, when $|\psi\rangle$ is taken as an approximation of the ground state in the RPA equations. More specifically, one may express $|\psi\rangle$ as a function of the exact ground state $|0\rangle$ (assumed to be a Slater determinant). According to the Thouless theorem, as $|\psi\rangle$ is a Slater determinant, such an expression would read

$$|\psi\rangle = \exp\left(\sum_{m,i} C_{mi} a_m^\dagger a_i\right)|0\rangle$$

The expectation value $\langle\psi|\hat{H}|\psi\rangle$ can then be expanded in terms of the C coefficients, and the stability condition is that the terms that are linear in these coefficients must vanish and that the quadratic ones must be positive or zero. One can show that the positiveness of the quadratic terms translates into

$$\mathscr{Z}(\nu)^\dagger \mathscr{S}\mathscr{Z}(\nu) \geq 0, \tag{2.31}$$

meaning that the stability matrix $\mathscr{S}$ is positive semi-definite. In a nutshell, the RPA collective modes are stable if the linear terms in the above-mentioned expansion of the energy vanish and the stability matrix is positive semi-definite. In other words, if the HF ground state is really a minimum of the energy, then the RPA equations have only real solutions — nothing guarantees that the reverse is true. We will go back to this result in Subsec. 3.2.2, where we tackle the stability condition in SRPA.

We next derive a relation between the RPA amplitudes X and Y, which is

imposed by requiring the orthonormality of any two excited states $|\lambda\rangle$ and $|\lambda'\rangle$ of the many-body system.

If we denote by $|0\rangle$ the correlated ground state, which is sought to be the exact ground state, the orthonormality requirement of the excited states reads

$$\langle\lambda'|\lambda\rangle = \delta_{\lambda\lambda'}\,, \tag{2.32}$$

and, in virtue of Eqs. (2.19) and (2.20), we also have

$$\langle\lambda'|\lambda\rangle \;=\; \langle 0|\,[Q_{\lambda'}, Q_\lambda^\dagger]\,|0\rangle\;. \tag{2.33}$$

Starting from the expression of the excitation operator (2.21) and of its conjugate operator

$$Q_\lambda \;:=\; \sum_{n,j}\Big(X^*_{nj}(\lambda)\,a_j^\dagger a_n - Y^*_{nj}(\lambda)\,a_n^\dagger a_j\Big)\,, \tag{2.34}$$

we calculate the relation between the coefficients of the excitation operator that arises from the orthonormality requirement. Let us therefore express the commutator $[Q_{\lambda'}, Q_\lambda^\dagger]$ in terms of these coefficients, and of the metric matrix elements:

$$\begin{aligned}[Q_{\lambda'}, Q_\lambda^\dagger] \;=\; \sum_{m,i,n,j}\Big(&X^*_{mi}(\lambda')X_{nj}(\lambda)[a_i^\dagger a_m, a_n^\dagger a_j] + Y^*_{mi}(\lambda')\,Y_{nj}(\lambda)[a_m^\dagger a_i, a_j^\dagger a_n]\\ &- Y^*_{mi}(\lambda')X_{nj}(\lambda)[a_i^\dagger a_m, a_j^\dagger a_n] - X^*_{mi}(\lambda')\,Y_{nj}(\lambda)[a_m^\dagger a_i, a_n^\dagger a_j]\Big).\end{aligned} \tag{2.35}$$

From the anticommutation relations (fermions), by taking the expectation value in the ground state and using Eqs. (2.32) and (2.33), the following orthonormality relation for any two RPA excited states $|\lambda\rangle$ and $|\lambda'\rangle$ may be derived:

$$\delta_{\lambda\lambda'} \;=\; \sum_{m,i,n,j}\Big(X^*_{mi}(\lambda')X_{nj}(\lambda)\,G_{mi,nj} - Y^*_{mi}(\lambda')\,Y_{nj}(\lambda)\,G^*_{mi,nj}\Big). \tag{2.36}$$

Note that, independently of the orthonormality requirement, the right-hand side of Eq. (2.36) can be written as $\mathscr{Z}(\lambda')^\dagger\mathscr{M}\mathscr{Z}(\lambda)$, where $\mathscr{M}$ is the metric matrix (see Eq. (2.28)) and $\mathscr{Z}(\lambda)$ is defined in Eq. (2.30). Hence

$$\langle\lambda'|\lambda\rangle \;=\; \mathscr{Z}(\lambda')^\dagger\mathscr{M}\mathscr{Z}(\lambda)\,. \tag{2.37}$$

Finally, we derive the explicit expression of the transition amplitude $\langle\lambda|\,\hat{F}\,|0\rangle$

of a given one-body operator $\hat{F}$. Such an operator has the from

$$\hat{F} = \sum_{\alpha,\beta} \langle\alpha|\hat{F}|\beta\rangle\, a^{\dagger}_{\alpha} a_{\beta}\,,$$

where the labels run over all single-particle states.

Making use of properties (2.19)-(2.20), the transition amplitude may be written as

$$\langle\lambda|\hat{F}|0\rangle = \left\langle 0\left|\left[Q_{\lambda},\hat{F}\right]\right|0\right\rangle .$$

Then, by a similar reasoning as that used to establish the orthonormality relation of excited states, one gets the following explicit relation:

$$\langle\lambda|\hat{F}|0\rangle = \sum_{m,i,n,j}\left(X^{*}_{mi}(\lambda)\langle n|\hat{F}|j\rangle - Y^{*}_{mi}(\lambda)\langle j|\hat{F}|n\rangle\right)G^{*}_{mi,nj}\,. \tag{2.38}$$

Let us stress that in Eq. (2.38), only the particle-hole components of the transition operator $\hat{F}$ are present, because of the particle-hole form of the operator Q_{λ}. This is of importance when considering the following identity, known as the energy-weighted sum rule (EWSR):

$$\sum_{\lambda}\omega_{\lambda}\left|\langle\lambda|\hat{F}|0\rangle\right|^{2} = \frac{1}{2}\left\langle 0\left|\left[\hat{F},\left[\hat{H},\hat{F}\right]\right]\right|0\right\rangle . \tag{2.39}$$

It turns out that this equation holds exactly when the HF ground state $|\mathrm{HF}\rangle$ replaces the correlated one $|0\rangle$ in both sides, and when $|\lambda\rangle$ are the RPA excited states[1], in virtue of the Thouless theorem [42]. This identity is useful in practice to indicate the quality of a given theoretical model and of practical applications.

It does not hold when the correlated ground state is maintained, because then all the components of $\hat{F}$ appear — not just the particle-hole ones. That is why extensions of RPA which assume a correlated ground state and consider only particle-hole excitations are said to violate the EWSR [45–47].

2.3.2 Unsufficiency and inconsistency of the standard RPA

In principle, the RPA ground state is not an independent-particle-like state, as the HF ground state is (Slater determinant). Indeed, the chosen form of the excitation operator (2.21) assumes a ground state where not all the hole states are filled and not all the particle states are empty (correlated ground state). Otherwise the backward term of this operator would always yield 0 when applied to the ground state, and would be pointless. In standard RPA

[1] It is the case within the quasiboson approximation; see Subsec. 2.3.2.

however, the following approximation, known as the quasiboson approximation (QBA), is used in the computation of matrix elements:

$$\begin{aligned} \left\langle 0 \left| \left[a_i^\dagger a_m, a_n^\dagger a_j \right] \right| 0 \right\rangle &= \delta_{mn}\delta_{ij} - \delta_{mn} \left\langle 0 \left| a_j a_i^\dagger \right| 0 \right\rangle - \delta_{ij} \left\langle 0 \left| a_n a_m^\dagger \right| 0 \right\rangle \\ &\simeq \delta_{mn}\delta_{ij} = \left\langle \mathrm{HF} \left| \left[a_i^\dagger a_m, a_n^\dagger a_j \right] \right| \mathrm{HF} \right\rangle \qquad (2.40) \\ \textit{i.e.} \quad G_{mi,nj} &\simeq \delta_{mn}\delta_{ij} \,. \qquad (2.41) \end{aligned}$$

This means that the HF ground state is used to approximate the RPA ground state, and this replacement is made in all the matrix elements. This approximation is inconsistent with the choice of the form of the excitation operator, as in Eq. (2.21), and violates the Pauli principle. In Sec. 5.2 we will present a method that may overcome this problem.

Note that within this approximation, the G block of the metric is equal to the identity, as may be seen in Eq. (2.41).

CHAPTER 3

A beyond-mean-field approach as a starting point: Second RPA

Contents

3.1 Towards the second random-phase approximation 23
3.2 The SRPA model 24
3.2.1 Derivation of the SRPA equations 24
3.2.2 Drawbacks of the SRPA model. 28

3.1 Towards the second random-phase approximation

The RPA and its extension that includes pairing correlations, the QRPA, have been extensively used to describe properties of both giant resonances and low-lying states, and have generally provided a satisfactory description of them [48]. But if one wants to account for the spreading width and the fragmentation of the excitation modes, one has to go beyond the RPA. A possible path in this direction is the use of more complex configurations than 1p1h ones. The SRPA includes 2p2h configurations in addition to the latter, and yields much more spread and fragmented spectra.

In fact, the SRPA model not only allows us to describe the Landau damping, which is a single-particle contribution to the width of excitation modes, already present at the RPA level. It also allows us to reproduce the broadening of excitations related to the spreading width, which corresponds to a dissipation of the energy to the system's internal degrees of freedom — here, the beyond-1p1h configurations —. The escape-width contribution to the width of an excited state can be described only in those models where the continuum is properly described, at variance with our approach where we discretize it using a basis. For a more detailed discussion on the three

contributions to the width, the reader may refer to Refs. [12, 49].

Until recently, extending the configuration space to 2p2h configurations was computationally unaffordable. To make computations tractable, drastic approximations were adopted in the past. For example, calculations were carried out relying on approximations such as using low-energy cutoffs for 2p2h configurations or using a diagonal approximation in the 2p2h sector of the matrix to be diagonalized, in some cases even neglecting the residual interaction between 2p2h configurations in the diagonal part [50–54].

More recently, there was a regain of interest for the SRPA model, especially because of the modern increase of computational capabilities. The SRPA equations could be solved with less restrictive energy cutoffs and avoiding the diagonal approximation [55–59]. The computation of rearrangement terms for EDF-type calculations based on density-dependent interactions was also implemented [60].

3.2 The SRPA model

3.2.1 Derivation of the SRPA equations

We derive here the SRPA equations by emphasizing the changes with respect to the RPA, as derived in Subsec. 2.3.1. Like in the RPA case, the present derivation is based on the equations-of-motion method [40], as may be found in Ref. [61], although alternative derivations were proposed, based on a variational approach [62] or on the small-amplitude limit of the time-dependent density matrix [63, 64].

The formal properties of the RPA and the SRPA are analogous [65], and as we did in the case of the RPA, we only present here the equations that are of particular interest for our study. Also, we derive the equations within the QBA.

The standard version of the SRPA is the mere extension of the RPA to 2p2h configurations. This leads to additional terms in the expression of the excitation operators, compared to the RPA ones (see Eq. (2.21)), in order to account for these higher configurations. The SRPA excitation operator is

then defined as

$$Q^\dagger_\nu := \sum_{m,i} \left(X_{mi}(\nu)\, \alpha^\dagger_{mi} - Y_{mi}(\nu)\, \alpha_{mi} \right) + \sum_{\substack{m,n>m \\ i,j>i}} \left(X_{mnij}(\nu)\, \alpha^\dagger_{mnij} - Y_{mnij}(\nu)\, \alpha_{mnij} \right), \tag{3.1}$$

where

$$\alpha^\dagger_{mi} := a^\dagger_m a_i\,, \tag{3.2}$$

$$\alpha^\dagger_{mnij} := a^\dagger_m a^\dagger_n a_j a_i\,. \tag{3.3}$$

As a consequence, in addition to the usual RPA amplitudes $X_{mi}(\nu)$ and $Y_{mi}(\nu)$ of the excitation operator, there are new forward and backward amplitudes to determine, respectively $X_{mnij}(\nu)$ and $Y_{mnij}(\nu)$.

The equations of motion have the same expression as Eq. (2.18), but it is now understood that the arbitrary operator R in this equation can also feature terms corresponding to 2p2h configurations, *i.e.* linear combinations of $\alpha^\dagger_{mnij}$ and α_{mnij}. Thus we see that the number of terms resulting from the computation of the commutators increases with respect to the RPA. Of course, one also has the same definition (2.19)-(2.20) of the excitation operator.

The equations of motion can then be written as a matrix equation identical to the RPA case (see Eq. (2.23))

$$\begin{pmatrix} A & B \\ B^* & A^* \end{pmatrix} \begin{pmatrix} X(\nu) \\ Y(\nu) \end{pmatrix} = \hbar\omega_\nu \begin{pmatrix} G & 0 \\ 0 & -G^* \end{pmatrix} \begin{pmatrix} X(\nu) \\ Y(\nu) \end{pmatrix}, \tag{3.4}$$

but where the matrices A, B and G and the vectors X and Y now contain additional elements, due to the inclusion of 2p2h configurations. To highlight what has formally changed from RPA to SRPA, let us first rename the RPA matrices and vectors by adding subscripts referring to 1p1h configurations: A_{11}, B_{11}, G_{11}, X_1 and Y_1. By considering the above SRPA excitation operator and by writing the equations of motion into a matrix form, the RPA matrices appear as subblocks of the — larger — SRPA blocks A, B and G and eigenvectors X and Y, such that[1]

$$A = \begin{pmatrix} A_{11} & A_{12} \\ A_{21} & A_{22} \end{pmatrix}, \quad B = \begin{pmatrix} B_{11} & B_{12} \\ B_{21} & B_{22} \end{pmatrix}, \quad G = \begin{pmatrix} G_{11} & G_{12} \\ G_{21} & G_{22} \end{pmatrix}, \tag{3.5}$$

[1] In the following notations of the matrix subblocks, we will use the subscripts '1' and '2', to refer to 1p1h and 2p2h configurations, respectively. For example: the A_{12} subblock contains elements written as $A_{pk,mnij}$; $X_1(\nu)$ contains elements written as $X_{mi}(\nu)$; $X_2(\nu)$ contains elements written as $X_{mnij}(\nu)$.

and

$$X(\nu) = \begin{pmatrix} X_1(\nu) \\ X_2(\nu) \end{pmatrix}, \quad Y(\nu) = \begin{pmatrix} Y_1(\nu) \\ Y_2(\nu) \end{pmatrix}. \tag{3.6}$$

The blocks that involve 2p2h configurations are defined as follows:

$$A_{pk,mnij} := \left\langle 0 \middle| \left[\alpha_{pk}, [\hat{H}, \alpha^\dagger_{mnij}] \right] \middle| 0 \right\rangle, \tag{3.7}$$
$$A_{mnij,pk} := \left\langle 0 \middle| \left[\alpha_{mnij}, [\hat{H}, \alpha^\dagger_{pk}] \right] \middle| 0 \right\rangle, \tag{3.8}$$
$$A_{mnij,pqkl} := \left\langle 0 \middle| \left[\alpha_{mnij}, [\hat{H}, \alpha^\dagger_{pqkl}] \right] \middle| 0 \right\rangle, \tag{3.9}$$
$$B_{pk,mnij} := -\left\langle 0 \middle| \left[\alpha^\dagger_{pk}, [\hat{H}, \alpha^\dagger_{mnij}] \right] \middle| 0 \right\rangle, \tag{3.10}$$
$$B_{mnij,pk} := -\left\langle 0 \middle| \left[\alpha^\dagger_{mnij}, [\hat{H}, \alpha^\dagger_{pk}] \right] \middle| 0 \right\rangle, \tag{3.11}$$
$$B_{mnij,pqkl} := -\left\langle 0 \middle| \left[\alpha_{mnij}, [\hat{H}, \alpha_{pqkl}] \right] \middle| 0 \right\rangle = 0, \tag{3.12}$$
$$G_{pk,mnij} := \left\langle 0 \middle| \left[\alpha_{pk}, \alpha^\dagger_{mnij} \right] \middle| 0 \right\rangle, \tag{3.13}$$
$$G_{mnij,pk} := \left\langle 0 \middle| \left[\alpha_{mnij}, \alpha^\dagger_{pk} \right] \middle| 0 \right\rangle = G^*_{pk,mnij}, \tag{3.14}$$
$$G_{mnij,pqkl} := \left\langle 0 \middle| \left[\alpha_{mnij}, \alpha^\dagger_{pqkl} \right] \middle| 0 \right\rangle = G^*_{pqkl,mnij}. \tag{3.15}$$

One still has

$$\begin{aligned} A_{mi,nj} &:= \left\langle 0 \middle| \left[\alpha_{mi}, [H, \alpha^\dagger_{nj}] \right] \middle| 0 \right\rangle, \\ B_{mi,nj} &:= -\left\langle 0 \middle| \left[\alpha_{mi}, [H, \alpha_{nj}] \right] \middle| 0 \right\rangle, \\ G_{mi,nj} &:= \left\langle 0 \middle| \left[\alpha_{mi}, \alpha^\dagger_{nj} \right] \middle| 0 \right\rangle = \delta_{mn}\rho_{ji} - \delta_{ji}\rho_{mn} = G^*_{nj,mi}, \end{aligned} \tag{3.16}$$

and, similarly to the RPA as in our derivation in Subsec. 2.3.1, the above definitions imply that the matrices A and G are hermitian and that B is symmetric. One thus has the following relations between blocks:

$$A^\dagger_{11} = A_{11} \qquad A^\dagger_{21} = A_{12} \qquad A^\dagger_{22} = A_{22} \tag{3.17}$$
$$B^\dagger_{11} = B^*_{11} \qquad B^\dagger_{21} = B^*_{12} \qquad B^\dagger_{22} = B^*_{22} = 0_{22} \tag{3.18}$$
$$G^\dagger_{11} = G_{11} \qquad G^\dagger_{21} = G_{12} \qquad G^\dagger_{22} = G_{22} \tag{3.19}$$

Let us now show how the normalization of eigenvectors is modified by the inclusion of 2p2h configurations.

As in the RPA, the normalization relation is obtained by requiring that the expectation value

$$\langle \lambda' | \lambda \rangle = \langle 0 | [Q_{\lambda'}, Q^\dagger_\lambda] | 0 \rangle$$

be equal to $\delta_{\lambda\lambda'}$. The commutator $[Q_{\lambda'}, Q^\dagger_\lambda]$ expanded using the expression (3.1) now contains sixteen terms, half of which are zero due to anticommutation relations. The remaining terms can be gathered using the definitions

(3.16), (3.13) and (3.15) of the G_{11}, G_{12} and G_{22} elements respectively, so as to obtain the following relation:

$$\begin{aligned}\langle\lambda'|\lambda\rangle \;=\; & \sum_{m,i,n,j}\Big(X^*_{mi}(\lambda')X_{nj}(\lambda)\,G_{mi,nj} - Y^*_{mi}(\lambda')\,Y_{nj}(\lambda)\,G^*_{mi,nj}\Big) \\ & + \sum_{\substack{p,m,k,i,\\ q>p,n>m,\\ l>k,j>i}}\Big(X^*_{pqkl}(\lambda')X_{mnij}(\lambda)\,G_{pqkl,mnij} \\ & \qquad - Y^*_{pqkl}(\lambda')\,Y_{mnij}(\lambda)\,G^*_{pqkl,mnij}\Big) \\ & + \sum_{\substack{p,m,k,i\\ n>m,j>i}}\Bigg(\Big(X^*_{pk}(\lambda')X_{mnkl}(\lambda) - Y_{pk}(\lambda)\,Y^*_{mnkl}(\lambda')\Big)\,G_{pk,mnij} \\ & \qquad - \Big(Y^*_{pk}(\lambda')\,Y_{mnkl}(\lambda) - X_{pk}(\lambda)X^*_{mnkl}(\lambda')\Big)\,G^*_{pk,mnij}\Bigg).\end{aligned} \tag{3.20}$$

One may notice at this point that, similarly to the RPA case, this expectation value can be related to the SRPA metric matrix and amplitudes:

$$\langle\lambda'|\lambda\rangle \;=\; \mathcal{Z}(\lambda')^\dagger\,\mathcal{M}\,\mathcal{Z}(\lambda)\,. \tag{3.21}$$

The general form of the normalization relation then reads:

$$\mathcal{Z}(\lambda')^\dagger\,\mathcal{M}\,\mathcal{Z}(\lambda) \;=\; \delta_{\lambda\lambda'}\,. \tag{3.22}$$

Let us proceed to some approximations that allow us to reduce the number of terms in the general expression (3.22):

1. The ground-state expectation value of pairs such as $a_\alpha a_\beta$ and $a^\dagger_\alpha a^\dagger_\beta$ ("anomalous correlators") are zero. The Wick theorem [39, 66] allows us to write any two-body expectation value (*e.g.* $\langle 0|\,a^\dagger_\alpha a^\dagger_\beta a_\gamma a_\delta\,|0\rangle$) as a linear combination of one-body expectation values (*e.g.*$\langle 0|\,a^\dagger_\alpha a_\beta\,|0\rangle$), among which some anomalous correlators may appear. This approximation thus implies that two-body density matrix elements, defined as

$$\rho_{\alpha\beta\gamma\delta}(0) \;:=\; \langle 0|\,a^\dagger_\gamma a^\dagger_\delta a_\beta a_\alpha\,|0\rangle\,, \tag{3.23}$$

can be expressed in terms of only one-body matrix elements

$$\rho_{\alpha\beta}(0) \;:=\; \langle 0|\,a^\dagger_\beta a_\alpha\,|0\rangle\,, \tag{3.24}$$

by the following relation[2]:

$$\forall(\alpha,\beta,\gamma,\delta),\;\; \rho_{\alpha\beta\gamma\delta} \;\simeq\; \rho_{\alpha\gamma}\,\rho_{\beta\delta} - \rho_{\alpha\delta}\,\rho_{\beta\gamma}\,. \tag{3.25}$$

[2]Where we have dropped the reference to the ground state for simplicity, as will hold in the following.

2. The one-body density matrix is assumed to be diagonal in the chosen single-particle basis, *i.e.*

$$\forall(\alpha,\beta),\ \rho_{\alpha\beta} = \delta_{\alpha\beta}\, n_\alpha\,, \tag{3.26}$$

where n_α is the occupation number of the single-particle state α.

Within these approximations, one can show that the G_{12} and G_{21} blocks of the SRPA metric $\mathscr{M}$ actually have only zero elements.

To conclude, the SRPA normalization relation simply reads

$$\begin{aligned}\delta_{\lambda\lambda'} \simeq & \sum_{m,i,n,j}\Big(X^*_{mi}(\lambda')X_{nj}(\lambda)\,G_{mi,nj} - Y^*_{mi}(\lambda')\,Y_{nj}(\lambda)\,G^*_{mi,nj}\Big) \\ & + \sum_{\substack{p,m,k,i,\\ q>p,n>m,\\ l>k,j>i}}\Big(X^*_{pqkl}(\lambda')X_{mnij}(\lambda)\,G_{pqkl,mnij} - Y^*_{pqkl}(\lambda')\,Y_{mnij}(\lambda)\,G^*_{pqkl,mnij}\Big).\end{aligned} \tag{3.27}$$

Continuing the correspondance with the RPA derivation of Subsec. 2.3.1, let us finally consider the SRPA transition amplitude $\langle\lambda|\,F\,|0\rangle$ of a one-body operator F. In this case, the only additional terms compared to the RPA case are those mixing 1p1h and 2p2h configurations, similar to the "12" terms of Eq. (3.22). Therefore, provided the approximations (3.25)-(3.26) hold, the expression of the transition amplitude of any one-body operator is actually the same as in the RPA (see Eq. (2.38)):

$$\langle\lambda|\,F\,|0\rangle = \sum_{m,i,n,j}\Big(X^*_{mi}(\lambda)\,\langle n|\,F\,|j\rangle - Y^*_{mi}(\lambda)\,\langle j|\,F\,|n\rangle\Big)\,G^*_{mi,nj}\,. \tag{3.28}$$

3.2.2 Drawbacks of the SRPA model

The standard form of the SRPA model suffers from several problems. Some of them are general in that they are present in all types of SRPA calculations. Others are related to the use of EDFs. We present each of them succinctly in this section.

General problems. Abnormal shift towards low energies and instabilities (Thouless theorem)

Instabilities (non-real eigenenergies) may appear in standard SRPA, contrary to standard RPA[3] provided the HF ground-state in the RPA does correspond to a true minimum of the energy[4]. Indeed, in contrast to the standard RPA, the fact that the reference state (the HF ground state) minimizes the energy is not sufficient anymore to guarantee stable solutions. As was highlighted by Papakonstantinou [67], this comes from the fact that a single Slater determinant cannot fulfill the stability condition in the SRPA case, namely the simultaneous positive semi-definiteness of the stability matrix and the cancellation of linear terms in the expansion of the Hamiltonian expectation value (see Subsec. 2.3.1). Of course, the latter expansion contains more terms than in the RPA case, due to the presence of 2p2h configurations, as may be seen in Ref. [62]. In summary, the Thouless theorem [42], applicable in the standard RPA, does not extend to the standard SRPA. However, it may be extended by means of a correction of the stability matrix, such as the subtraction procedure [68], which we discuss in Chap. 4.

Note that the onset of instabilities when including 2p2h configurations is not specific to the EDF framework, but arises also when other types of interactions are used, for example functionals derived from realistic nucleon-nucleon interactions [56].

The very large and unphysical shift towards low energies that is found in SRPA spectra compared to RPA spectra may also he related to the instability problems of the SRPA model, as analyzed in Ref. [67].

Illustrations of this shift are shown on Figs. 3.1 to 3.3.

Figure 3.1 is extracted from Ref. [57] and displays the ^{16}O isoscalar (IS) and isovector (IV) monopole responses, in both the RPA and the SRPA. One observes that the whole SRPA spectrum is shifted by several MeVs towards low energies with respect to the RPA, similarly in the isoscalar and in the isovector case (upper and lower panels, respectively). The used Skyrme parametrization is SGII [69, 70].

On Fig. 3.2, which was extracted from Ref. [56], the same behavior is found. This figure shows the isoscalar quadrupole response of ^{48}Ca (upper

[3] By "standard" we mean that the quasiboson approximation is used (see Subsec. 2.3.2).

[4] The standard RPA may have instabilties (for example in the quadrupole case close to the phase transition to quadrupole deformation, or in the charge-exchange case) due to a failure of the minimization of the expectation value $\langle \mathrm{HF}|\hat{H}|\mathrm{HF}\rangle$ in the variational procedure.

panel) with a realistic interaction, derived from the Argonne V18 potential [71] using the unitary correlation operator (UCOM) [72, 73], and the isovector dipole response of ^{16}O (lower panel) with the Brink-Boeker (BB) interaction [74]. One sees in addition that the effect of the diagonal approximation is marginal.

Figure 3.3 was published in Ref. [75] and displays strength distributions for several multipolarities L in the metal cluster Na_9^+, which is positively charged. Metal clusters are treated within the jellium approximation where the ionic structure is described as a positively charged uniform background interacting with delocalized valence electrons [76]. The interaction acting between the jellium and the electrons and between the delocalized electrons is the Coulomb interaction. The energy scale is different in metal clusters (then, the shift is of the order of the eV) than in nuclei (generally a shift of several MeVs), and in this case, the effect of the diagonal approximation is more important than in Ref. [56]. In particular, the dipole response (upper right panel) shows that the shift is indeed unphysical, for in the SRPA results, the dipole $S = 0$ state is located further from the experimental result than the RPA, with a worse reproduction obtained from the full SRPA (all 2p2h couplings) than from the SRPA with diagonal approximation.

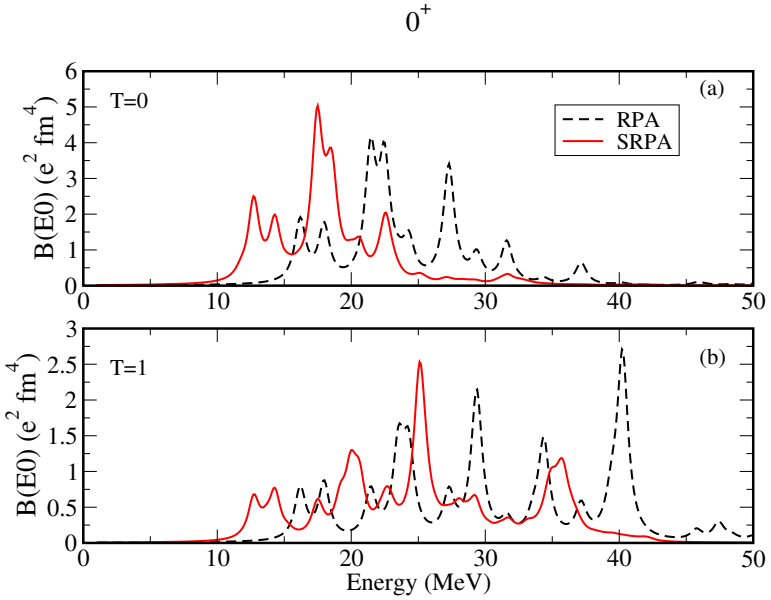

Figure 3.1: RPA [dashed (black) lines] and SRPA [full (red) lines] for the isoscalar (upper panel) and isovector (lower panel) monopole strength distributions in ^{16}O. The calculations are performed with the Skyrme parametrization SGII. In SRPA, the cutoff on 2p2h configurations is 120 MeV. From Ref. [57].

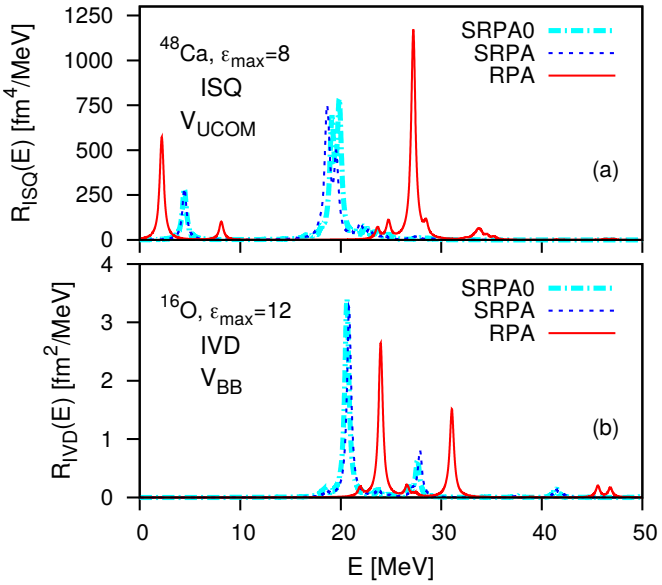

Figure 3.2: (a) Isoscalar (IS) quadrupole response of ^{48}Ca in a single-particle basis with $\epsilon_{\max} = 8$ and using V_{UCOM}. (b) Isovector (IV) dipole response of ^{16}O in a single-particle basis with $\epsilon_{\max} = 12$ and $l_{\max} = 8$ and using V_{BB}. Results are obtained with the RPA, solving the full SRPA problem and using the diagonal approximation (SRPA0). $l_{\max}$ and $\epsilon_{\max}$ represent respectively the cutoff in orbital angular momentum and the number of energy quanta in the highest oscillator shell considered. In all cases, the Lorentzian folding width is $\Gamma = 0.5$ MeV. From Ref. [56].

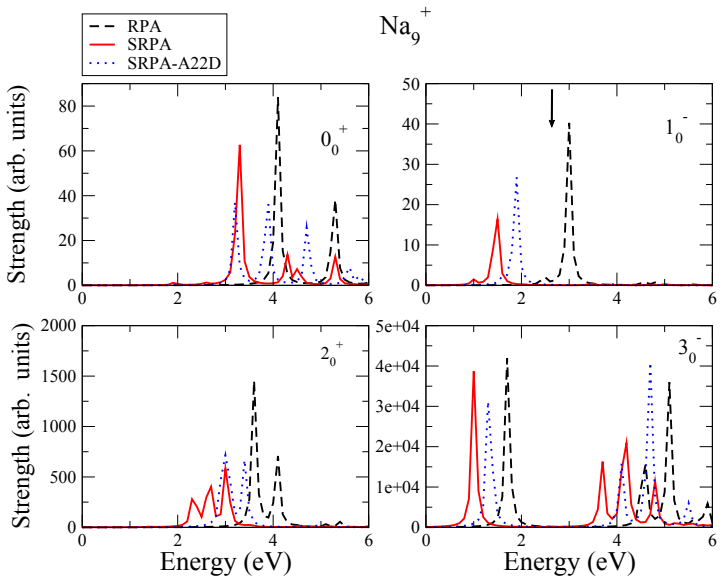

Figure 3.3: Natural parity $L = 0$, 1 (upper panel) and $L = 2$, 3 (lower panel) spin = 0 multipole strength distributions for the Na_9^+ metal cluster. Solid (red) lines refer to SRPA results, while the dashed (black) ones refer to RPA calculations. SRPA-A22D dotted (blue) lines show the SRPA results when the diagonal approximation is used. The arrow roughly indicates the positions of the experimental dipole plasmon peak [77]. From Ref. [75].

Problems related to EDFs. Double-counting and possible ultraviolet divergence

Let us recall that all the present studies are carried out in the framework of EDFs. When EDFs are used, beyond-RPA approaches generate a double counting of correlations [25]. Indeed, effective interactions contain parameters which are adjusted to reproduce selected properties of nuclei. In general, these adjustments have been performed using mean-field calculations, but the measured quantities that they aim to reproduce contain correlations. This implies that some correlations are indeed implicitly accounted for in the numerical values of the adjusted parameters. Now the SRPA is a beyond-MF method, because of the inclusion of 2p2h configurations, therefore it is designed to describe correlations which are absent in a simple MF model. If EDFs adjusted at the MF level are used, there is a risk of overcounting correlations.

Eliminating the double counting of correlations would thus mean in this case subtracting those correlations which are already accounted for in the numerical values of the parameters and leaving only the genuine beyond-mean-field effects (what Tselyaev calls dynamic correlations [68]).

As already mentioned in Sec. 2.1, the most used interactions in the EDF framework are the Skyrme and Gogny interactions. In the Skyrme case, all the terms are of zero range, whereas in the Gogny case, some terms have zero range and others finite range (gaussians). When the mean-field approximation is overcome, the zero range of the used interaction may generate ultraviolet divergences and the obtained results acquire a cutoff dependence.

This divergence was for example studied analytically in Ref. [78], where second-order calculations of the equation of state of infinite matter are carried out with Skyrme interactions.

In cases where ultraviolet divergences occur, regularization schemes are required.

CHAPTER 4

A correction of SRPA: Subtracted SRPA

"Prends un siège Cinna, et assieds-toi par terre
Et si tu veux parler, commence par te taire."
Raymond Rua.

Contents

4.1 Principle of the subtracted SRPA (SSRPA) 33
4.1.1 SRPA as an energy-dependent RPA-like problem 33
4.1.2 Benefits and practical use of the subtraction method 35
4.2 Results: Assessment of the correction capabilities of SSRPA 40
4.2.1 Residual interaction in SSRPA calculations 40
4.2.2 Dipole response and polarizability in ^{48}Ca 43
4.2.3 Quadrupole response: systematics on selected nuclei 51
4.2.4 Beyond-mean-field effects on the effective masses 58

4.1 Principle of the subtracted SRPA (SSRPA)

4.1.1 SRPA as an energy-dependent RPA-like problem

In this section, we show a derivation which will be used to introduce our subtraction method.

We first remind the matrix form of the (S)RPA equations:

$$\begin{pmatrix} A & B \\ B^* & A^* \end{pmatrix} \begin{pmatrix} X(\nu) \\ Y(\nu) \end{pmatrix} = \hbar\omega_\nu \begin{pmatrix} G & 0 \\ 0 & -G^* \end{pmatrix} \begin{pmatrix} X(\nu) \\ Y(\nu) \end{pmatrix}. \tag{4.1}$$

Let us consider the SRPA case and denote by N_1 and N_2 respectively the number of 1p1h and 2p2h configurations. A, B and G therefore belong to $\mathscr{M}_{N_1+N_2}(\mathbb{C})$ in the general case. Defining the dimension of the problem as $D := 2(N_1 + N_2)$, the stability matrix belongs to $\mathscr{M}_D(\mathbb{C})$.

Making the matrix subblocks appear explicitly, one has:

$$\begin{pmatrix} A_{11} & A_{12} & B_{11} & B_{12} \\ A_{21} & A_{22} & B_{21} & B_{22} \\ B_{11}^* & B_{12}^* & A_{11}^* & A_{12}^* \\ B_{21}^* & B_{22}^* & A_{21}^* & A_{22}^* \end{pmatrix} \begin{pmatrix} X_1(\nu) \\ X_2(\nu) \\ Y_1(\nu) \\ Y_2(\nu) \end{pmatrix} = \hbar\omega_\nu \begin{pmatrix} G_{11} & G_{12} & 0 & 0 \\ G_{21} & G_{22} & 0 & 0 \\ 0 & 0 & -G_{11}^* & -G_{12}^* \\ 0 & 0 & -G_{21}^* & -G_{22}^* \end{pmatrix} \begin{pmatrix} X_1(\nu) \\ X_2(\nu) \\ Y_1(\nu) \\ Y_2(\nu) \end{pmatrix}. \tag{4.2}$$

Now, as we have derived in Subsec. 3.2.1, the different matrix subblocks are linked to one another by the properties (3.17) to (3.19), and we have shown that $G_{12} = 0_{12}$ under two approximations. In these conditions, the SRPA equations (4.2) become

$$\begin{cases} A_{11}X_1(\nu) + A_{12}X_2(\nu) + B_{11}Y_1(\nu) + B_{12}Y_2(\nu) = \hbar\omega_\nu G_{11}X_1(\nu) & (4.3) \\ A_{12}^\dagger X_1(\nu) + A_{22}X_2(\nu) + {}^tB_{12}Y_1(\nu) = \hbar\omega_\nu G_{22}X_2(\nu) & (4.4) \\ B_{11}^\dagger X_1(\nu) + B_{12}^* X_2(\nu) + A_{11}^* Y_1(\nu) + A_{12}^* Y_2(\nu) = -\hbar\omega_\nu G_{11}^* Y_1(\nu) & (4.5) \\ B_{12}^\dagger X_1(\nu) + {}^tA_{12}Y_1(\nu) + A_{22}^* Y_2(\nu) = -\hbar\omega_\nu G_{22}^* Y_2(\nu). & (4.6) \end{cases}$$

In Eqs. (4.4) and (4.6), the X_2 and Y_2 vectors can be factorized independently from one another, by defining two new matrices for each eigenvalue ω:

$$M(\omega) := \hbar\omega G_{22} - A_{22}, \tag{4.7}$$
$$P(\omega) := -\left(\hbar\omega G_{22}^* + A_{22}^*\right). \tag{4.8}$$

Hence, if one assumes that M and P are invertible, an expression for these two vectors is

$$X_2(\nu) = M(\omega_\nu)^{-1}\left(A_{12}^\dagger X_1(\nu) + {}^tB_{12}Y_1(\nu)\right), \tag{4.9}$$
$$Y_2(\nu) = P(\omega_\nu)^{-1}\left(B_{12}^\dagger X_1(\nu) + {}^tA_{12}Y_1(\nu)\right). \tag{4.10}$$

If so, one can replace X_2 and Y_2 in Eqs. (4.3) and (4.5) to transform these equations into the following ones:

$$\begin{cases} \left[A_{11} + A_{12}M(\omega_\nu)^{-1}A_{12}^\dagger - B_{12}P(\omega_\nu)^{-1}B_{12}^\dagger\right]X_1(\nu) \\ + \left[B_{11} + A_{12}M(\omega_\nu)^{-1}{}^tB_{12} - B_{12}P(\omega_\nu)^{-1}{}^tA_{12}\right]Y_1(\nu) \\ \qquad = \hbar\omega_\nu G_{11}X_1(\nu) & (4.11) \\ \left[B_{11}^\dagger + B_{12}^* M(\omega_\nu)^{-1}A_{12}^\dagger - A_{12}^* P(\omega_\nu)^{-1}B_{12}^\dagger\right]X_1(\nu) \\ + \left[A_{11}^* + B_{12}^* M(\omega_\nu)^{-1}{}^tB_{12} - A_{12}^* P(\omega_\nu)^{-1}{}^tA_{12}\right]Y_1(\nu) \\ \qquad = -\hbar\omega_\nu G_{11}^* Y_1(\nu). & (4.12) \end{cases}$$

The system (4.11)-(4.12) would resemble an RPA-like problem, if the factor of Y_1 in Eq. (4.12) were the Hermitian conjugate of that of X_1 in Eq. (4.11) (and similarly for the two other factors). This condition is fulfilled if $M(\omega_\nu)$ and $P(\omega_\nu)$ are their own complex conjugates.

It then seems relevant to introduce the following two N_1^2-matrices:

$$A'_{11}(\omega) := A_{11} + A_{12}M(\omega)^{-1}A_{12}^\dagger - B_{12}P(\omega)^{-1}B_{12}^\dagger, \tag{4.13}$$

$$B'_{11}(\omega) := B_{11} + A_{12}M(\omega)^{-1^t}B_{12} - B_{12}P(\omega)^{-1^t}A_{12}. \tag{4.14}$$

Note that these matrices depend on the excitation energy ω_ν, unlike the RPA matrices A_{11} and B_{11}.

The system (4.11)-(4.12) can now be written in matrix form:

$$\begin{pmatrix} A'_{11}(\omega_\nu) & B'_{11}(\omega_\nu) \\ B'^*_{11}(\omega_\nu) & A'^*_{11}(\omega_\nu) \end{pmatrix} \begin{pmatrix} X_1(\nu) \\ Y_1(\nu) \end{pmatrix} = \hbar\omega_\nu \begin{pmatrix} G_{11} & 0 \\ 0 & -G^*_{11} \end{pmatrix} \begin{pmatrix} X_1(\nu) \\ Y_1(\nu) \end{pmatrix}. \tag{4.15}$$

In the end, provided the matrices $M(\omega_\nu)$ and $P(\omega_\nu)$ are real and invertible for each eigenvalue ω_ν, the initial problem of dimension $D = 2(N_1+N_2)$ has been reduced a problem of dimension N_1, involving the inversion of two N_2^2-matrices ($M(\omega_\nu)$ and $P(\omega_\nu)$) — this inversion is needed to set up the new block matrices, but also to calculate X_2 and Y_2 (according to Eqs. (4.9) and (4.10)). Of course, Eq. (4.15) is not properly speaking an eigenvalue problem, because the matrices themselves depend on the solution.

The above derivation can be summarized in the following way:
If $M(\omega_\nu) = \hbar\omega_\nu G_{22} - A_{22}$ and $P(\omega_\nu) = -\left(\hbar\omega_\nu G^*_{22} + A^*_{22}\right)$ are real and invertible for each ω_ν, then:

$$\text{SRPA problem (4.2)} \iff \begin{cases} \text{Inversion of } M(\omega_\nu) \text{ and } P(\omega_\nu) \text{ for each } \omega_\nu \\ \text{Energy-dependent RPA-like problem (4.15)} \end{cases}$$

4.1.2 Benefits and practical use of the subtraction method

Historically, the subtraction procedure was introduced by Tselyaev [79] as a means to address the problem of spurious states in the quasiparticle-time-blocking-approximation (QTBA) approach. Let us recall at this point that spurious states are excitations of the many-body system that correspond to given symmetries, such as translational of rotational invariance. They do not correspond to physical excited modes and are therefore expected to have zero excitation energies. Tselyaev's method consisted in finding a sufficient condition for the response function to have poles at zero excitation energy corresponding to the spurious states. Later, Tselyaev showed that, in the

case of beyond-RPA approaches, this procedure also allows for the elimination of correlations that might already be accounted for in the values of the parameters of the effective interaction (in EDF models), as already discussed in Subsec. 3.2.2 (double counting of correlations) [68].

It was shown [68] that the subtraction procedure also solves the stability problem of SRPA (see Subsec. 3.2.2). In fact, the SRPA stability matrix resulting from the subtraction is positive semi-definite, which allows for an extension of the Thouless theorem to SRPA [42, 67].

In Ref. [68], the latter features of this subtraction procedure are highlighted for a category of RPA-like problems into which the problem (4.15) falls, which is of interest for our study. To present how the procedure is translated in the SRPA case, we briefly introduce here the needed quantities from the response function formalism.

Let us first define the RPA matrix Ω^{RPA}, in terms of the RPA stability and metric matrices, $\mathscr{S}^{\mathrm{RPA}}$ and $\mathscr{M}^{\mathrm{RPA}}$ respectively:

$$\Omega^{\mathrm{RPA}} := \mathscr{M}^{\mathrm{RPA}^{-1}} \mathscr{S}^{\mathrm{RPA}} . \tag{4.16}$$

The RPA response function [38] is defined as

$$R^{\mathrm{RPA}}(\omega) := -(\omega - \Omega^{\mathrm{RPA}})^{-1} \mathscr{M}^{\mathrm{RPA}} , \tag{4.17}$$

and the (dynamic) polarizability Π_F^{RPA}, which determines the distribution of the transition strength due to an external field represented by the single-particle operator F, has the following definition:

$$\Pi_F^{\mathrm{RPA}}(\omega) := -\left\langle F \left| R^{\mathrm{RPA}}(\omega) \right| F \right\rangle . \tag{4.18}$$

The so-called static polarizability is the value of the polarizability at $\omega = 0$. This quantity can be derived as $-2m_{-1}$ [80], where $m_{-1} := \int_0^\infty S(E) E^{-1} \mathrm{d}E$ is the inverse energy-weighted moment of the strength function S, which contains all the information of the spectrum. Now, the general idea is that EDF functionals are built so as to encapsulate contributions to the correlations, because they contain parameters adjusted with mean-field calculations to reproduce measured observables. In a DFT spirit, these functionals may be regarded as "universal functionals" tailored to describe correlated many-body systems. Following this idea, the standard mean-field RPA would then provide the supposedly exact value of the static polarizability. On the other side, when beyond-MF models are employed (such as the SRPA model), correlations which are absent in a mean-field calculation are explicitly included. If a traditional EDF functional is used, double counting of correlations may

occur.

Therefore it is sensible to impose that the inverse energy-weighted moment of the strength m_{-1} (related to the static polarizability and calculated with the beyond-MF approach of interest) be equal to the RPA m_{-1}, so that correlations are accounted for without double counting. As already pointed out in Subsec. 3.2.2, this subtraction concerns static contributions ($\omega = 0$), keeping the benefits of the beyond-MF approach with respect to RPA in the description of excited states (dynamic contributions to correlations are taken into account).

The procedure then amounts to impose that the beyond-RPA and the RPA static polarizabilities be equal. In our case, the beyond-MF approach is the SRPA, and, as we have shown in the previous section, the SRPA can be expressed as an energy-dependent RPA-like problem, which we will label RPA$'$ in the formulae. The prescription reads

$$\Pi_F^{\mathrm{RPA}'}(0) = \Pi_F^{\mathrm{RPA}}(0). \tag{4.19}$$

As we have seen, the stability matrix of this RPA-like problem depends on the excitation energy:

$$\mathcal{S}^{\mathrm{RPA}'}(\omega) := \begin{pmatrix} A'_{11}(\omega) & B'_{11}(\omega) \\ B'^{*}_{11}(\omega) & A'^{*}_{11}(\omega) \end{pmatrix}, \tag{4.20}$$

and so does the corresponding RPA matrix $\Omega^{\mathrm{RPA}'}(\omega) := \mathcal{M}^{\mathrm{RPA}'-1}\mathcal{S}^{\mathrm{RPA}'}(\omega)$ (where $\mathcal{M}^{\mathrm{RPA}'} = \mathcal{M}^{\mathrm{RPA}}$; see Eq. (4.15)), by definition. Making use of the definitions (4.18), (4.17) and (4.16), we get

$$\begin{aligned} \Pi_F^{\mathrm{RPA}'}(0) &= -\left\langle F \left| \Omega^{\mathrm{RPA}'}(0)^{-1} \mathcal{M}^{\mathrm{RPA}'} \right| F \right\rangle \\ &= -\left\langle F \left| \mathcal{S}^{\mathrm{RPA}'}(0)^{-1} \mathcal{M}^{\mathrm{RPA}'2} \right| F \right\rangle, \end{aligned}$$

which shows that the prescription (4.19) can equivalently be formulated on the stability matrices:

$$\mathcal{S}^{\mathrm{RPA}'}(0) = \mathcal{S}^{\mathrm{RPA}}. \tag{4.21}$$

According to the definition of the stability matrices, we conclude that this requirement translates into the equality of the RPA-like blocks at zero energy and standard RPA blocks:

$$\begin{cases} A'_{11}(0) = A_{11} \\ B'_{11}(0) = B_{11}. \end{cases} \tag{4.22}$$

Now the RPA-like blocks were defined as the RPA ones to which an energy-

dependent term (self-energy) is added (see Eqs. (4.13) and (4.14)):

$$A'_{11}(\omega) = A_{11} + W_A(\omega), \tag{4.23}$$
$$B'_{11}(\omega) = B_{11} + W_B(\omega), \tag{4.24}$$

where we define

$$W_A(\omega) := A_{12}M(\omega)^{-1}A_{12}^{\dagger} - B_{12}P(\omega)^{-1}B_{12}^{\dagger}, \tag{4.25}$$
$$W_B(\omega) := A_{12}M(\omega)^{-1^t}B_{12} - B_{12}P(\omega)^{-1^t}A_{12}. \tag{4.26}$$

One would have satisfied the prescription (4.22) if one had have, in place of the $A'_{11}(\omega)$ and $B'_{11}(\omega)$ blocks, respectively the following ones:

$$A^{\mathrm{S}}_{11}(\omega) := A'_{11}(\omega) - W_A(0) = A_{11} + W_A(\omega) - W_A(0), \tag{4.27}$$
$$B^{\mathrm{S}}_{11}(\omega) := B'_{11}(\omega) - W_B(0) = B_{11} + W_B(\omega) - W_B(0). \tag{4.28}$$

As is apparent in Eqs. (4.27) and (4.28), the RPA-like problem is cleared from the static contribution to the correlations, while having the dynamic correlations preserved.

A way of satisfying the prescription would be to choose beforehand the A_{11} and B_{11} blocks to be $A_{11} - W_A(0)$ and $B_{11} - W_B(0)$ respectively. In other words, let us suppose that one has a SRPA problem (4.2), where the A_{11} and B_{11} blocks are subtracted in this way. The derivation carried out in Subsec. 4.1.1 can be followed for this subtracted SRPA problem, and the corresponding RPA-like blocks exactly fulfill the prescription (4.22). This is how the subtraction method is performed in practice in our numerical applications.

As a conclusion, the SSRPA model amounts to a correction of the RPA block matrices, while setting up all the other matrices in the usual way, followed by the resolution of the subsequent SRPA problem. The major cost of this procedure is the computation of the terms to subtract, namely $W_A(0)$ and $W_B(0)$. As one can see in their respective definitions (4.25) and (4.26), their computation involves the inversion of the M and P matrices, which are matrices of size N_2^2 (see Eqs. (4.7) and (4.8)). The large number of 2p2h configurations (N_2), compared to that of 1p1h ones (N_1), may result in non-negligible computational effort when performing this procedure.

Gambacurta *et al.* [81] showed that the subtraction procedure also eliminates the ultraviolet divergences when zero-range interactions, such as Skyrme interactions, are used. Figure 4.1 illustrates this. There, the isoscalar monopole response of ^{16}O computed with the Skyrme parametrization SGII

is displayed for several cutoff values. These cutoff values are put both on the corrective terms (self-energy) and on the 2p2h sector of the SSRPA matrix to be diagonalized. For a numerical simplification of such a test, the diagonal approximation was used in the computation of the corrective terms (in the matrix to be inverted).

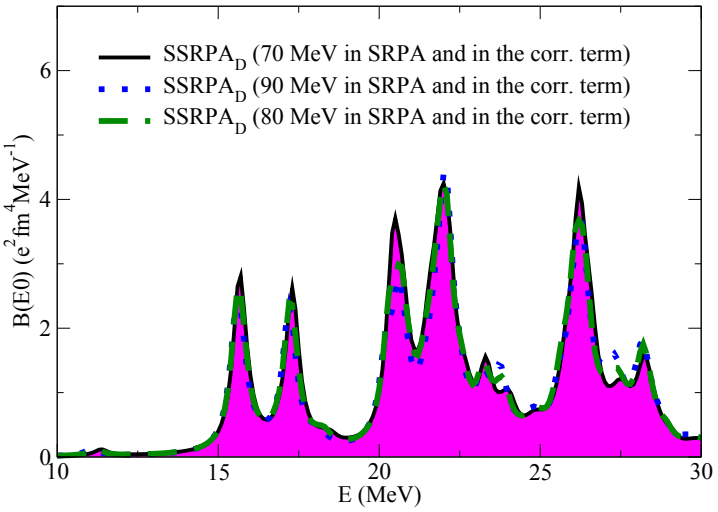

Figure 4.1: Isoscalar monopole response of ^{16}O in the diagonal approximation for the computation of the corrective terms, with cutoff at 70 (black line and magenta area), 80 (green dashed line), and 90 (blue dotted line) MeV. From Ref. [81].

The choice of the cutoff in the corrective terms is crucial to guarantee that the m_{-1} moment of the strength is conserved with respect to RPA. As an illustration, Fig. 4.2 shows the ratios of the moments m_{-1}, m_0 and m_1 of the quadrupole strength distribution in ^{16}O with the parametrization SGII (the ratios are taken with respect to the RPA values). The subscripts F and D indicate whether the matrix to be inverted (in the corrective terms) is computed without approximations or in the diagonal approximation, respectively. A cutoff of 50 MeV is employed for the SRPA and the SSRPA calculations. Three cutoff values, 40, 45 and 50 MeV, are used in the corrective terms. One may observe that the m_{-1} moment is fully conserved only when the matrix to invert in the corrective terms is treated without the diagonal approximation and the 2p2h cutoff values used in the SSRPA diagonalization and in the corrective terms are the same.

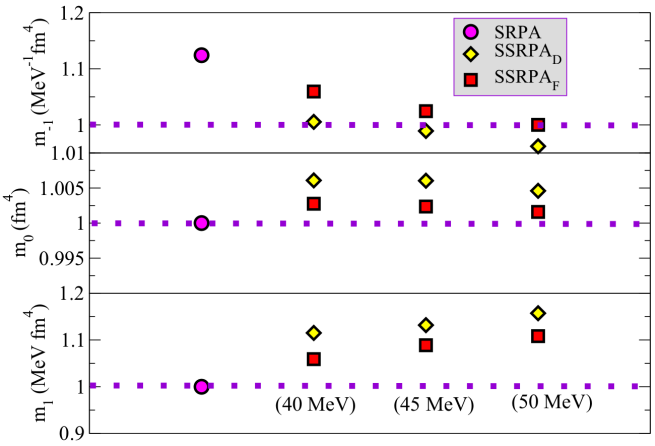

Figure 4.2: Ratios of the moments m_{-1} , m_0 , and m_1 of the quadrupole strength distribution in the SRPA (purple circles), the full SSRPA (SSRPA$_F$, red squares), and the SSRPA with diagonal approximation in the corrective terms (SSRPA$_D$, yellow diamonds) to those in the RPA for increasingly high cutoffs in the correction terms, at 40, 45, and 50 MeV. From Ref. [81].

4.2 Results: Assessment of the correction capabilities of SSRPA

4.2.1 Residual interaction in SSRPA calculations

In all the applications that will be presented in this manuscript, the adopted phenomenological interaction is the Skyrme interaction in its most currently used form (and not containing tensor terms), that is:

$$\begin{aligned} V(\mathbf{r_1},\mathbf{r_2}) = \; & t_0(1+x_0P_\sigma)\delta(\mathbf{r}) + \frac{1}{6}t_3(1+x_3P_\sigma)\rho(\mathbf{R})^\alpha\delta(\mathbf{r}) \\ & + \frac{1}{2}t_1(1+x_1P_\sigma)[\mathbf{P'}^2\delta(\mathbf{r}) + \delta(\mathbf{r})\mathbf{P}^2] + t_2(1+x_2P_\sigma)\mathbf{P'}\cdot\delta(\mathbf{r})\mathbf{P} \\ & + iW_0\sigma\cdot[\mathbf{P'}\times\delta(\mathbf{r})\mathbf{P}], \end{aligned}$$

The density-dependent term may be recognized as the second term of the first line. Two gradient terms appear in the second line, one of s-wave type (t_1) and the other of p-wave type (t_2). The last line describes the spin-orbit

contribution. The employed notation is the following:

$$\mathbf{r} = \mathbf{r_1} - \mathbf{r_2}\,, \quad \mathbf{R} = \frac{1}{2}(\mathbf{r_1} + \mathbf{r_2})\,, \tag{4.29}$$

$$\mathbf{P} = \frac{1}{2i}(\nabla_1 - \nabla_2)\,, \tag{4.30}$$

$$\sigma = \sigma_1 + \sigma_2\,, \quad P_\sigma = \frac{1}{2}(1 + \sigma_1 \cdot \sigma_2)\,.$$

$\mathbf{P}'$ is the complex conjugate of $\mathbf{P}$ (acting on the left), σ are the spin matrices and P_σ are spin-exchange operators. The parameters are t_i, x_i ($i \in \{0,1,2,3\}$), α (power of the density-dependent term), and W_0 (spin-orbit parameter).

This interaction is used to carry out the HF calculations for the ground state.

The residual interaction for the SRPA and SSRPA applications is derived from the same Skyrme interaction. In the first applications [57, 58, 81], calculations were not fully self-consistent because the Coulomb and spin-orbit contributions were not included in the residual interaction. Only starting from the application of Ref. [82], which will be described in Subsec. 4.2.2, these two contributions were fully taken into account.

Owing to the presence of a density-dependent term in the Skyrme interaction, the so-called rearrangement terms must be properly included in the residual interaction. This important aspect was addressed in Ref. [60] and will be discussed in what follows.

Rearrangement terms are a peculiarity of cases where a density-dependent interaction is used and are produced by the second derivative of the functional with respect to the density. They are also present in the diagonal matrix elements of A, containing single-particle energies.

In Ref. [83], a derivation of rearrangement terms was presented in the context of the shell model. Reference [84] was a first attempt to derive rearrangement terms for beyond-RPA matrix elements. However, Ref. [60] is the first derivation of all the terms for SRPA-type calculations, which, in addition, allows one to recover the RPA rearrangement terms in the RPA limit. The variational procedure of Ref. [62] is extended to the case of density-dependent forces. The ground-state $|\psi\rangle$ is written as

$$|\psi\rangle = \mathrm{e}^S\,|\mathrm{HF}\rangle\,,$$

where

$$S = \sum_{m,i} C_{mi} a_m^\dagger a_i + \frac{1}{2} \sum_{m,n,i,j} C_{mnij} a_m^\dagger a_n^\dagger a_j a_i \,.$$

We introduce the coefficients

$$c_{\alpha\beta\gamma\delta} := C_{\alpha\beta\gamma\delta} - C_{\alpha\beta\delta\gamma} \,.$$

The Hamiltonian with a density-dependent interaction is written as

$$\hat{H} = \hat{T} + \hat{V}(\rho) = \sum_{\mu,\mu'} T_{\mu\mu'} a_\mu^\dagger a_{\mu'} + \frac{1}{4} \sum_{\mu,\nu,\mu',\nu'} v_{\mu\nu\mu'\nu'}(\rho) a_\mu^\dagger a_\nu^\dagger a_{\nu'} a_{\mu'} \,,$$

where

$$v_{\alpha\beta\gamma\delta}(\rho) := \langle \alpha\beta | \hat{V}(\rho) | \gamma\delta \rangle - \langle \alpha\beta | \hat{V}(\rho) | \delta\gamma \rangle \,.$$

Assuming that the coefficients C_{mi} and C_{mnij} are small, one may expand the expectation values of one- and two-body operators in powers of S and one may truncate this expansion at second order.

Let us start with the one-body density matrix:

$$\begin{aligned}
\rho_{\alpha\beta}(\psi) &= \langle \psi | a_\beta^\dagger a_\alpha | \psi \rangle = \langle \mathrm{HF} | \, \mathrm{e}^{S^\dagger} a_\beta^\dagger a_\alpha \mathrm{e}^S \, | \mathrm{HF} \rangle \\
&= \langle \mathrm{HF} | \left(1 + S^\dagger + \frac{1}{2} S^{\dagger 2} + \cdots \right) a_\beta^\dagger a_\alpha \left(1 + S + \frac{1}{2} S^2 + \cdots \right) | \mathrm{HF} \rangle \\
&\simeq \rho_{\alpha\beta}^{(0)} + \langle \mathrm{HF} | \left(a_\beta^\dagger a_\alpha S + S^\dagger a_\beta^\dagger a_\alpha \right) | \mathrm{HF} \rangle \\
&\quad + \langle \mathrm{HF} | \left(\frac{1}{2} a_\beta^\dagger a_\alpha S^2 + S^\dagger a_\beta^\dagger a_\alpha S + \frac{1}{2} S^{\dagger 2} a_\beta^\dagger a_\alpha \right) | \mathrm{HF} \rangle \,,
\end{aligned}$$

where $\rho_{\alpha\beta}^{(0)}$ is the HF density, the second term on the third line is the linear contribution $\delta\rho^{(1)}$ and the term on the last line is the quadratic contribution $\delta\rho^{(2)}$ to the variation of the density $\delta\rho = \delta\rho^{(1)} + \delta\rho^{(2)}$. Terms beyond the quadratic contribution are neglected.

The mean value of the Hamiltonian can be written as

$$\begin{aligned}
\left\langle \hat{H} \right\rangle &= \left\langle \mathrm{HF} \left| \hat{H} \right| \mathrm{HF} \right\rangle + \sum_{m,i} \left(C_{mi}^* \lambda_{mi}(\rho) + C_{mi} \lambda_{im}(\rho) \right) \\
&\quad + \sum_{\substack{m,n>m \\ i,j>i}} \left(c_{mnij}^* v_{mnij}(\rho) + c_{mnij} v_{ijmn}(\rho) \right) + F^{(2)} \,,
\end{aligned}$$

where $F^{(2)}$ contains all the quadratic contributions in the C coefficients (see Eq. (8) in Ref. [62]). The quantities λ are defined as

$$\lambda_{\alpha\beta}(\rho) = T_{\alpha\beta} + \sum_k v_{\alpha k \beta k}(\rho) \,.$$

The A and B matrices are derived as second derivatives of $\langle \hat{H} \rangle$ with respect to the coefficients. For instance:

$$
\begin{aligned}
A_{mi,pk} &= \left[\frac{\partial^2 \langle \hat{H} \rangle}{\partial C^*_{mi} \partial C_{pk}} \right]_{C=C^*=0}, \\
A_{mi,pqkl} &= \left[\frac{\partial^2 \langle \hat{H} \rangle}{\partial C^*_{mi} \partial c_{pqkl}} \right]_{C=C^*=0}, \\
A_{mnij,pqkl} &= \left[\frac{\partial^2 \langle \hat{H} \rangle}{\partial c^*_{mnij} \partial c_{pqkl}} \right]_{C=C^*=0}, \\
B_{mi,pk} &= \left[\frac{\partial^2 \langle \hat{H} \rangle}{\partial C^*_{mi} \partial C^*_{pk}} \right]_{C=C^*=0}.
\end{aligned}
$$

Of course, when the interaction is not density-dependent, only the $F^{(2)}$ terms of $\langle \hat{H} \rangle$ contribute. Otherwise, rearrangement terms appear.

Let us now expand the antisymmetrized interaction $\hat{v}$ around $\rho^{(0)}$ up to quadratic terms:

$$
\begin{aligned}
v_{\alpha\beta\gamma\delta} \simeq\ & v_{\alpha\beta\gamma\delta}(\rho^{(0)}) + \sum_{a,b} \left[\frac{\partial v_{\alpha\beta\gamma\delta}}{\partial \rho_{ab}} \right]_{\rho=\rho^{(0)}} \delta\rho_{ab} \\
& + \frac{1}{2} \sum_{a,b,c,d} \left[\frac{\partial^2 v_{\alpha\beta\gamma\delta}}{\partial \rho_{ab} \partial \rho_{cd}} \right]_{\rho=\rho^{(0)}} \delta\rho_{ab} \delta\rho_{cd} .
\end{aligned}
$$

Using this expansion, the rearrangement terms for the beyond-RPA matrix elements may be found (see Ref. [60] for details). For example, for the matrix elements coupling 1p1h and 2p2h configurations, one has

$$
\begin{aligned}
A^{(\mathrm{rearr})}_{mi,pqkl} &= \left[\frac{\partial v_{klpq}}{\partial \rho_{im}} \right]_{\rho=\rho^{(0)}} \rho_{im}, \\
B^{(\mathrm{rearr})}_{mi,pqkl} &= \left[\frac{\partial v_{klpq}}{\partial \rho_{mi}} \right]_{\rho=\rho^{(0)}} \rho_{mi} .
\end{aligned}
$$

4.2.2 Dipole response and polarizability in ^{48}Ca

This study consisted in the first application of the SSRPA model to analyze the dipole strength and polarizability in ^{48}Ca [82].

The electric dipole polarizability is a quantity of importance, because it might provide information on the slope and density dependence of the symmetry energy in the equation of state of nuclear matter [85]. Its determi-

nation has various implications in nuclear physics: for instance in nuclear structure for the description of the neutron-skin thickness of neutron-rich nuclei [86, 87], or in nuclear astrophysics, where the concerned quantities are the radius, proton fraction, and cooling of neutron stars [88–90].

The electric dipole response of atomic nuclei has been extensively studied in different experiments and with different probes. For example recently the low-lying dipole response in ^{48}Ca has been measured in Darmstadt. These measurements in the low-energy region of the ^{48}Ca spectrum, based on the (γ, γ') reaction [91, 92], showed that only certain types of beyond-MF calculations — among which SRPA — could provide results in reasonable agreement with the data, as far as fragmentation is concerned [57, 92, 93]. Also, a recent study [94] suggested that the inclusion of complex configurations was necessary to account for this low-lying strength. The RPA model is unable to reproduce the strength below 10 MeV because either it does not provide any strength at these low energies, or if some strength is predicted, only the Landau damping is present, and therefore no sufficient fragmentation is found. On the contrary, the SRPA model provides some strength at energies lower than 10 MeV and leads naturally to such an additional fragmentation, due to the mixing between 1p1h and 2p2h configurations.

More recently, experimental studies were conducted to reach both the low-energy and giant resonance regions [95, 96] of the dipole spectrum. In particular, the experiment of Ref. [96], which was carried out at the RCNP facility in Osaka, employing the (p, p') reaction at forward angle, concerned ^{48}Ca. Future studies are planned at ELI-NP in Bucharest [97, 98].

In Ref. [82], two different parametrizations of the Skyrme interaction were used: SLy4 [99–101] and SGII. As these two parametrizations were adjusted without the so-called J^2 terms, where J is the spin–orbit density, the J^2 terms were not included in the mean field and in the residual interaction used in our calculations. This holds also for all the other calculations that will be illustrated later in this manuscript. The 1p1h cutoff was set to 100 MeV, the 2p2h cutoff to 60 MeV with SGII and to 70 MeV with SLy4. It was verified that the choice of the cutoff on the 1p1h configurations guarantees that the isoscalar and isovector EWSRs are preserved (deviations are less than 1 %). It was also checked that the 2p2h cutoffs were high enough so to have results that were practically cutoff-independent. In addition, a diagonal approximation was applied in the corrective terms of the subtraction.

	Exp	SRPA SGII	SSRPA SGII	SRPA SLy4	SSRPA SLy4
$\sum B(E1)$	0.068 ± 0.008	0.563	0.078	1.012	0.126
$\sum_i E_i B_i(E1)$	0.570 ± 0.062	4.618	0.621	8.795	1.062
Centroid	8.38	8.20	7.96	8.69	8.43

Table 4.1: Experimental and theoretical $\sum B(E1)$ (in e^2 fm^2) and $\sum_i E_i B_i(E1)$ (in MeV e^2 fm^2) summed between 5 and 10 MeV. The third line reports the corresponding centroid energies in MeV. The experimental values are extracted from Ref. [92].

Let us first present the results obtained in the low-energy region (between 5 and 10 MeV). A previous work [58] tackled the dipole response of ^{48}Ca in particular, calculated in SRPA, with a focus on the low-lying strength. The present work differs in that it makes use of the subtraction procedure, and in that all the terms of the residual interaction are included (spin-orbit and Coulomb terms were neglected in Ref. [58]).

In the study of Ref. [58], where no subtraction procedure was used, the dipole strength integrated up to 10 MeV was largely overestimated. On the contrary, the present calculations use a subtraction procedure, which, as we discussed in Subsec. 4.1.2, avoids the occurrence of instabilities and UV divergences. As the abnormal downward shift of the strength is also corrected by the subtraction, the integrated low-lying $B(E1)$ transition probability becomes much more compatible with experiments. This improvement can be seen in Table 4.1: the m_0 (integrated strength) and m_1 moments calculated with subtraction are much closer to the experimental values than in standard SRPA. For example, with the SGII parametrization, which gives the best results in this case, we obtain less than 15 % discrepancy in SSRPA against a factor of more than 8 in standard SRPA. Although the SLy4 parametrization leads to less satisfactory results in this energy region in particular, the subtraction brings nevertheless a significant improvement over RPA and SRPA. With the two parametrizations used here, no strength is found below 10 MeV with RPA.

Regarding the position of the peaks below 10 MeV, Fig. 4.3 displays the experimental data (upper panel) and the SRPA results with and without subtraction (lower panel) computed with the parametrization SGII. One observes that SSRPA results are in overall better agreement with the experimental peak positions than standard SRPA. Although the corresponding re-

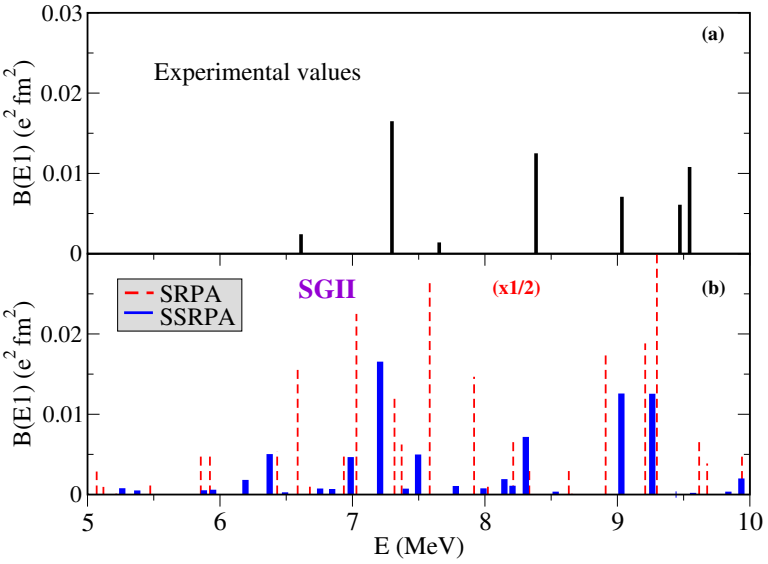

Figure 4.3: (a) Experimental $B(E1)$ values [91]; (b) Theoretical distributions of the transition probabilities $B(E1)$ calculated with the standard SRPA (dashed red bars; the values have been divided by 2) and with the SSRPA (blue thick bars), employing the Skyrme parametrization SGII.

sults with the SLy4 parametrization are less satisfactory (see Fig. 4.4), the subtraction allows for a reduction of the strength also in this case, which is an improvement compared with standard SRPA results.

Note that we also performed calculations for ^{40}Ca: for this nucleus, no strength below 10 MeV is found, in agreement with the experiments of Refs. [91, 92].

We next focus on the GDR region. The experimental values of the centroid energy E_C and width Γ, reported in Ref. [96], are respectively 18.9 ± 0.2 MeV and 3.9 ± 0.4 MeV. In our calculations, these quantities are computed according to the formulas

$$E_C = \frac{m_1}{m_0} \tag{4.31}$$

$$\Gamma = \sqrt{m_2/m_0 - (m_1/m_0)^2}, \tag{4.32}$$

where

$$m_k := \sum_i E_i^k B_i(E1) \tag{4.33}$$

is the energy-weighted moment of order k.

Figure 4.5 shows the strength distributions calculated with the parametrization SGII in RPA, SRPA, and SSRPA, compared with the experimental distri-

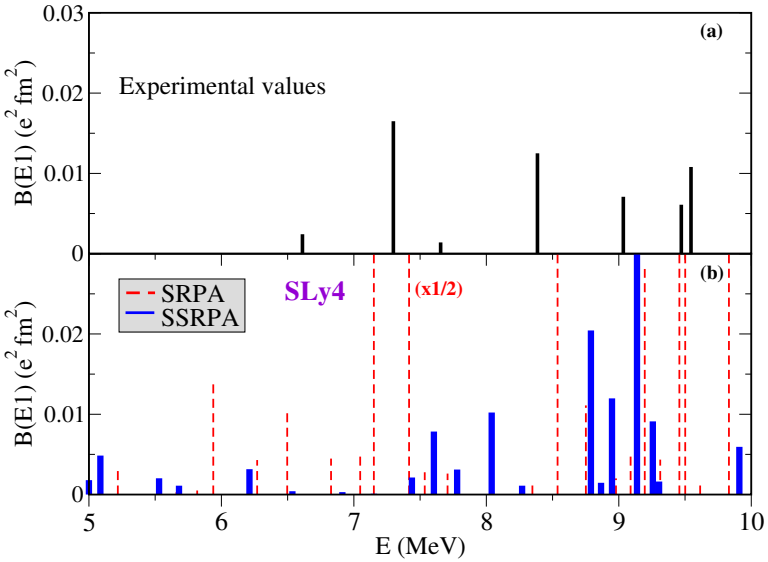

Figure 4.4: Same as Fig. 4.3, but the theoretical results are obtained this time with the Skyrme parametrization SLy4.

butions of Ref. [96]. One obtains a good reproduction of the experimental width in SSRPA, a notable correction of the downward shift present in SRPA, but still with an underestimation of the centroid of about 1.5 MeV. A similar width is obtained in SRPA and SSRPA ($\Gamma = 2.5$ MeV), which confirms that the subtraction does not remove the beyond-MF contribution to the width. The missing width with respect to the above-mentioned experimental value could reside in the escape width (not taken into account in this study) or in higher-order configurations (3p3h, *etc.*).

With the SLy4 parametrization (Fig. 4.6), despite an overall worse reproduction of experimental data, one observes similar improvements of SSRPA with respect to SRPA and RPA. For all the theoretical results shown in Figs. 4.5 and 4.6, a folding with a Lorentzian having a width of 0.25 MeV is done. This of course produces an artificial spreading for the RPA case.

To better appreciate the width reproduction given by the SSRPA results, the distributions of Figs. 4.5 and 4.6 are displayed with an artificial shift on Fig. 4.7. The differences between the results obtained with the two parametrizations may be connected to the properties of the interaction. In fact, Ref. [102] suggested a relation between the GDR excitation energy and the symmetry energy, which is confirmed here: the parametrization SLy4, which corresponds to a higher symmetry energy (32 MeV), predicts a lower centroid energy than that predicted by SGII for which the symmetry energy is around 27 MeV.

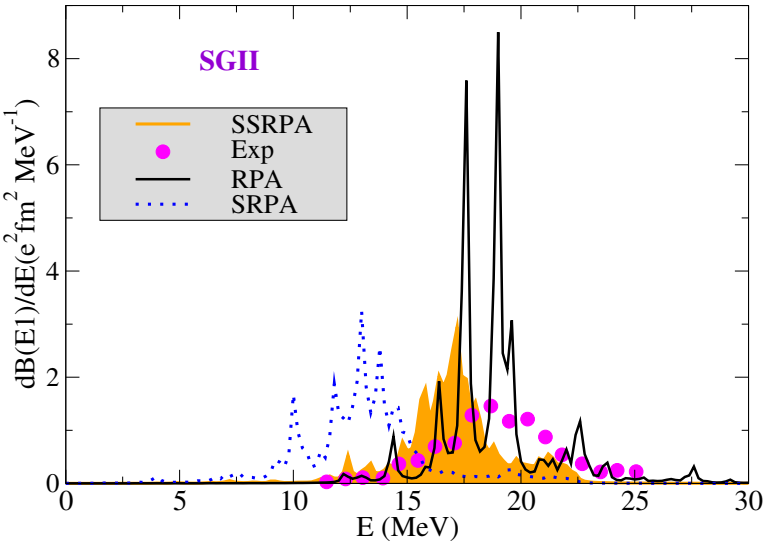

Figure 4.5: Dipole strength distributions evaluated with RPA (solid black line), SRPA (blue dotted line), and SSRPA (orange line and area), compared with the experimental distributions (magenta circles) of Ref. [96]. The SGII Skyrme interaction is used.

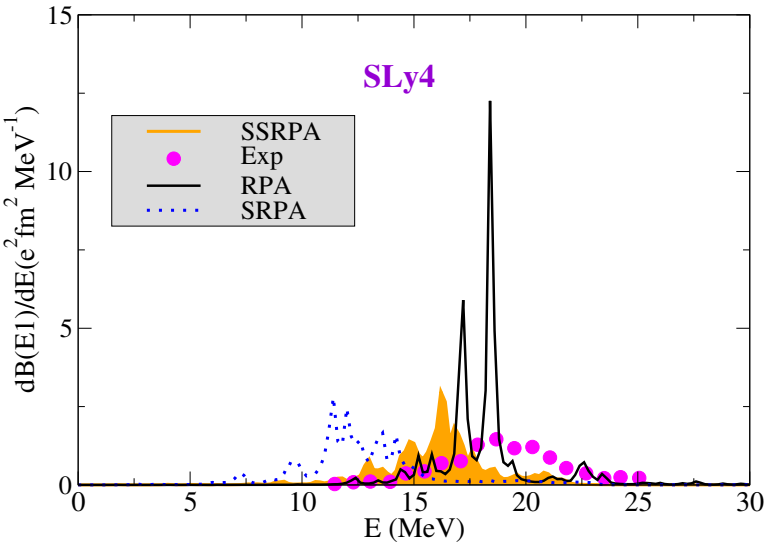

Figure 4.6: Same as Fig. 4.5 but with the Skyrme interaction SLy4.

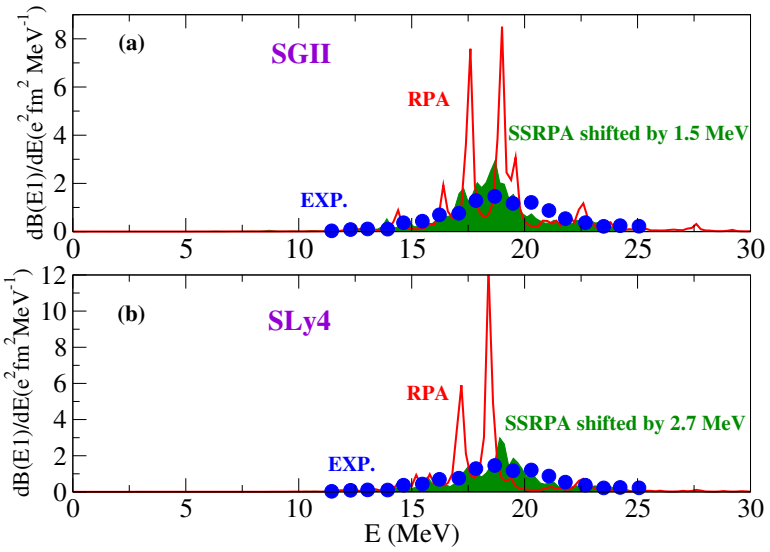

Figure 4.7: (a) SSRPA results shifted by 1.5 MeV (green area) compared with the RPA strength (red line) and with the experimental values (blue circles), obtained with the parametrization SGII. (b) Same as (a) but the results are obtained with the parametrization SLy4 and the shift of the SSRPA spectrum is larger (2.7 MeV).

We note that results for ^{40}Ca in the GDR region were compared with the results obtained for ^{48}Ca and with experimental data. For ^{40}Ca, our calculations yield a less spread and fragmented distribution than for ^{48}Ca, in contrast to the very resembling distributions reported in Ref. [96], but in agreement with Ref. [103], which employed the relativistic quasiparticle time-blocking approximation.

Lastly, we computed the electric dipole polarizability

$$\alpha_{\mathrm{D}} = \frac{8\pi}{9} \int \frac{B_i(E1)}{E_i} \mathrm{d}E_i \tag{4.34}$$

Experimentally [96], the contribution to the electric dipole polarizability below 10 MeV is negligible, and is of 1.73 ± 0.18 fm^3 between 10 MeV and 25 MeV. As our results are more satisfactory with the SGII parametrization than with the SLy4 one, we will focus our discussion on the SGII results for the polarizability.

Below 10 MeV, we indeed obtain negligible values of α_{D} in RPA and SSRPA, respectively $6{\cdot}10^{-4}$ fm^3 and $3{\cdot}10^{-3}$ fm^3. We may next represent the polarizability calculated by varying the upper limit of the integral in Eq. (4.34). Figure 4.8 shows such a trend. The measurement of Ref. [96] was done up to 25 MeV. However, 25 Mev as upper limit of the integral in Eq. (4.34) is

not enough to obtain a saturated value for α_D. The experimental values of Ref. [96] were for this reason extrapolated to plot the polarizability up to 60 MeV (using for this extrapolation results available for ^{40}Ca).

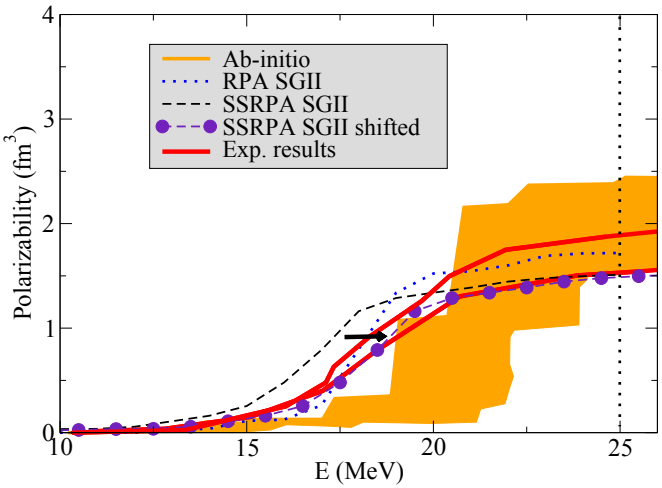

Figure 4.8: Electric dipole polarizability as a function of the excitation energy. The orange area corresponds to *ab initio* results [104, 105] and the area between the two solid red lines to experimental results reported in Ref. [96]. In particular, the measurement illustrated in Ref. [96] provides the values in the band up to the vertical dashed line located at 25 MeV. Results obtained with the RPA (blue dotted line) and the SSRPA (black dashed line) models are displayed. The violet circles and dashed line represent these latter results shifted upwards by 1.5 MeV. The Skyrme interaction SGII is used.

We compute the SSRPA trend of α_D up to 25 MeV (vertical dotted line in Fig. 4.8), owing to the huge computational effort required for these calculations.

Ab initio results are also shown in the figure and represented by an orange area. They are obtained with coupled-cluster calculations [104, 105]. The orange band corresponds to the use of different chiral Hamiltonians [106].

As a first observation, it is clear on Fig. 4.8 that both the RPA and the *ab initio* polarizabilities have a too steep slope, compared with the experiments. This means that these RPA and *ab initio* results fail to reproduce the experimental spreading of the transition probability. Contrary to RPA, which gives a centroid energy in between the two experimental curves, the *ab initio* results additionally overestimate the position of the centroid. In contrast, our SSRPA model with the SGII parametrization produces a slope which is compatible with the experimental data (as the shifted SSRPA curve shows), despite an underestimation of the centroid energy. This result indicates that our SSRPA is able to correctly account for the spreading of the electric dipole excitation in ^{48}Ca.

Notice that the RPA and the SSRPA curves do not converge to the same value on Fig. 4.8. Yet as discussed in Subsec. 4.1.2, the subtraction procedure requires that the RPA and SSRPA inverse moments m_{-1} be equal, and therefore that the converged values of α_{D} be equal. Of course, this discrepancy may be explained first by the fact that one should integrate up to an energy much higher than 25 MeV to obtain converged values for α_{D}. Also, this discrepancy may be explained by our use of the diagonal approximation in the corrective terms.

To conclude, our SSRPA model allows for improvements in the description of both the low-lying and GDR transition probabilities in ^{48}Ca, with respect to standard RPA and SRPA. A particular advantage of the SSRPA is the ability to account for the spreading of the electric dipole excitation in the giant resonance region, as seen by the satisfactory reproduction of the slope of the polarizability.

4.2.3 Quadrupole response: systematics on selected nuclei

In this section, we apply the SSRPA model to perform a systematic study of the centroids and the widths of the IS GQR for several nuclei, from medium-mass to heavy systems. The corresponding published article is Ref. [107].

From the experimental point of view, the IS GQR was extensively analyzed since its discovery more than forty years ago [108–110]. The first measurements were summarized in the 1980s in a review on giant resonances [111] and in a systematic study dedicated to the GMR and to the GQR for several medium-mass and heavy nuclei, up to ^{208}Pb [112]. The IS GQR and GMR could be identified and distinguished from each other using inelastic α scattering at small angles. Measurements for ^{48}Ca [113], ^{90}Zr [114], and Sn and Sm nuclei [115, 116] are also available, based on inelastic scattering of α particles. Data taken on unstable nuclei were recently published: a measurement was first done on ^{56}Ni, based on the reaction ^{56}Ni(d,d') [117] and, more recently, a measurement was performed on ^{68}Ni using inelastic α and deuteron scattering [118].

High-resolution experiments based on proton inelastic scattering have been performed at iThemba LABS to investigate the fine structure of GQR excitations for ^{40}Ca [119], ^{58}Ni, ^{90}Zr, ^{120}Sn and ^{208}Pb [120].

In this work, we extract the experimental data for the centroid energies

from Ref. [112] for almost all nuclei, with the exception of ^{48}Ca [113], ^{112}Sn, ^{114}Sn, ^{148}Sm, ^{150}Sm and ^{152}Sm [115]. Data on the IS GQR are also available for Sn isotopes in Ref. [116]. The widths reported in Ref. [116] are in some cases very different compared to those obtained with other measurements [112, 115]. Due to this ambiguity, we showed in Ref. [107] a systematic comparison with the experimental results only for the centroid energies. Fragmentation and fine structure are compared with the experimental results only for some selected cases in which high-precision (p, p') data are available.

Of course, SRPA-based models are not the only beyond-MF approaches allowing for a proper description of the fragmentation and the width of excited state. Several microscopic approaches have been introduced in recent decades to describe the widths and the damping properties of collective excitations. Some illustrations are the quasiparticle-phonon model [121–123], particle-phonon (or quasiparticle-phonon) coupling models [49, 124–127], particle-phonon coupling models based on the so-called time-blocking approximation [79, 128], and, more recently, the relativistic quasiparticle time-blocking approximation [103, 129].

We perform RPA and SSRPA calculations with the SLy4 parametrization of the Skyrme interaction. The single-particle space is chosen large enough to assure that the EWSR are preserved within 1 %. For the 2p2h space in the SSRPA calculations, we use a cutoff of 60 MeV for medium-mass nuclei (^{30}Si, ^{34}Si, ^{36}S, ^{40}Ca, ^{48}Ca, ^{56}Ni and ^{68}Ni) and of 50 MeV for the heavy ones (^{90}Zr, ^{114}Sn, ^{116}Sn, ^{120}Sn, ^{132}Sn and ^{208}Pb). We checked that these cutoff values provide stable results.

Unlike in the study presented in Subsec. 4.2.2, the centroid energies E_C and widths Γ were not estimated using the formulas (4.31) and (4.32) based on moments of the strength. Indeed, this method is not adequate in all cases: on the one hand, spectra obtained with SRPA-based calculations may be strongly fragmented, making the estimation based on moments artificially underestimate the widths; on the other hand, RPA calculations for some nuclei produce a single significant peak, leading to an overestimated width if Eq. (4.32) is used.

We choose instead to compute E_C and Γ by fitting a Lorentzian function to the distribution obtained after folding. Such a method is similar to that used in Ref. [130]. The folding of the discrete spectra is performed using Lorentzian functions of width 100 keV, which is adapted to the high density of states observed in SSRPA results. We verified that such folding did not

produce any artificial effect on the spreading, neither in SSRPA nor in RPA.

As the first part of this study, we make a systematic analysis of the centroid and width of thirteen spherical-expected nuclei: ^{30}Si, ^{34}Si, ^{36}S, ^{40}Ca, ^{48}Ca, ^{56}Ni, ^{68}Ni, ^{90}Zr, ^{114}Sn, ^{116}Sn, ^{120}Sn, ^{132}Sn and ^{208}Pb.

The trend of the centroids obtained in SSRPA is displayed versus the mass number on Fig. 4.9, along with the corresponding RPA results and available experimental values. Nuclei for which a comparison between our theoretical results and the corresponding experimental data may be done are identified in the figure by vertical dotted red lines. We observe that the SSRPA centroids are systematically located at lower energies than the RPA values, and therefore usually reproduce the experimental data better than RPA, which tends to overestimate them.

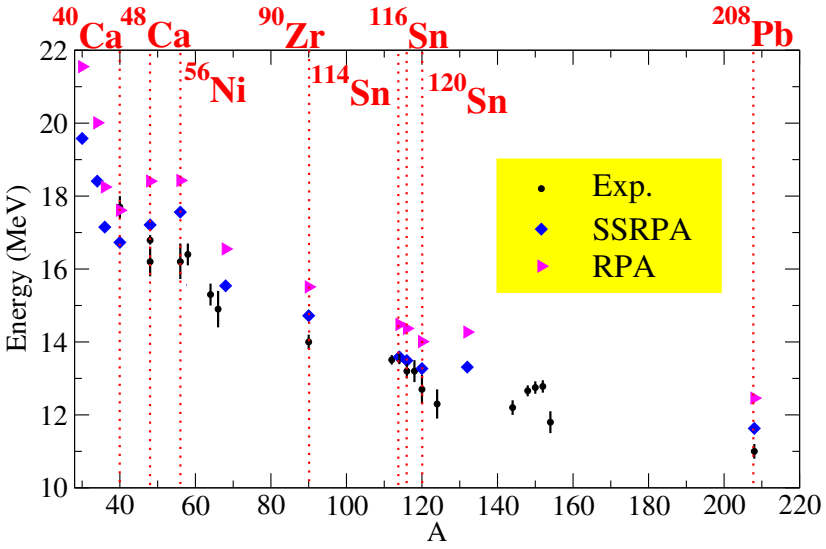

Figure 4.9: Centroids of the IS GQR. The experimental data are displayed as black circles (with their associated error bars) and are extracted from Refs. [112, 113, 115, 117]. SSRPA (RPA) values are plotted as blue diamonds (magenta triangles). At $A = 48$, there are two experimental measurements, for ^{48}Ti and for ^{48}Ca. The experimental point corresponding to ^{48}Ca is the highest one. Theoretical calculations are performed for the nuclei ^{30}Si, ^{34}Si, ^{36}S, ^{40}Ca, ^{48}Ca, ^{56}Ni, ^{68}Ni, ^{90}Zr, ^{114}Sn, ^{116}Sn, ^{120}Sn, ^{132}Sn and ^{208}Pb.

We mention here that the centroid energies of the IS GQR can be related to the effective mass, which we discuss in a separate work with an emphasis on beyond-MF effects on the effective mass (see Subsec. 4.2.4).

As far as the widths are concerned, our SSRPA results are shown on Fig. 4.10 together with RPA results. In this case, we decided not to represent the experimental data, due to the above-mentioned ambiguities concerning

the corresponding widths in the literature.

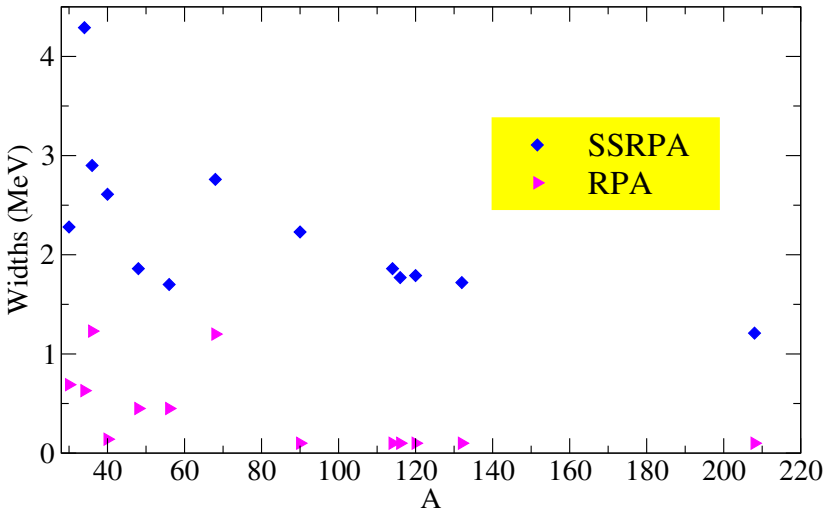

Figure 4.10: Theoretical widths calculated with the fit of a Lorentzian distribution within RPA and SSRPA models.

As expected, we observe that the SSRPA widths are systematically larger than the RPA ones, due to the additional spreading brought by the coupling between 1p1h and 2p2h configurations. The escape width, not present in our applications, might modify some of our results, especially for light nuclei. However, the escape width is expected to be less important than the spreading width.

A further observation can be made on Fig. 4.10: the widths tend globally to decrease going from light to heavy nuclei, suggesting that there is more fragmentation in the former than in the latter. Since this effect is observed already at the RPA level, we deduce that the higher fragmentation for lighter nuclei is produced by a stronger Landau damping. This single-particle effect was already discussed in Refs. [119, 131, 132]. We notice that, for ^{40}Ca, we do not find any important effect related to the Landau damping, the RPA width being particularly small. For this nucleus, the beyond-MF effects coming from the mixing with 2p2h configurations are particularly important and produce a strong increase of the width going from RPA to SSRPA.

In a second step of our study, we select nuclei for which high-precision (p,p') data (40 keV resolution) are available: ^{40}Ca, ^{90}Zr, ^{120}Sn, and ^{208}Pb. We compare our theoretical results with both RPA and experimental spectra, and analyze in detail their fine structure and fragmentation.

We present in Fig. 4.11 the SSRPA strength distribution (violet bars) for

the nucleus ^{40}Ca. To better compare it with the corresponding experimental spectrum (b), a folded curve is also plotted (black solid line and grey area), obtained by folding the discrete distribution with a Lorentzian of width equal to 40 keV, which corresponds to the experimental energy resolution.

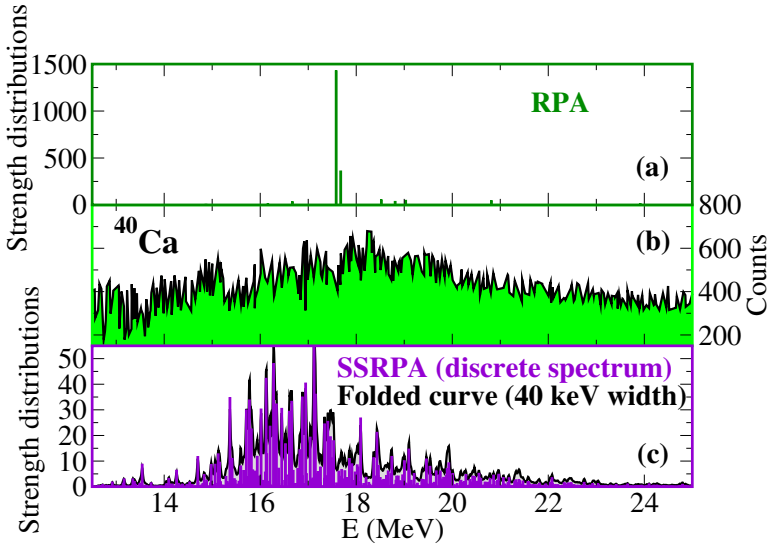

Figure 4.11: (a) RPA strength distributions calculated for the nucleus ^{40}Ca; (b) Experimental spectrum [119] for the IS GQR for ^{40}Ca; (c) SSRPA strength distributions calculated for the nucleus ^{40}Ca. For the cases of the RPA and SSRPA discrete spectra, units are e^2 fm^4. For the SSRPA folded case, units are e^2 fm^4 MeV^{-1}.

This is the only case shown in Fig. 4.9 where the SSRPA underestimates the experimental centroid energy, whereas the RPA value is closer to it. However, the significant advantage of using the SSRPA model instead of RPA is clearly indicated by Fig. 4.11. Our RPA distribution displays a unique dominant peak, whereas the SSRPA strength distribution is much more fragmented and extends over a larger energy region where the experimental data are spread.

Figure 4.12 shows the same quantities as in Fig. 4.11 but for the nucleus ^{90}Zr. In this case, the RPA centroid is larger by more than 1 MeV compared to the experimental value (Fig. 4.9). The SSRPA value is located at lower energies, in better agreement with data. Again, a relevant improvement with respect to RPA is observed in the strength fragmentation (unique dominant peak in RPA). The same comments may be extended to Figs. 4.13 and 4.14, where results for ^{120}Sn and ^{208}Pb are presented.

We observe that the comparison with the experimental fine structure shows a qualitative global agreement in the sense that our model provides a fragmented response in the same energy region. We note however that, for

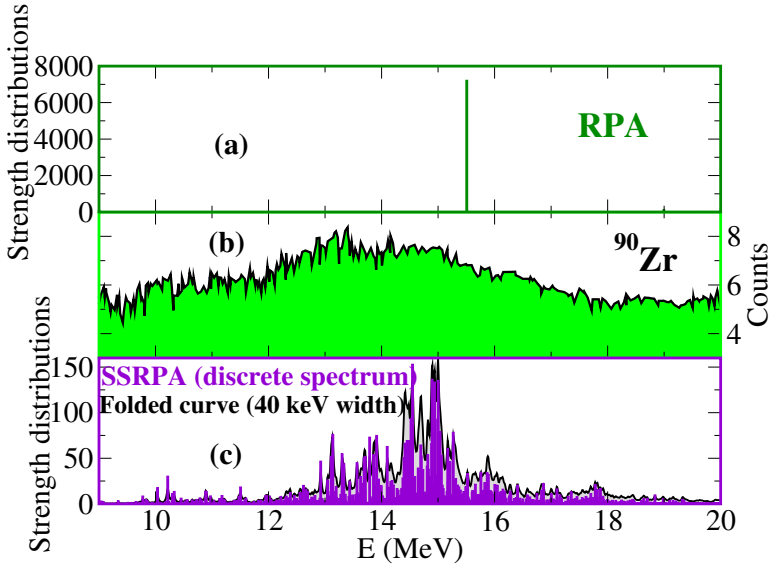

Figure 4.12: Same as in Fig. 4.11 but for the nucleus ^{90}Zr. The experimental data are this time extracted from Ref. [120]. For the cases of the RPA and SSRPA discrete spectra, units are e^2 fm^4. For the SSRPA folded case, units are e^2 fm^4 MeV^{-1}.

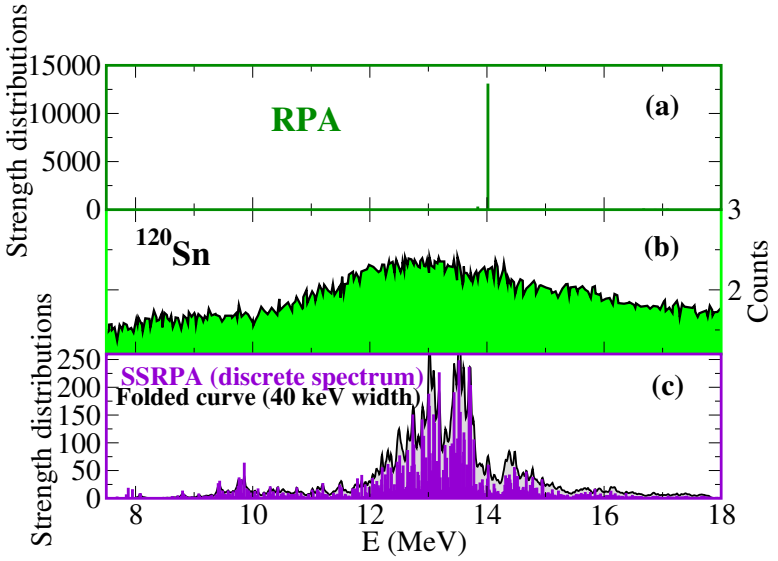

Figure 4.13: Same as in Fig. 4.12 but for the nucleus ^{120}Sn. For the cases of the RPA and SSRPA discrete spectra, units are e^2 fm^4. For the SSRPA folded case, units are e^2 fm^4 MeV^{-1}.

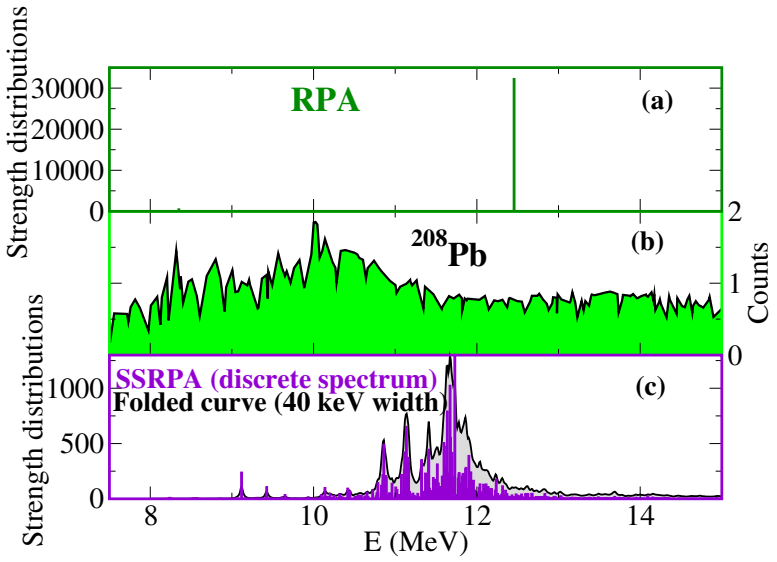

Figure 4.14: Same as in Fig. 4.13 but for the nucleus ^{208}Pb. For the cases of the RPA and SSRPA discrete spectra, units are e^2 fm^4. For the SSRPA folded case, units are e^2 fm^4 MeV^{-1}.

all these nuclei, the energy window where the experimental strength is distributed is broader than the range where the SSRPA response is located. This is probably related to missing effects in our theoretical model, such as the inclusion of higher-order configurations and of fragmentation effects induced by the coupling with the continuum, not taken into account here.

We also notice that our ^{40}Ca results are different from those of Ref. [119]. In that study, the used potential was derived from the realistic interaction Argonne V18 with the UCOM, and the SRPA calculations were performed without subtraction. Compared with our results, the RPA spectrum is more fragmented, its centroid strongly overestimates the experimental value, and the SRPA spectrum is much less dense than ours. These differences may probably be ascribed to the use of a potential derived from a realistic interaction (Argonne V18) which generates, at the HF level, a single-particle spectrum with very large interlevel spacings. This is the reason why the RPA centroid is located so high in energy. And this is probably also the reason why the coupling with 2p2h configurations in the SRPA model is not able in that case to produce a dense strength distribution, in spite of the huge number of elementary 2p2h configurations.

In a last part, we verify the ability of the subtraction procedure to eliminate the ultraviolet divergences, which may appear in SRPA-based calculations based on zero-range forces. Such a property of the SSRPA was already

noticed in Ref. [81]. We illustrate it in the case of ^{40}Ca, by displaying the strength distribution for four values of the 2p2h cutoff (Fig. 4.15). Visually, one may observe the cutoff independence, which is confirmed by the stability of the numerical value of the centroid. For example, the value 16.74 MeV of the centroid at a cutoff of 60 Mev is modified by less than 1 % when increasing the cutoff to 70 MeV.

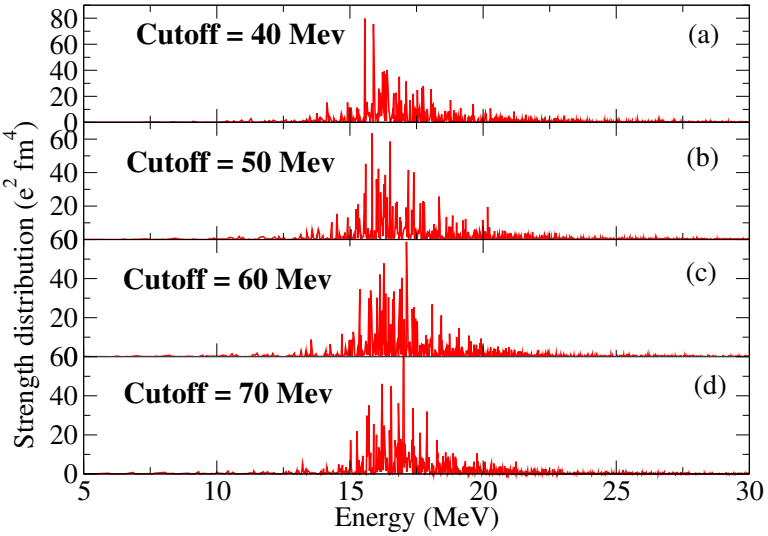

Figure 4.15: Strength distributions obtained for the nucleus 40 Ca with four different cutoff values for the 2p2h configurations: 40 (a), 50 (b), 60 (c), and 70 (d) MeV.

In summary, this systematic analysis of centroids and widths demonstrated the improvement brought by the SSRPA model over the RPA: a better reproduction of the experimental centroids is achieved for nearly all the studied nuclei, the spreading width and fragmentation of the spectra are increased, and their fine structure is in better agreement with the available high-resolution experiments.

Additionally, the ability of the subtraction procedure to remove the divergent contribution leading to cutoff-independent results was further confirmed.

4.2.4 Beyond-mean-field effects on the effective masses

This study tackles the relation between the frequency of axial breathing modes and effective masses in nuclear physics, using the SSRPA model with Skyrme forces. We present here a method which allows for a microscopic description of beyond-mean-field (BMF) effects. This work was published in

Ref. [133].

The Landau's theory of interacting Fermi systems [134, 135] provides an elegant description of low-energy excitations in Fermi liquids. The complex dynamics of the interacting particles is simplified through the concept of quasiparticles having an effective mass m^* induced by the interparticle interaction. The study of m^* meets a broad interest in several branches of many-body physics. Since m^* is related to the propagation of particles in a medium and, more specifically, to the density of states in many-body systems [37], it has an important impact on several observables such as the energies of axial compression modes in atomic gases [136] and in nuclei [137, 138], the specific heat of a low-temperature Fermi gas [37], or the maximum mass of a neutron star [139].

The effective mass is usually evaluated through the computation of the self-energy (see for instance Refs. [37, 140]), and may be provided by Quantum Monte Carlo calculations. References [141, 142] show for example Quantum Monte Carlo calculations for the polaron in atomic gases which are strongly imbalanced. Similar calculations done this time for nuclear systems can be found in Refs. [33, 143].

The centroid energies of isoscalar giant quadrupole resonances (axial breathing modes) of nuclei may be related to the effective mass in nuclear matter [137, 138]. In particular, a relation exists between the frequency of axial breathing modes and $\sqrt{m/m^*}$. This relation can be derived within the Landau theory of Fermi liquids using the local-density approximation. The measured centroids were then used to phenomenologically constrain the effective mass (see Ref. [4] and references therein).

For a particle of energy E and momentum k, the effective mass m^* is defined by the relation

$$\frac{1}{m^*} := \frac{\mathrm{d}E}{\mathrm{d}k}\frac{1}{\hbar^2 k} \tag{4.35}$$

where

$$E = \frac{\hbar^2 k^2}{2m} + \Sigma_k + \Sigma_{k,E}\,. \tag{4.36}$$

In Eq. (4.36), $\Sigma_k + \Sigma_{k,E}$ is the self-energy, sum of the MF contribution Σ_k (from the leading order of the Dyson equation in the perturbative many-body expansion) and of a BMF energy-dependent contribution $\Sigma_{k,E}$. The self-energy does not have any energy dependence in the MF approximation. An explicit energy dependence is acquired only when the MF approximation is overcome.

Using the definition of m^* in Eq. (4.35), one can write

$$\begin{aligned}\frac{m^*}{m} &= \left(1-\frac{\partial\Sigma_{k,E}}{\partial E}\right)\cdot\left(1+\frac{m}{\hbar^2 k}\frac{\partial\Sigma_k}{\partial k}\right)^{-1} \\ &= \frac{m^*_E}{m}\cdot\frac{m^*_k}{m},\end{aligned} \tag{4.37}$$

where the above expression defines the so-called E-mass m^*_E/m and k-mass m^*_k/m, using the same notations as in Refs. [137, 144–147]. In the MF approximation, where the self-energy may only have a k dependence, the E-mass is equal to 1. In the case of a zero-range interaction without gradient terms, for example, also the k-mass would be equal to 1 in the MF approximation, and one should go to second order to have a k-mass different from 1. The t_1 and t_2 terms of the Skyrme interaction provide a k-mass different from 1 in the MF approximation. The effective mass is modified by BMF effects, which is visible by an E-mass not equal to 1 anymore.

We exploit here the above-mentioned relation between the energies of axial breathing modes and the effective mass to propose a new method to estimate BMF effects on the effective mass of nuclear matter: we calculate the BMF centroids of axial breathing modes in SSRPA; then, assuming the relation between these excitation modes and the effective mass, we use a linear fit performed on MF centroids to extract the BMF effective masses, and deduce the E-masses. Determining the E-masses in this way allows us to quantify the BMF effects induced by our SSRPA model.

More specifically, we first calculated the IS GQR centroids of the medium-mass nucleus ^{48}Ca and the heavier nucleus ^{90}Zr in RPA, using four Skyrme parametrizations SkP [148], SGII, SLy4, and Ska [149]. These parametrizations have MF effective masses respectively equal to 1, 0.79, 0.7 and 0.61 in nuclear matter. The RPA centroids of ^{48}Ca and ^{90}Zr are displayed on Fig. 4.16 as a function of $\sqrt{m/m^*}$, where we use the values of the MF effective mass in nuclear matter for each interaction. The experimental values of the centroids are represented as orange bands. For each nucleus, we performed a linear fit on the four centroids (blue dotted lines). To estimate the BMF effects on the effective masses, we then calculated these centroids with our SSRPA model, choosing the SLy4 and the SGII parametrizations as illustrations, and reported them on the linear fits. We observe that the centroids are located at lower energies for the SSRPA model with respect to the corresponding RPA values. Such a lowering of the energies implies that the associated effective mass increases with respect to the MF value. For ^{48}Ca

(^{90}Zr), the extracted effective mass for nuclear matter increases from 0.7 in the MF case to 0.834 (0.769) for the BMF calculations of the IS GQR with SLy4. With SGII, the effective mass for matter increases from 0.79 to 0.837 (0.842) from the calculations done for ^{48}Ca (^{90}Zr).

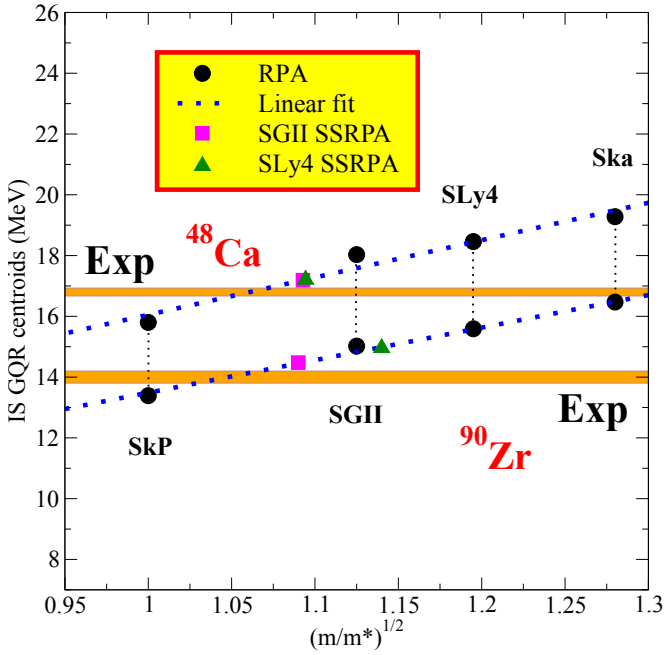

Figure 4.16: IS GQR centroid energies for ^{48}Ca and ^{90}Zr as a function of $\sqrt{m/m^*}$. The RPA centroids (black circles) are reported for four Skyrme parametrizations and associated to the corresponding MF effective masses in nuclear matter. A linear fit is done on these points (blue dotted lines). The SSRPA-SLy4 and SSRPA-SGII centroids are reported on the blue dotted lines (green triangles and magenta squares, respectively). The experimental values are also displayed by orange bands.

Using Eq. (4.37), we can then extract the average values of the E-mass, equal to 1.19 (1.06) with SLy4 (SGII) for ^{48}Ca and to 1.10 (1.07) with SLy4 (SGII) for ^{90}Zr. BMF effects produce an increase of the E-mass ranging from 6 to 16 %, the largest variation from 1 occurring for ^{48}Ca and the SLy4 parametrization.

We observe in Fig. 4.16 that, for ^{48}Ca, the SSRPA centroid energies obtained with the two parametrizations SLy4 and SGII are very similar, leading to very similar values of m^*/m. Since the MF effective mass is not the same for the two parametrizations, this implies a stronger BMF modification of the E-mass for the case of SLy4 (where the MF effective mass is lower). On the other side, the SSRPA centroids obtained with SLy4 and SGII are slightly different for ^{90}Zr, leading to a higher value of m^*/m for the case of SGII. The two BMF E-masses are very similar to one another for this nucleus.

Remaining at the MF level, one may associate a theoretical error to the effective mass of matter, related to the use of different parametrizations of the interaction. One may wonder how this error behaves when going beyond the MF. We show on Fig. 4.17(a) (MF) and Fig. 4.17(b) (BMF) estimations of the theoretical errors on the ratio m^*/m: the yellow area corresponds to the discrepancy between SGII and SLy4, and the grey area corresponds to the additional discrepancy when the Ska interaction is used ($m^*/m = 0.61$). This parametrization is also employed to provide an estimation of the typical MF error bar on effective masses, knowing that, for most Skyrme parametrizations, MF effective masses have values located between 0.6 and 0.8.

For example, in the MF case, there is a discrepancy of 11 % on the m^*/m ratio if one considers SLy4 and SGII. If the three parametrizations are considered, the MF error bar is 23 %. In the BMF case (lower panel), the m^*/m ratio is extracted using the method explained above, for several nuclei covering three different regions of the nuclear chart: ^{48}Ca, ^{90}Zr and ^{120}Sn. We observe that, (not) including the Ska BMF values in Fig. 4.17(b) (green symbols), the discrepancy window is of (9 %) 22 %. We may thus infer that our extraction method of a BMF effective mass for nuclear matter does not produce an overall error larger than the one already induced with MF calculations and related to the dependence on the used parametrization — even if, in the BMF case, there is an additional dependence on the nucleus.

Note that this method for extracting BMF effective masses is general and can be employed with other BMF models than SSRPA.

The effective mass can be related to the density of states [150]: BMF changes of the m^* value induce a different single-particle spectrum, which is compressed if the m^* is increased. This BMF modification of single-particle spectra is well known for instance in models based on the particle-vibration coupling (see for example Refs. [147, 151]). It is worth mentioning that a compression of single-particle spectra was also predicted in Ref. [152] within a self-consistent RPA applied to metal clusters. Generalized single-particle energies were computed from the A matrix elements. In this extension of RPA, a matrix (which would reduce to HF single-particle energies in the standard RPA limit) is diagonalized using the correlated one-body density matrix that is provided self-consistently from the model. Such generalized single-particle energies are compared with the HF spectrum and a compression of the spectrum can be observed (see Fig.4 of Ref. [152]).

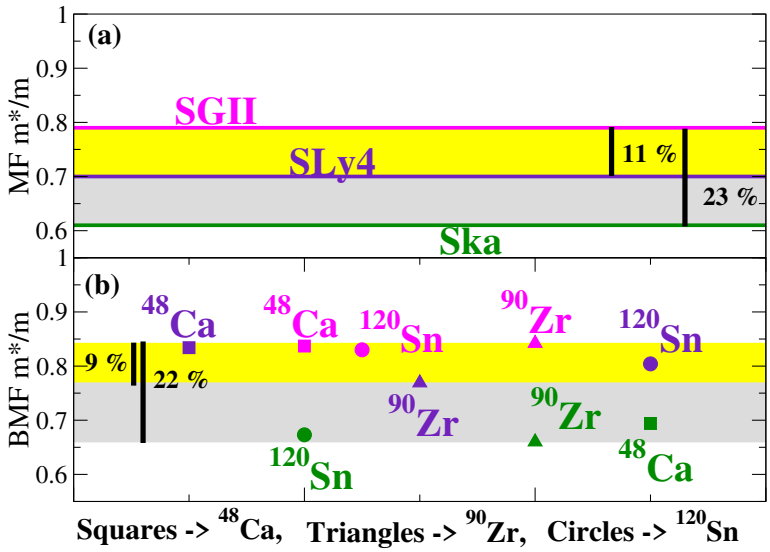

Figure 4.17: (a) Theoretical error associated to the MF effective mass for nuclear matter induced by two Skyrme parametrizations, SLy4 (indigo) and SGII (magenta) (yellow band) and three Skyrme parametrizations, SLy4, SGII, and Ska (green) (yellow plus grey band); (b) Same as in panel (a) but for the BMF effective mass. The three colors represent the three interactions as in panel (a). Squares, triangles, and circles represent the BMF effective masses extracted from ^{48}Ca, ^{90}Zr, and ^{120}Sn, respectively.

The lowering of the excitation energies provided by SRPA-based models (with respect to the RPA spectrum) is a general feature of the model that does not occur only in nuclear systems. The same type of effect was found for instance also for metal clusters in Refs. [75, 153]. In all cases, one thus expects an increase of the effective mass (E-mass larger than 1) and, consequently, an effective compression of the single-particle spectrum.

In the following, we analyze this aspect in more detail for the nuclei ^{48}Ca and ^{90}Zr. We recall that the SRPA problem can be written as a energy-dependent RPA-like problem, where self-energy corrections provide a renormalization of the diagonal matrix elements A_{11} in particular (see Eqs. (4.23) and (4.25)). Since such matrix elements contain the single-particle excitation energies, this renormalization certainly induces a BMF renormalization of the 1p1h single-particle spectrum. By performing the subtraction procedure, the rescaling of the matrix element A_{11} is further modified by the subtraction of the zero-energy self-energy.

As an illustration, we discuss the case of the parametrization SLy4. Figure 4.18 shows the diagonal matrix elements A_{11} calculated for the nucleus ^{48}Ca for the first three 1p1h configurations entering in the construction of the collective quadrupole excitations. In this case, the three configurations are

neutron configurations. We present RPA and SSRPA results. In the case of SSRPA, to compute the rescaling effect induced by BMF calculations, the energy-dependent self-energy correction is calculated at an energy value given by the SSRPA centroid of the IS GQR. This guarantees that we make this estimation in the region of the GQR.

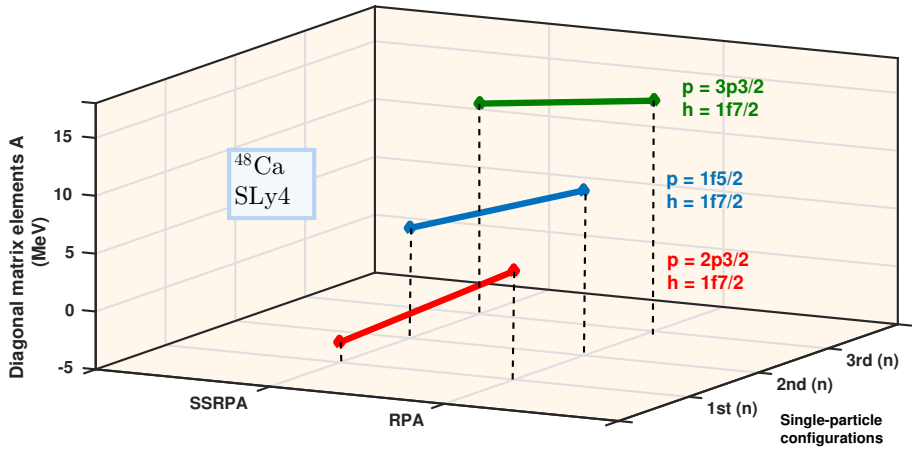

Figure 4.18: RPA and SSRPA diagonal matrix elements A_{11} calculated with the parametrization SLy4 for the nucleus ^{48}Ca for the first three single-particle configurations (which are neutron configurations). The BMF results are calculated using in the energy-dependent matrix elements an energy value equal to the IS GQR centroid obtained in SSRPA.

We notice that the BMF rescaling of the matrix element is more pronounced for the first configuration and becomes less important at increasing energies. We have observed that this effect is indeed strongly quenched for the highest-energy 1p1h configurations.

Also, the BMF modification produces in all cases a global reduction of the matrix element (and, consequently, a reduction of the single-particle excitation energy). Such a reduction implies an effective compression of the single-particle spectrum, consistent with the enhancement of the effective mass indicated by our previous analysis done on the values of the centroid energies.

Figure 4.19 shows the same quantities as Fig. 4.18, but for the nucleus ^{90}Zr. In this case, the third single-particle configuration is a proton configuration.

For the two nuclei, ^{48}Ca and ^{90}Zr, the third single-particle configuration entering in the construction of the quadrupole collective phonon is located in the same energy region as the IS GQR. One can thus in this case provide an

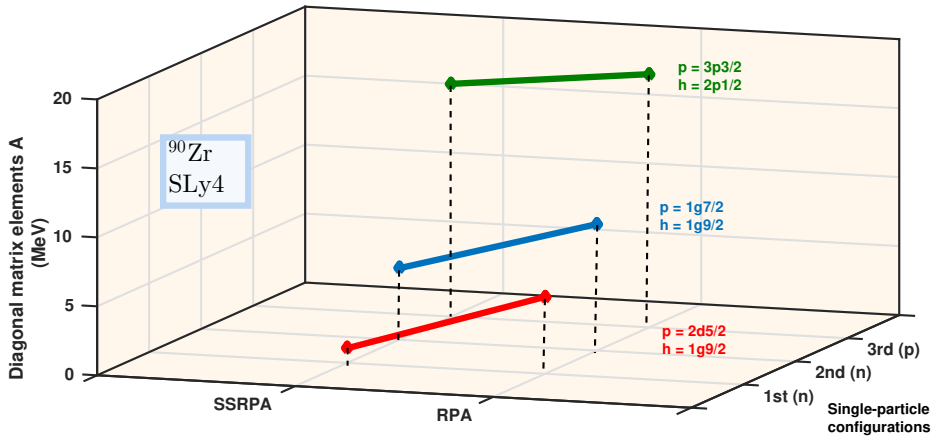

Figure 4.19: Same as in Fig. 4.18 but for ^{90}Zr. One of the configurations is in this case a proton configuration.

intuitive physical interpretation of the BMF renormalization effects. Such effects may be regarded in the same spirit as in particle-phonon-coupling models: the unperturbed 1p1h excitation mode couples with the collective phonon because the two excitation energies are close to one another. The resulting effect is the lowering of the centroid for the collective phonon, the formation of a spreading width for the collective excitation due to the mixing with 2p2h configurations, and the compression of the single-particle spectrum that we deduce from the fact that our effective single-particle excitation energies are systematically reduced.

Let us focus on this third 1p1h configuration and on the nucleus ^{48}Ca (the SSRPA matrix element A_{11} is reduced by 11.6 % with respect to RPA).

To push further this analysis, we computed the SSRPA energy-dependent self-energy correction of Eq. (4.27). We have done this calculation for the third single-particle configuration, for the nucleus ^{48}Ca and the parametrization SLy4. We denote this self-energy by Σ_3: the quantity $1-\partial\Sigma_3/\partial E$ should correspond to an estimation of the E-mass for the third 1p1h configuration (see Eq. (4.37)). The derivative of Σ_3 with respect to the energy is negative, which leads to values for the E-mass larger than 1. This quantity goes to 1 in the static limit where we recover the MF result. Consistently with the previous extraction of the average E-mass from the centroid of the collective axial modes, we noticed that, at the energy value of the third 1p1h configuration (for which the computation is performed) this estimation of the E-mass provides the value of 1.16, which is very close to the one previously found for ^{48}Ca and SLy4 (1.19).

Analogous results were obtained for the heavier nucleus ^{90}Zr and the parametrization SGII. In general, we did not identify any particular difference between the results obtained for the two nuclei, despite their different mass.

To conclude, we proposed here an original and general method to extract BMF effective masses of nuclear matter, based on centroid energies of axial breathing modes of nuclei. We highlighted the increase of the effective mass induced by BMF effects, as well as the subsequent compression of the single-particle spectrum.

We took advantage of the SSRPA model, which, as we showed before, is a robust BMF model against instabilities, divergences and double-counting of correlations.

CHAPTER 5

Extensions of the model

"Certainty is either conventional, or mistaken."

Contents

5.1 Treating nuclei with partially-filled orbitals: Equal-filling approximation . . . 67
5.1.1 Within the HF approximation . . . 68
5.1.2 With a superfluid ground state . . . 69
5.1.3 Results . . . 73
5.2 Going beyond the QBA . . . 77
5.2.1 An extension of RPA and SRPA with renormalization factors: Formalism . 80
5.2.2 An extension of RPA and SRPA with renormalization factors: Results . . . 84

5.1 Treating nuclei with partially-filled orbitals: Equal-filling approximation

In all our applications of the RPA and SRPA models described in the previous chapters, spherical symmetry was assumed. This constitutes an important simplification when it comes to practical calculations. In addition, we only treated nuclei where the last orbitals of the single-particle spectrum are fully occupied for both neutrons and protons.

However, this is surely a limitation which did not allow us to treat most of the open-shell nuclei present in the nuclear chart.

With the perspective of enriching our SSRPA model, our aim here is to extend it so that nuclei with partially-filled orbitals can be described. One simple such extension can be performed using the equal-filling approximation (EFA).

The EFA originally consists in considering, in odd-mass nuclei, that the unpaired nucleon occupies a state and its time-reversed companion with equal probabilities. In the case of spherical symmetry, where one has $(2j+1)$-degenerate orbitals of total angular momentum j, this occupation probability

is distributed over all substates of the given (partially-filled) orbital, meaning that all single-particle states of magnetic angular momentum m_j have an occupancy of $\frac{1}{2j+1}$. An interpretation and a justification of the EFA in terms of quantum statistical mechanics were proposed in Ref. [154]. This justification showed that the EFA can be extended beyond the mean field and, consequently, may indeed have a quite large range of applicability. The very important advantage of using the EFA is that time-reversal symmetry (and thus spherical symmetry) can be maintained.

In the next sections, we show how we use this extension to treat even-even nuclei having their last orbital partially occupied. The occupation of this orbital is distributed over the magnetic angular momenta m_j.

First, we apply the EFA within the HF approximation, where all the occupation numbers are 1 and 0, except for the last (partially-filled) orbital where the occupation is shared among the $(2j+1)$-degenerate states.

As a second step, by applying EFA renormalization factors to all the single-particle wave functions, we propose to use such a procedure to introduce occupation number different from 1 and 0 in the ground state. This is done with the objective of making an estimation of the effect of some correlations.

In particular, occupation numbers modulated by pairing correlations (treated through the BCS approximation) are used. Some links with the QRPA and quasiparticle SRPA (QSRPA) are discussed.

5.1.1 Within the HF approximation

To begin with, calculations for the ground state have to be performed. For the HF calculation, the EFA translates into a renormalization of the wave function of the last occupied orbital P — which is partially filled — by a factor equal to $\sqrt{\frac{\phi}{2j_P+1}}$, where ϕ is the number of occupied states on this orbital. This accounts for the partial occupation of the orbital P. The occupation is shared between the $(2j_P+1)$-degenerate states.

Going to RPA or SSRPA calculations, the wave function of the partially-filled orbital has to be renormalized by a factor equal to $\sqrt{n_\alpha}$ or $\sqrt{1-n_\alpha}$, where n_α is the occupation number of the state α, according to whether this state plays the role, in a given matrix element, of a hole or of a particle, respectively[1].

These modifications concern the A and B matrix elements, and also apply to the transition amplitudes $\langle\lambda|\hat{F}|0\rangle$ of a given one-body operator $\hat{F}$ (see

[1] See also Ref. [155].

Eq. (2.38)). For example, the expression for the transition amplitudes is modified as follows:

$$\langle\lambda|\,\hat{F}\,|0\rangle \;=\; \sum_{m,i,n,j}\Big(X^{*}_{mi}(\lambda)\,\langle n|\,\hat{F}\,|j\rangle - Y^{*}_{mi}(\lambda)\,\langle j|\,\hat{F}\,|n\rangle\Big)\sqrt{n_j(1-n_n)}\,. \tag{5.1}$$

To do this, we have extended our numerical codes which are now able to treat also nuclei having a last orbital with a partial occupation.

These kinds of calculations of course still remain in the framework of the HF approximation.

5.1.2 With a superfluid ground state

Having extended our SRPA model to nuclei with partially-filled orbitals, we aim in this section at presenting how pairing correlations can be included, to study the effects of superfluidity. The RPA and SRPA, as derived in Subsec. 2.3.1 and Subsec. 3.2.1 respectively, do not account for pairing, and one should go to extensions such as the QRPA and the QSRPA to fully take into account pairing correlations in superfluid nuclei.

In this thesis work, we have performed a first step along this direction by making an estimation of pairing correlations with the use of BCS occupation numbers included in EFA-type renormalization factors.

We first present the main derivation steps of the BCS model, which is detailed for example in [38], before explaining our approach within the EFA.

We start with a trial wave function of the BCS type:

$$|\mathrm{BCS}\rangle \;:=\; \prod_{\alpha>0}\left(u_\alpha + v_\alpha a^{\dagger}_{\alpha}a^{\dagger}_{\bar{\alpha}}\right)|-\rangle\;, \tag{5.2}$$

where $\bar{\alpha}$ represents the conjugate (time-reversed if time-reversal invariance is assumed), and u_α and v_α are the variational parameters, related to one another by the normalization condition

$$|u_\alpha|^2 + |v_\alpha|^2 \;=\; 1\,. \tag{5.3}$$

These coefficients enter in the unitary transformations which define the quasi-particle operators $\alpha^{\dagger}_{\mu}$ and α_μ:

$$\begin{aligned}\alpha^{\dagger}_{\mu} &:= u_\mu a^{\dagger}_{\mu} - v_\mu a_{\bar{\mu}}\,,\\ \alpha_{\mu} &:= u_\mu a_{\mu} - v_\mu a^{\dagger}_{\bar{\mu}}\,.\end{aligned}$$

The BCS state Eq. (5.2) does not have the good number of particles N.

For this reason, one has to impose the condition

$$\left\langle \mathrm{BCS}\left|\hat{N}\right|\mathrm{BCS}\right\rangle = N\,, \tag{5.4}$$

where $\hat{N}$ is the particle-number operator. This guarantees that the number of particles is conserved in average.

Assuming once again a Hamiltonian of the form

$$\hat{H} = \sum_{\mu,\mu'} T_{\mu\mu'} a^\dagger_\mu a_{\mu'} + \frac{1}{4} \sum_{\mu,\nu,\mu',\nu'} v_{\mu\nu\mu'\nu'} a^\dagger_\mu a^\dagger_\nu a_{\nu'} a_{\mu'}\,, \tag{5.5}$$

one determines the coefficients u_α and v_α by minimization of the energy. To ensure that the condition (5.4) is satisfied, the minimization is performed on the expectation value of the variational Hamiltonian H':

$$\hat{H}' := \hat{H} - \lambda \hat{N}\,. \tag{5.6}$$

From the variational condition

$$\frac{\partial}{\partial N} \langle \mathrm{BCS}|\hat{H}'|\mathrm{BCS}\rangle = 0\,, \tag{5.7}$$

the Lagrange multiplier λ can be derived as

$$\lambda = \frac{\partial}{\partial N} \langle \mathrm{BCS}|\hat{H}'|\mathrm{BCS}\rangle = \frac{\partial}{\partial N} E\,, \tag{5.8}$$

which is the chemical potential.

As the BCS wave function (5.2) is completely determined by the variational parameters which are related to each other by the relation (5.3), the variational equations reads

$$\left(\frac{\partial}{\partial v_\alpha} + \frac{\partial}{\partial u_\alpha}\frac{\partial}{\partial v_\alpha}\right) \langle \mathrm{BCS}|\hat{H}'|\mathrm{BCS}\rangle = 0\,. \tag{5.9}$$

Using Eqs. (5.2) and (5.5), the above derivatives finally yield the set of BCS equations:

$$\forall \alpha > 0, \quad 2\tilde{\epsilon} u_\alpha v_\alpha + \Delta_\alpha (v_\alpha^2 - u_\alpha^2) = 0\,, \tag{5.10}$$

with

$$\tilde{\epsilon} := \frac{1}{2}\left(t_{\alpha\alpha} + t_{\bar{\alpha}\bar{\alpha}} + \sum_\mu (v_{\alpha\mu\alpha\mu} + v_{\bar{\alpha}\mu\bar{\alpha}\mu}) v_\mu^2 \right) - \lambda$$

and the gap parameter

$$\Delta_\alpha := -\sum_{\mu>0} v_{\alpha\bar{\alpha}\mu\bar{\mu}} u_\mu v_\mu\,.$$

The normalization condition (5.3) and the requirement $v_\alpha^2 = 1$ and $u_\alpha^2 = 0$

when $\Delta_\alpha = 0$ (no pairing interaction) lead to the following solutions of the BCS equations:

$$v_\alpha^2 = \frac{1}{2}\left(1 - \frac{\tilde{\epsilon}_\alpha}{\sqrt{\tilde{\epsilon}_\alpha^2 - \Delta_\alpha^2}}\right), \tag{5.11}$$

$$u_\alpha^2 = \frac{1}{2}\left(1 + \frac{\tilde{\epsilon}_\alpha}{\sqrt{\tilde{\epsilon}_\alpha^2 - \Delta_\alpha^2}}\right). \tag{5.12}$$

From the particle-number requirement (5.4), the actual computation of the variational parameters (5.11) and (5.12) can be carried out by iterations.

In our approach, we use BCS calculations to compute the occupation probabilities n_α (occupation numbers), which thereby contain pairing correlations. These correlated occupation numbers are then used as input in the factors $\sqrt{n_\alpha}$ and $\sqrt{1-n_\alpha}$. We shall call this approach the BCS-based EFA.

Before describing the practical applications that were carried out, let us make a link with the Q(S)RPA case. We consider the QRPA case as an illustration.

The A and B matrix elements have the following form in QRPA [41]:

$$\begin{aligned} A^{\mathrm{QRPA}}_{\alpha\beta,\gamma\delta} &= \delta_{\alpha\gamma}\delta_{\beta\delta}(E_\alpha + E_\beta) \\ &+ \langle\alpha\beta|\,\hat{V}\,|\gamma\delta\rangle\,(u_\alpha u_\beta u_\gamma u_\delta + v_\alpha v_\beta v_\gamma v_\delta) \\ &+ \left\langle\alpha(\beta)^{-1}\right|\hat{V}\left|\gamma(\delta)^{-1}\right\rangle(u_\alpha v_\beta u_\gamma v_\delta + v_\alpha u_\beta v_\gamma u_\delta) \\ &- \left\langle\alpha(\beta)^{-1}\right|\hat{V}\left|\delta(\gamma)^{-1}\right\rangle(u_\alpha v_\beta v_\gamma u_\delta + v_\alpha u_\beta u_\gamma v_\delta), \end{aligned} \tag{5.13}$$

$$\begin{aligned} B^{\mathrm{QRPA}}_{\alpha\beta,\gamma\delta} &= -\langle\alpha\beta|\,\hat{V}\,|\gamma\delta\rangle\,(u_\alpha u_\beta v_\gamma v_\delta + v_\alpha v_\beta u_\gamma u_\delta) \\ &+ \left\langle\alpha(\beta)^{-1},\gamma(\delta)^{-1}\right|\hat{V}\,|\mathrm{QRPA}\rangle\,(u_\alpha v_\beta u_\gamma v_\delta + v_\alpha u_\beta v_\gamma u_\delta) \\ &- \left\langle\alpha(\beta)^{-1},\delta(\gamma)^{-1}\right|\hat{V}\,|\mathrm{QRPA}\rangle\,(u_\alpha v_\beta v_\gamma u_\delta + v_\alpha u_\beta u_\gamma v_\delta), \end{aligned} \tag{5.14}$$

where E_α is the energy of the quasiparticle α.

The RPA limit for the matrices A and B may be easily found by imposing

$$\begin{cases} v_m = v_n = u_i = u_j = 0 \\ u_m = u_n = v_i = v_j = 1\,, \end{cases}$$

because u_α^2 and v_α^2 represent the probabilities by which a single-particle state α is unoccupied and occupied, respectively. This means that, in general,

$$v_\alpha^2 = n_\alpha\,; \quad u_\alpha^2 = 1 - n_\alpha\,.$$

One can recognize in Eqs. (5.13) and (5.14) the particle-hole matrix ele-

ments

$$\left\langle \alpha(\beta)^{-1} \middle| \hat{V} \middle| \gamma(\delta)^{-1} \right\rangle = \langle \alpha\delta | \hat{V} | \beta\gamma \rangle = v_{\alpha\delta\beta\gamma}\,,$$
$$\left\langle \alpha(\beta)^{-1}, \gamma(\delta)^{-1} \middle| \hat{V} | \mathrm{QRPA} \right\rangle = \langle \alpha\gamma | \hat{V} | \beta\delta \rangle = v_{\alpha\gamma\beta\delta}\,.$$

The interaction matrix elements entering in the RPA matrices A and B, with the EFA approximation, are renormalized by factors of the type

$$\sqrt{n_i n_j (1-n_m)(1-n_n)}\,. \tag{5.15}$$

In terms of the u and v coefficients of the BCS ground state, the expression (5.15) may be written as

$$v_i v_j u_m u_n\,,$$

which is the same as in the particle-hole matrix elements of the QRPA matrices A and B (see Eqs. (5.13) and (5.14)).

We may then conclude that, by applying the EFA procedure and by using BCS occupation numbers, our matrix elements have the same structure as some of the QRPA matrix elements.

In particular, for the BCS-based EFA in the RPA case, we have $uvuv$-type matrix elements. For the BCS-based EFA in the SSRPA case, we have $v_i u_m u_n u_p$, $v v_j v_k u_m$, $u_m u_n u_p u_q$, $v_i v_j v_k v_l$ and $v_i v_k u_p u_m$-type matrix elements.

Even if we are not performing a full quasiparticle calculation, we are thus using a simplified procedure to describe pairing effects. One thing to note is that we did not introduce a pairing interaction for some specific matrix elements of the residual interaction. The pairing interaction is used only for the ground-state calculation.

Note that in this extension, the pairing results in a smearing of the occupancies, so that in practice all the states acquire an occupation number different from the sharp 1 and 0 values. Now as in the HF-based EFA presented in Subsec. 5.1.1, we allow for any orbital having a fractional occupancy to play the role of particle- or hole-state orbital in the configurations.

As a consequence, this extension with pairing correlations generates an additional non-negligible computational cost, due to the more numerous configurations that are allowed, compared to the HF-based EFA. Thus in practice, it was necessary to restrict this allowance, by imposing an artificial tolerance criterion on the occupation numbers: only those orbitals whose occupation numbers have, in absolute value, a difference greater than the tolerance with respect to the HF values 1 and 0 are allowed to play both roles (hole- and particle-state respectively) — the other orbitals are treated as pure hole- or particle-states, meaning that their role can only be of one

type. Numerical details are provided in the next section.

5.1.3 Results

In this subsection, we present the applications of our RPA and SSRPA models in the EFA. As explained in Subsec. 5.1.1 and Subsec. 5.1.2 respectively, these applications can be either based on a HF ground state or on a BCS ground state, depending on how the input occupation numbers are calculated.

A recent study [156] reported the first γ-ray spectroscopy of the ^{52}Ar nucleus as well as an analysis of the lowest 2^+ states of other even-even Argon isotopes with $N > 20$. The experiment, conducted at the Radioactive Isotope Beam Factory (RIBF) in Japan, employed the ^{53}K$(p,2p)^{52}$Ar reaction at $\sim$210 MeV/u to investigate the low-lying spectrum of ^{52}Ar. The main goal was to determine how the $N = 34$ subshell closure, suggested only in ^{54}Ca so far, would evolve below $Z = 20$.

The results of several theoretical phenomenological and *ab initio* calculations were confronted to the currently available experimental values for the considered Argon isotopes.

Figure 5.1 is extracted from Ref. [156], where we focus on the region $N > 28$. We are indeed interested in the trend from $N = 28$ to $N = 34$. At $N = 28$ and $N = 34$, the experimental measurements lead to two maxima, indicating that these two nuclei have a shell-closure nature.

The experimental values shown on the figure are taken from Ref. [156] and from Refs. [157, 158].

One can see that large-scale shell model calculations with the SPDF-U [159] and SPDF-MU [160, 161] (*original* and *modified*) interactions give a satisfactory reproduction of the experimental data, especially of the $N = 28$ shell closure and of the rise of the lowest 2^+ (denoted as 2^+_1) observed in ^{52}Ar. Calculations in the valence-space in-medium similarity renormalization group (VS-IMSRG) approach with the 1.8/2.0(EM) [162–164] and the N^{2}LO$_{\text{sat}}$ [3] interactions reproduce reasonably well the experiments. Coupled-cluster calculations [156] are not in favour of the $N = 34$ closure persistence and reproduce less well the experimental results. They are obtained using the DCE-EOM and 2PR-EOM methods with the 1.8/2.0(EM) interaction.

It is interesting to see what information our RPA and SSRPA calculations can provide in this context. We therefore decided to perform systematic calculations of the quadrupole response of Argon isotopes from $N = 28$ to $N = 34$.

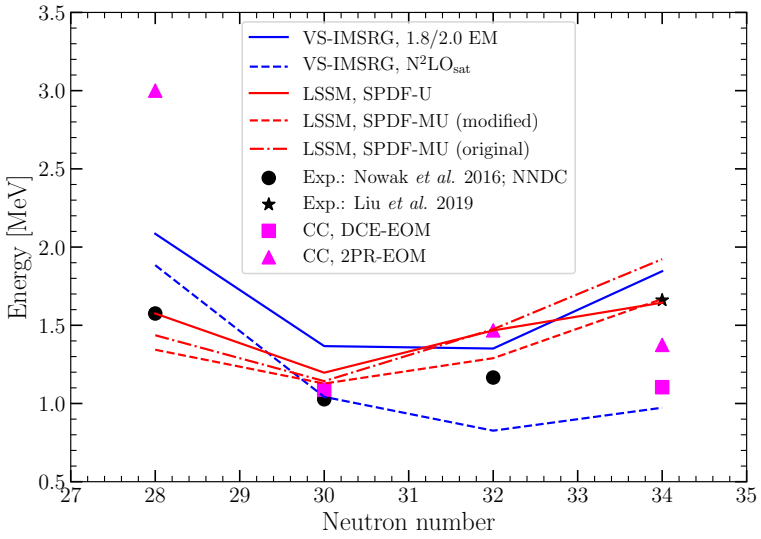

Figure 5.1: Experimental 2_1^+ energies for even-even Ar isotopes compared with theory: VS-IMSRG with the chiral interaction 1.8/2.0(EM) [162–164] and N^2LO_{sat} [3], coupled-cluster calculations (CC) [156] using the DCE-EOM and 2PR-EOM methods with the 1.8/2.0(EM) interaction, and large-scale shell model (LSSM) calculations with the SDPF-U [159] and the so-called original [161] and modified [160] SDPF-MU interactions. Experimental data are taken from Ref. [156] ('Liu *et al.*') and from Refs. [157, 158] ('Nowak *et al.*' and 'NNDC').

Let us recall that in both the HF-based and BCS-based calculations, the EFA factors are applied to the A and B matrices and to transition amplitudes of one-body operators. In BCS-based calculations, the tolerance on occupancies[2] is chosen to be 0.1: single-particle states with occupation numbers in $[0;0.1]$ and $[0.9;1]$ are respectively considered as pure particle states and pure hole states. In HF-based calculations, where for a given isospin there is at most one orbital with a fractional occupancy, the tolerance value is chosen to be close to zero[3], so that the partially-filled orbitals are always treated as both hole and particle state orbitals when building the (S)RPA configurations.

The cutoff on 1p1h configurations is set to 100 MeV, in both RPA and SSRPA calculations. In SSRPA, to keep the calculations more tractable, a 40-MeV 2p2h cutoff is adopted. Moreover, the same 2p2h cutoff is applied for the matrices involved in the subtracted self-energy, and the diagonal approximation is used to compute these subtracted terms.

In the case where occupation numbers are calculated using BCS calculations, the pairing interaction has the following form:

$$V(\mathbf{r},\mathbf{r}') = V_0\left(1-\eta\left(\frac{\rho(\mathbf{r})}{\rho_0}\right)^{\gamma}\right)\delta(\mathbf{r}-\mathbf{r}'). \tag{5.16}$$

In Eq. (5.16), the pairing strength V_0 is set to 400 MeV·fm^3. This choice leads to reasonable values of the average proton pairing gap ($\sim$1.2 MeV) along the isotope chain we consider, and to the correct description of the neutron shell closure $N = 28$ for ^{46}Ar. The η parameter is set to 0.5, and we take $\gamma = 1$. $\rho(\mathbf{r})$ is the isoscalar nucleonic density and $\rho_0 = 0.16$ fm^{-3}. This parameterization is adopted for both neutrons and protons. In both cases, ten single-particle states located above the last occupied HF state are included, and are active for pairing.

For this systematic analysis, all the RPA and SSRPA calculations are carried out with the SLy4 Skyrme parameterization, which we extensively used in previous applications (see Sec. 4.2).

We shall start by reporting the HF-based and BCS-based RPA results of our calculations. They are displayed on Fig. 5.2 with the same experimental values as in Fig. 5.1. It is clear that these RPA results do not reproduce the rises of the 2_1^+ energies for ^{46}Ar and ^{52}Ar and even predict the opposite trend. We note also that the effect of adding pairing correlations is to increase the

[2] See the corresponding discussion in Subsec. 5.1.2.

[3] The value is not exactly 0 in practice because of the numerical noise that can generate small fluctuations of the occupation numbers around the values 0 and 1 for filled orbitals.

excitation energies.The trend remains very similar from the HF-based to the BCS-based calculation. These results would thus seem opposed to the experimental observation of a shell closure in ^{46}Ar and ^{52}Ar.

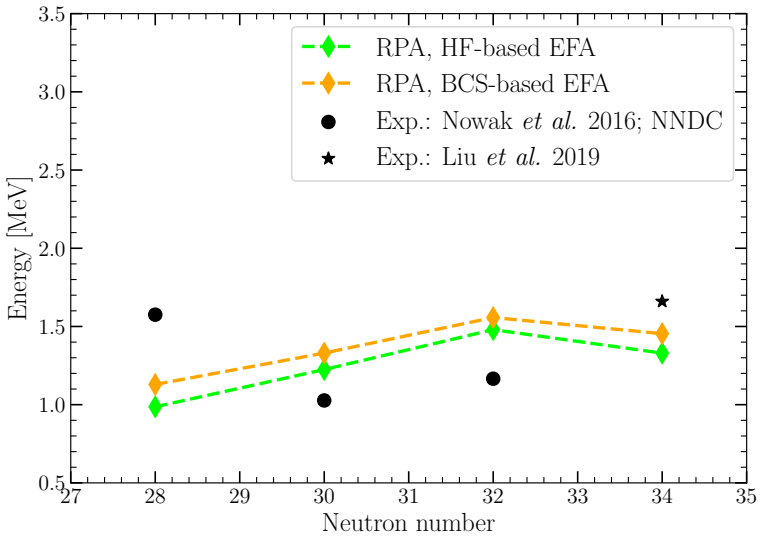

Figure 5.2: Lowest 2^+ energies in $N = 28$ to $N = 34$ Argon isotopes, calculated in RPA with EFA. Occupation numbers used as input are computed in HF ("HF-based") and BCS ("BCS-based") calculations. Experimental values are the same as in Fig. 5.1.

One may next study the evolution of these energies when including 2p2h configurations. The comparison between the HF-based and the BCS-based EFA in SSRPA is presented on Fig. 5.3. In this case, we observe again the higher position of the energies in presence of pairing, but there is a notable deviation of the HF-based with respect to the BCS-based values for ^{52}Ar: while the tendency is to a decrease in the HF case, the inclusion of pairing leads to a continual increase from ^{46}Ar to ^{52}Ar. This suggests that the addition of pairing correlations in SRPA-type calculations can substantially affect the description of the low-lying spectrum of some nuclei. In the present case, the original absence of pairing would not allow for a conclusion in favor of the persistence of the shell closure in ^{52}Ar, whereas the trend obtained with our BCS-based approach agrees with the experimental observation of Liu *et al.*

Finally, the results of the BCS-based RPA and SSRPA are compared on Fig. 5.4. This allows for a direct comparison of the two models where pairing effects are estimated through BCS occupation numbers. Going from RPA to SSRPA, the trend at the minima $N = 28$ and $N = 34$ is partly rectified. One can conclude that it is the mixing with 2p2h configurations which leads to

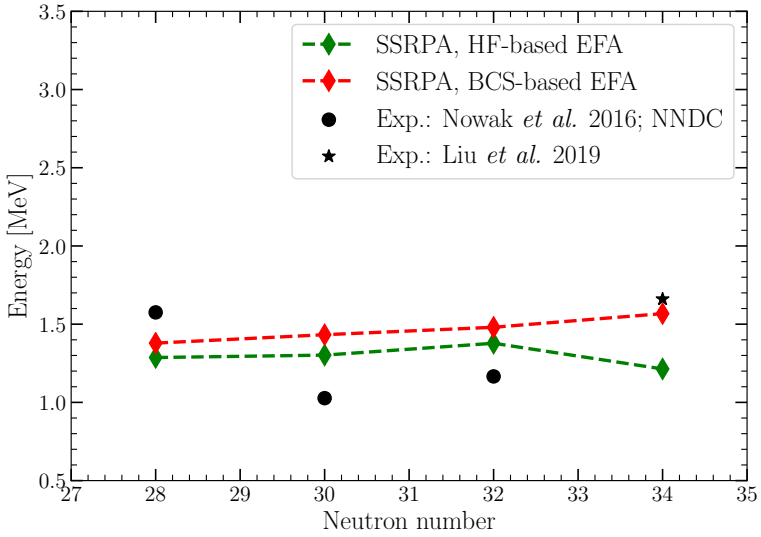

Figure 5.3: Lowest 2^+ energies in $N = 28$ to $N = 34$ Argon isotopes, calculated in SSRPA (2p2h cutoff of 40 MeV) with EFA. Occupation numbers used as input are computed in HF ("HF-based") and BCS ("BCS-based") calculations. Experimental values are the same as in Fig. 5.1.

this correction towards a better agreement with the experimental values.

To conclude, the BCS-based EFA approach that we introduced allows for an estimation of the effect of pairing in RPA and SRPA. While not modifying substantially the results in RPA, more important modifications are observed when including 2p2h configurations, towards a better agreement with experimental data. This supports the importance of including pairing correlations within SRPA-type calculations to improve the description of low-lying states of certain nuclei. Of course, as pointed out previously, this is only a simplified inclusion of pairing correlations.

5.2 Going beyond the QBA

As discussed in Subsec. 2.3.2, the standard RPA resolution relies on the QBA to set up the matrix elements, because the exact (correlated) ground state is *a priori* unknown. We remind here that this approximation, which in practical applications is equivalent to using the HF ground state when building the matrix elements, is inconsistent and has the obvious drawback of bounding the applications to the MF framework.

In principle, the form of the RPA excitation operators implies that the

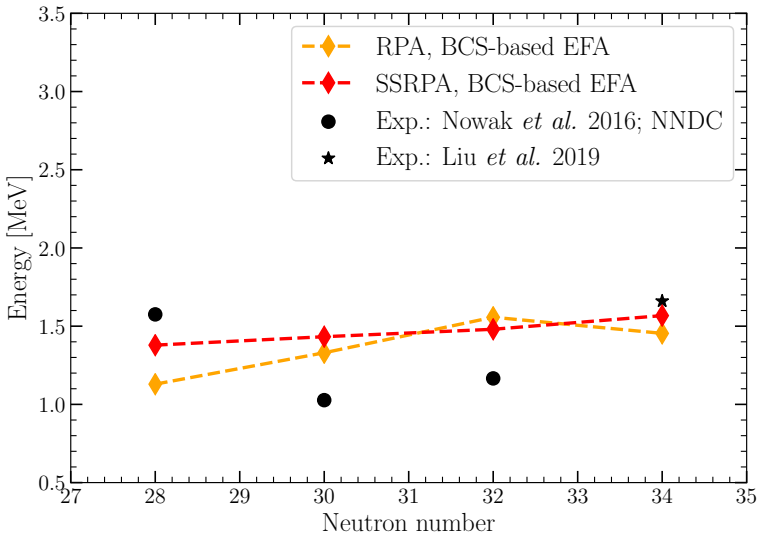

Figure 5.4: Lowest 2^+ energies in $N = 28$ to $N = 34$ Argon isotopes, calculated in RPA and SSRPA with EFA. Occupation numbers used as input are computed in BCS calculations. Experimental values are the same as in Fig. 5.1.

RPA ground state is correlated. Replacing such a correlated ground state with the HF ground state thus induces a clear inconsistency in the model. This also produces a violation of the Pauli principle. In addition, within the RPA model, the use of the QBA leads to a fully harmonic spectrum (no anharmonicities in the multiphonon spectrum).

To go beyond this approximation, various formal developments were made in the past. In the pioneering studies of Refs. [40, 165], the so-called renormalized RPA was introduced for the first time, where renormalization factors depending on the occupation numbers of single-particle states appeared. Such occupation numbers were different from 1 and 0 because a correlated ground state was used instead of the HF ground state (the QBA was not adopted). In these first studies, the single-particle energies were estimated by measurements (centroids extracted from pickup or stripping reactions). Applications to the study of low-lying states [166, 167] and of double beta decay [168–170] were carried out. In these latter applications, single-particle energies were this time computed microscopically.

Such a renormalized RPA model is a simplification of the so-called self-consistent RPA [171–174] where two-body densities are simplified by an antisymmetrized product of single-particle densities.

Several directions were explored to overcome the QBA, in some cases by constructing theories based on a boson formalism [175–183] and, in other cases, remaining within a fermionic space [47, 152, 166, 184–191]. In the cases where boson-expansion methods were used, the operator $Q^{\dagger}_{\nu}$ was defined in terms of the boson operators. Fermion operators of interest were replaced by their boson images through a mapping procedure. By truncating the boson Hamiltonian at two-boson terms, a boson formulation of RPA could be obtained. A higher level of approximation was reached if the boson image of the Hamiltonian included higher-order terms.

It is known that enlarging the RPA model by avoiding the QBA generates violations of the EWSRs. These violations were cured by including, in addition to particle-hole configurations, also particle-particle and hole-hole configurations [45–47, 192].

In Ref. [187], renormalized operators

$$B^{\dagger}_{mi} := \sum_{p,k} N_{mi,pk} a^{\dagger}_{p} a_{k} \tag{5.17}$$

were introduced to construct the excitation operators:

$$Q^{\dagger}_{\nu} := \sum_{m,i} \left(X_{mi}(\nu) B^{\dagger}_{mi} - Y_{mi}(\nu) B_{mi} \right) \tag{5.18}$$

It was assumed a diagonal one-body density matrix

$$\langle 0 | \, a^{\dagger}_{\beta} a_{\alpha} \, | 0 \rangle \; = \; \delta_{\alpha\beta} \, n_{\alpha}$$

and the following choice was made:

$$N_{mi,pk} \; = \; \delta_{mp} \delta_{ik} (n_i - n_m)^{-1/2} \; := \; \delta_{mp} \delta_{ik} D^{-1/2}_{mi} \, . \tag{5.19}$$

In the above equations, n_{α} is the occupation number of the single-particle state α.

Then, through a linearization of the equations of motion, expressions for the matrices A and B containing the one-body density matrix were obtained. Thanks to the number operator method [193], the one-body density matrix elements were derived as functions of the amplitudes X and Y of the RPA excitation operator. This led to a set of non-linear equations which were solved iteratively. One limitation was that the one-body density matrix was assumed to be diagonal in the HF basis. This limitation was overcome in Ref. [188]. However, the ansatz (5.17) and the choice (5.19) were still adopted.

To avoid this, it was proposed in Ref. [152] to work with operators which are not renormalized. By linearizing the equations of motion, a set of RPA-

type equations was obtained, again depending on the one-body density matrix, the latter being related to the X and Y amplitudes by the use of the number operator method. A similar procedure was employed in Ref. [153] to extend the SRPA model. The importance of avoiding the QBA in the SRPA model was underlined by Papakonstantinou [67] as already mentioned.

5.2.1 An extension of RPA and SRPA with renormalization factors: Formalism

In this thesis work, the extended SRPA model of Ref. [153] is used. We remind that this extension is based on a similar procedure as that employed in a previous study made for the RPA case [152]. These two models were referred to as extended SRPA (ESRPA) and extended RPA (ERPA) in the two articles, respectively. They were both applied to the study of collective excitations in metal clusters. The novelty of the present work resides in the further development of these extended models and their application to atomic nuclei.

Let us start with the ERPA case. This model was developed as an improvement of other extensions of RPA presented in Refs. [187, 188]. In the extension introduced in Ref. [187] the particle-hole operators are renormalized (Eq. (5.17)). By defining the correlated ground state $|0\rangle$ as the vacuum of the operators Q_ν (where $Q_\nu^\dagger$ are given by Eq. (5.18)), by assuming that the one-body density matrix is diagonal and by adopting the choice (5.19), RPA-like equations may be derived where the matrices A and B are now expressed as

$$A_{mi,nj} := \Big\langle 0\Big|\Big[B_{mi}, \hat{H}, B_{nj}^\dagger\Big]\Big|0\Big\rangle, \tag{5.20}$$

$$B_{mi,nj} := -\Big\langle 0\Big|\Big[B_{mi}, \hat{H}, B_{nj}\Big]\Big|0\Big\rangle, \tag{5.21}$$

and

$$G_{mi,nj} := \Big\langle 0\Big|\Big[B_{mi}, B_{nj}^\dagger\Big]\Big|0\Big\rangle, \tag{5.22}$$

having introduced the antisymmetrized double-commutators:

$$[a,b,c] := \frac{1}{2}\Big(\big[a,[b,c]\big] + \big[[a,b],c\big]\Big). \tag{5.23}$$

The usual orthonormality conditions as in standard RPA may be found:

$$\delta_{\lambda\lambda'} = \sum_{m,i,n,j}\Big(X_{mi}^*(\lambda')X_{nj}(\lambda) - Y_{mi}^*(\lambda')Y_{nj}(\lambda)\Big). \tag{5.24}$$

To simplify this complicated problem, the linearization of the equations of motion is carried out. In the computation of the commutator of the Hamiltonian $\hat{H}$ with a particle-hole operator, the two-body terms are contracted with respect to $|0\rangle$. In this way, one obtains expressions for the matrices A and B where only the one-body density matrix appears. Thus, the matrices A and B depend on the occupation numbers which, in turn, depend on the amplitudes X and Y. This non-linear problem is solved iteratively.

The fact that the one-body density matrix is assumed to be diagonal in Ref. [187] in the HF basis is a clear limitation. This limitation is overcome in Ref. [188], which is however still based on Eqs. (5.17) and (5.18).

To go beyond such a strong constraint, an improvement of the model was then proposed in Ref. [152].

The form of the excitation operator $Q^\dagger_\nu$ is this time the same as in standard RPA (see Eq. (2.21)), and the system to solve is that of Eq. (2.23), with the matrix elements defined in Eqs. (2.24) to (2.26). The solutions X and Y of the problem satisfy the orthonormality condition (2.36).

Assuming the expression (2.1) of the Hamiltonian, and using the linearization of the equations of motion, the density-dependent expressions of the matrix elements are obtained:

$$\begin{aligned} A_{mi,nj} = \frac{1}{2}\Bigg(& h_{mn}\rho_{ji} + h_{ij}\rho_{nm} - \delta_{ij}\sum_p h_{pn}\rho_{pm} - \delta_{mn}\sum_k h_{kj}\rho_{ki} \\ & + \sum_{k,l} v_{mkln}\rho_{il}\rho_{jk} + \sum_{p,q} v_{ipqj}\rho_{mq}\rho_{np} + 2\sum_{k,p} v_{kpni}\rho_{jk}\rho_{mp} \\ & + (m,i \longleftrightarrow n,j)\Bigg), \end{aligned} \tag{5.25}$$

$$B_{mi,nj} = -\Bigg(\sum_{p,q}\left(v_{ijpq}\rho_{np}\rho_{mq}\right) + \sum_{k,l}\left(v_{klnm}\rho_{jk}\rho_{il}\right) \tag{5.26}$$

$$+ \sum_{p,k}\left(v_{kipn}\rho_{jk}\rho_{mp}\right) + \sum_{p,k}\left(v_{kjpm}\rho_{ik}\rho_{np}\right)\Bigg), \tag{5.27}$$

where the $h_{\alpha\beta}$ quantity was defined as in Eq. (2.11).

One always has

$$G_{mi,nj} = \delta_{mn}\,\rho_{ji} - \delta_{ji}\,\rho_{nm}\,. \tag{5.28}$$

As already mentioned, the elements of the one-body density matrix are expressed in terms of the X and Y amplitudes through the number operator

method. One obtains

$$\rho_{mm'} = \sum_{\nu,\nu} S(\nu,\nu') \sum_{p,i} \sum_{q,j} Y_{pi}(\nu) Y^*_{qj}(\nu') \sum_k G_{mk,pi} G^*_{m'k,qj}\,, \tag{5.29}$$

$$\rho_{ii'} = \delta_{ii'} - \sum_{\nu,\nu} S(\nu,\nu') \sum_{p,k} \sum_{q,j} Y_{pk}(\nu) Y^*_{qj}(\nu') \sum_m G_{mi,pk} G^*_{mi',qj}\,, \tag{5.30}$$

where

$$S(\nu,\nu') = \delta_{\nu\nu'} - \frac{1}{2} \sum_{m,i,n,j} X_{mi}(\nu) X^*_{nj}(\nu') \sum_{p,k} G_{pk,mi} G^*_{pk,nj}\,. \tag{5.31}$$

As was done in Ref. [152], one may diagonalize the h matrix to obtain "generalized single-particle energies" $h_{\alpha\beta} = \epsilon_\alpha \delta_{\alpha\beta}$, and use the subsequent single-particle basis.

In our model we do not diagonalize the one-body density matrix. Instead, we assume it to be diagonal. Such additional approximation in our model results in the following expressions for the matrix elements, where we separate the kinetic and the interaction parts:

$$A_{mi,nj} = \delta_{mn}\delta_{ij}(\epsilon_m - \epsilon_i)(n_i - n_m) + v_{mjin}(n_i - n_m)(n_j - n_n)\,, \tag{5.32}$$

$$B_{mi,nj} = v_{mnij}(n_i - n_m)(n_j - n_n)\,, \tag{5.33}$$

$$G_{mi,nj} = \delta_{mn}\delta_{ij}(n_i - n_m)\,. \tag{5.34}$$

One may express in a similar fashion the transition amplitude $\langle\lambda|\,\hat{F}\,|0\rangle$ of a one-body operator $\hat{F}$. We already derived such an expression in Subsec. 2.3.1 (see Eq. (2.38)). Notice that this quantity also depends on the one-body density via the elements of the G matrix.

We now present the corresponding equations for the SRPA case, following the same approximation framework as in Ref. [153].

The A_{11}, B_{11} and G_{11} blocks of the SRPA stability matrix are the same as in Eqs. (5.32) to (5.34). The elements of the remaining (non-zero) SRPA blocks can be derived in a similar way. As an example of such a derivation, the case of the A_{12} elements is presented in App. 1. We provide here only

the final expressions for the SRPA block matrices:

$$A_{pk,mnij} = \mathscr{A}(i,j)\,\delta_{kj} v_{ipmn}\,\chi^{(3\mathrm{p1h})} - \mathscr{A}(m,n)\,\delta_{pn} v_{ijmk}\,\chi^{(3\mathrm{h1p})}, \tag{5.35}$$

$$\begin{aligned} A_{mnij,pqkl} = {} & \mathscr{A}(i,j)\,\mathscr{A}(m,n)\,\delta_{ik}\delta_{mp}\delta_{jl}\delta_{nq}(\epsilon_m + \epsilon_n - \epsilon_i - \epsilon_j)\,\chi_{mi,nj} \\ & + \mathscr{A}(i,j)\,\delta_{ik}\delta_{jl} v_{mnpq}\,\chi^{(4\mathrm{p})} \\ & + \mathscr{A}(m,n)\,\delta_{mp}\delta_{nq} v_{ijkl}\,\chi^{(4\mathrm{h})} \\ & + \mathscr{A}(i,j)\,\mathscr{A}(m,n)\,\mathscr{A}(k,l)\,\mathscr{A}(p,q)\,\delta_{jl}\delta_{nq} v_{mkip}\,\chi^{(2\mathrm{p2h})} \end{aligned} \tag{5.36}$$

$$G_{mnij,pqkl} = \mathscr{A}(i,j)\,\mathscr{A}(m,n)\,\delta_{ik}\delta_{mp}\delta_{jl}\delta_{nq}\,\chi_{mi,nj}\,, \tag{5.37}$$

where the renormalizing factors that contain occupation numbers are defined as follows:

$$\chi_{mi,nj} := n_i n_j (1 - n_m - n_n) - n_m n_n \left(1 - n_i - n_j\right) \tag{5.38}$$

$$\chi^{(3\mathrm{p1h})} := n_k n_i (1 - n_m - n_n) + \frac{1}{2}\chi_{pm,in} \tag{5.39}$$

$$\chi^{(3\mathrm{h1p})} := n_i n_j \left(1 - n_m - n_p\right) + \frac{1}{2}\chi_{im,jk} \tag{5.40}$$

$$\chi^{(4\mathrm{p})} := \chi_{mi,nj}\left(1 - \frac{n_m + n_n + n_p + n_q}{2}\right) \tag{5.41}$$

$$\chi^{(4\mathrm{h})} := -\chi_{mi,nj}\left(1 - \frac{n_i + n_j + n_k + n_l}{2}\right) \tag{5.42}$$

$$\chi^{(2\mathrm{p2h})} := \chi_{mi,nj}\frac{n_i + n_k - n_m - n_p}{2}\,. \tag{5.43}$$

Notice that, because of our approximation framework, the expressions of the matrix elements with density matrices reduce to expressions with only occupation numbers.

Having derived these beyond-QBA expressions of the matrix elements, one needs to compute the occupation numbers to evaluate the renormalizing factors prior to solving the SRPA problem. The practical way we address this problem will be described in detail in Subsec. 5.2.2.

The expressions for the occupation numbers are derived via the number operator method introduced in Ref. [193]. The expressions used in our calculations are based on the simplification $G_{mi,nj} = \delta_{mn}\delta_{ij}$ and contain only terms with up to a quadratic dependence in the amplitudes ($O(|X^2|)$ and

$O(|Y^2|)$). One has in this scheme

$$n_m \simeq \frac{1}{2}\sum_{\nu}\sum_{i}|Y_{mi}(\nu)|^2 + O(|Y^4|)\,, \tag{5.44}$$

$$n_i \simeq 1 - \frac{1}{2}\sum_{\nu}\sum_{m}|Y_{mi}(\nu)|^2 + O(|Y^4|)\,. \tag{5.45}$$

More involved expressions, keeping the full expression for $G_{mi,nj}$ and going up to terms in $O(|Y^4|)$, can be derived [187]. However such expressions are not considered in our approach. We provide the main steps of the number operator method in App. 2.

5.2.2 An extension of RPA and SRPA with renormalization factors: Results

We provide in this section the details of our applications of the extensions of RPA and SRPA introduced in the previous subsection, and discuss the corresponding results.

Let us remind that our aim in this particular study is to achieve a renormalization of SRPA as per Eqs. (5.32) to (5.37), by using occupation numbers calculated self-consistently in RPA. As was underlined and suggested in Ref. [67], the drawbacks of the SRPA model related to the stability and to the Thouless theorem may be cured by going towards a model where the ground state is not the HF one but a correlated ground state. One can thus hope that, if the ground state calculated with the RPA amplitudes is sufficiently correlated (with occupation numbers noticeably different from 1 and 0), the SRPA model with renormalization factors (depending on such occupation numbers) may be an alternative method to the subtraction procedure, leading to the same type of corrections.

This is indeed what was found in practice in Ref. [153] in the application carried out to describe dipole strength distributions in metal clusters (where these excitations are vibrations of the delocalized valence electrons against the ionic core, which is approximated by a jellium). Whereas the standard SRPA produces in Ref. [153] the well-known unphysical downward shift of the excitation energies compared to RPA, the extension of the SRPA based on a correlated ground state leads to an important correction of the spectrum, which is shifted to higher energies.

This is consistent with what was discussed a long time ago from a formal point of view by Takayanagi *et al.* [194, 195]. If a correlated ground state

is used, the SRPA model may be rewritten in such a way that a modified response function is obtained (compared to the case of the standard SRPA), where the self-energy is corrected by the inclusion of a new term (recall that a corrective term to the self-energy is also introduced by the subtraction procedure).

However, this procedure based on a correlated ground state (with renormalization factors) is working efficiently only for cases where such renormalization factors induce non negligible ground state modifications.

Now, the correlations that RPA-based models are able to describe are those which are related to the amplitudes X and Y. In particular, they depend on the amplitudes Y (to what extent they are different from zero). It turns out that, for metal clusters, these amplitudes are quite large. We have then checked how this procedure works for atomic nuclei.

We base our implementation of the renormalized RPA on the `skyrme_rpa` program [196]. This program was extended to allow for iterative renormalized RPA calculations.

Our approach consisted in the following two steps:

1. Calculate the occupation numbers in iterative renormalized RPA, using Eqs. (5.44) and (5.45). The first calculation (iteration 0) is performed in standard RPA (the iteration process is therefore initialized by HF occupation numbers). The procedure is stopped when convergence is reached, that is when the RPA eigenenergies at a given iteration are considered identical to those of the previous one.

2. Use the occupation numbers resulting from the last RPA iteration as input for a renormalized SRPA calculation. The occupation numbers are taken into account via the renormalizing factors defined in Eqs. (5.38) to (5.43).

Note that, according to the number operator method, the computation of the occupation numbers is all the more accurate as more multipolarities J^π are taken into account in the iterative process. In fact, for a given nucleus, our method allows us to include a desired number of multipolarities in the iterative calculation, so that they all finally contribute to the converged occupation numbers. In the cases presented in this section, five multipolarities J^π were included at each iteration of the occupation-number computation: 0^+, 2^+, 4^+, 1^-, 3^-.

We recall that, inherently to the number operator method, the total number of particles (neutrons and protons) is recovered when summing all the

occupation numbers — this serves also as a test, and was systematically verified for all our calculations.

We exemplify here our results by presenting the case of the monopole response of ^{16}O, using the SLy4 interaction. The energy cutoff was set to 100 MeV for single-particle states and to 100 MeV for 1p1h configurations, in both RPA and SRPA calculations. In SRPA, the 2p2h cutoff was set to 60 MeV.

As far as the RPA iterations are concerned for this nucleus, it was found that five iterations are enough to obtain eigenvalues converged up to 10^{-4} MeV. In addition, it appears that the difference between the converged and the initial values of the eigenenergies usually does not exceed 0.1 MeV.

Occupation numbers calculated iteratively for ^{16}O are displayed on Fig. 5.5. One observes the depletion of states that are occupied in HF, and the corresponding population of particle states, the latter being spread over the whole remaining single-particle basis. One can notice that the modification of the occupation numbers with respect to 1 and 0 is extremely weak.

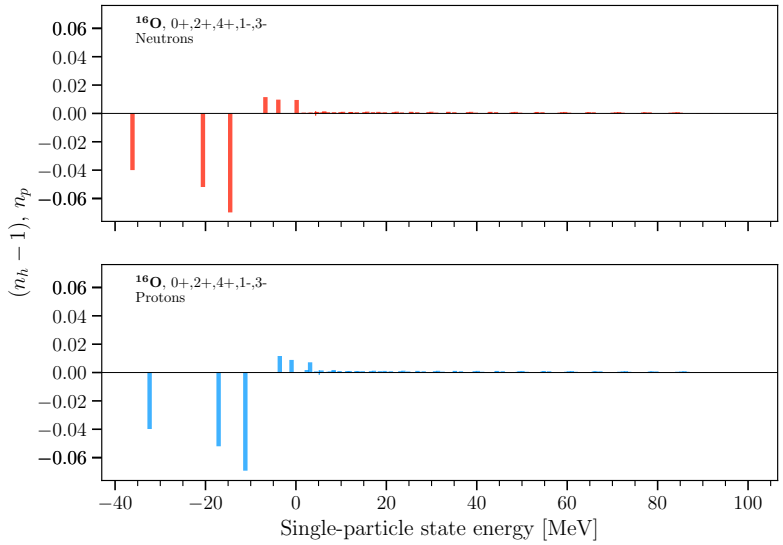

Figure 5.5: Occupation numbers n_p for particle states and opposite of depletion numbers $1-n_h$ for hole states, calculated iteratively with renormalized RPA for the ^{16}O nucleus. The upper panel displays the values for neutrons, the lower panel for protons. The indicated multipolarities were included at each step of the RPA iterations.

Figure 5.6 represents the same occupation numbers computed this time in the case where only the multipolarity of the final SRPA calculation ($J^\pi = 0^+$)

was included in the iterative RPA calculations. This figure shows that the effect on the occupation numbers of adding different multipolarities in the iterative process is non-negligible: the total depletion of hole-states is increased by around 4 % (the most depleted hole state having an occupation number of 0.93), when all the above-mentioned five multipolarities were added, instead of only the $J^\pi = 0^+$.

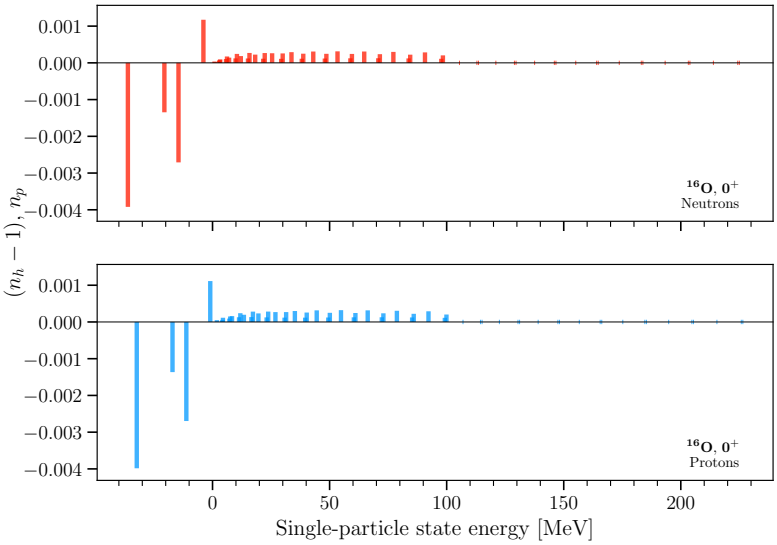

Figure 5.6: Same as Fig. 5.5, but where only the multipolarity $J^\pi = 0^+$ was included in the iterative RPA calculations for the computation of occupation numbers.

Now feeding back the converged values of occupation numbers to a ^{16}O SRPA calculations, a modification of the spectrum is indeed observed, as can be seen on Fig. 5.7.

From this result we made the following observations:

- The observed renormalization has the expected effect: the whole spectrum is pushed towards higher energies. Indeed, this behavior tends to correct (though insufficiently) the unphysical shift observed in standard SRPA.
- The renormalization is weak (usually of a few hundreds of keV in the GR region). By fitting a Lorentzian function to the distribution obtained after folding in each case, the centroids estimated in this way are located at 19.8 MeV in standard SRPA, and at 20.3 MeV in renormalized SRPA.

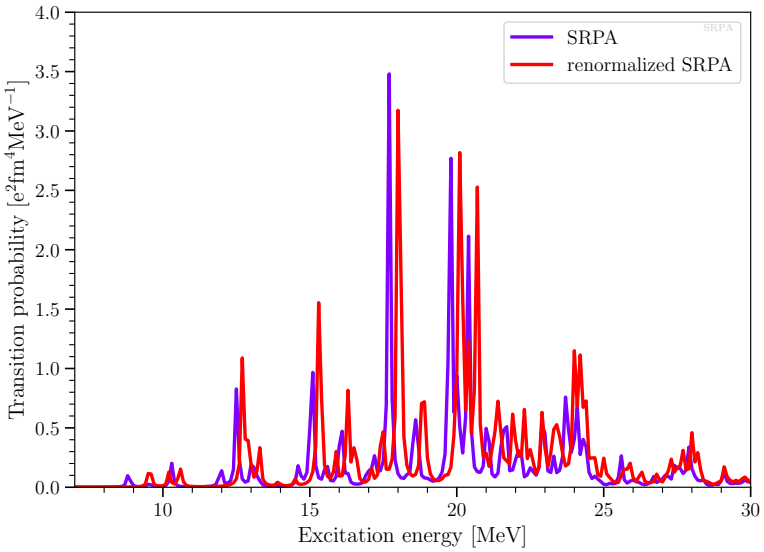

Figure 5.7: Monopole response of ^{16}O calculated with the SLy4 interaction in SRPA (no renormalization) and in SRPA renormalized with RPA occupation numbers. The transition probability was folded with Lorentzian functions of width 0.1 MeV. The folded spectrum was rescaled to the maximum value of the discrete spectrum. The energy cutoff for 2p2h configurations is 60 MeV.

We checked that a similar behavior is obtained with the SGII interaction, and with higher 2p2h energy cutoffs in SRPA. As an additional illustration, we show on Fig. 5.8 the quadrupole response of the same nucleus, evaluated with a 2p2h cutoff of 30 MeV (the same behavior is obtained by increasing the value of the cutoff).

The very low effect of such a renormalization demonstrates that ground-state correlations coming only from self-consistent RPA calculations are not sufficient to correct for the strong shift observed in standard SRPA.

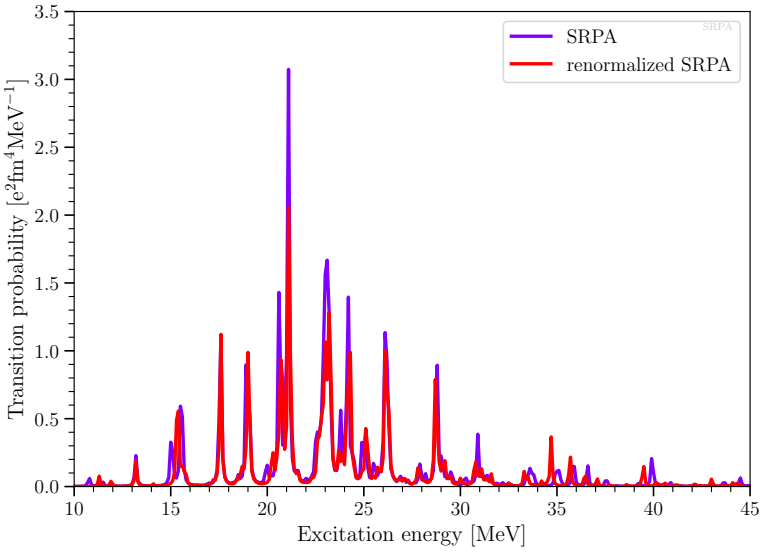

Figure 5.8: Quadrupole response of ^{16}O calculated with the SLy4 interaction in SRPA (no renormalization) and in SRPA renormalized with RPA occupation numbers. The transition probability was folded with Lorentzian functions of width 0.1 MeV. The folded spectrum was rescaled to the maximum value of the discrete spectrum. The energy cutoff for 2p2h configurations is 30 MeV.

CHAPTER 6

General conclusions & perspectives

With the initial aim of improving the description of nuclear excitation spectra, this thesis work contributed to the assessment and the development of beyond-mean-field methods. These methods address the nuclear many-body problem by coupling single-particle degrees of freedom with more complex configurations and correlations. We summarize here the main results of our studies, and provide insights to possible further developments and perspectives.

We have highlighted the need to overcome the mean-field approximation, used in particular in RPA on top of the HF method, to account for the spreading and the fragmentation of excitation spectra observed experimentally. The SRPA as a mere extension of RPA to 2p2h configurations is a possible approach to go beyond the mean field, but it has important drawbacks. An anomalously large shift of the excitation spectra to lower energies is found in SRPA, compared to the RPA case. Instabilities and imaginary solutions may be obtained due to the fact that the Thouless theorem is not valid in the standard SRPA. In addition, if traditional interactions are employed where the parameters are adjusted at the mean-field level, a risk of double counting correlations exists. If such interactions have a zero range, as is the case for Skyrme interactions, an ultraviolet divergence is generated beyond the mean field, which is visible in a dependence on the cutoff put on 2p2h configurations. We therefore built our developments on a corrected version of SRPA based on a subtraction procedure — the Subtracted SRPA (SSRPA) — which allows us to solve all these drawbacks.

We first carried out an extensive analysis of the capabilities of the SSRPA. Applying this model to the dipole response and the electric polarizability in ^{48}Ca, we first showed the gain in accuracy it allows in accounting for the position of the low-lying excitation energies with the SGII Skyrme parametrization. While the centroids of the giant dipole resonance provided

by the SSRPA are still underestimating the experimental data, an important improvement is observed in the description of the spreading, as seen by the satisfactory reproduction of the slope of the electric dipole polarizability.

We next performed a systematic application of our SSRPA model to the quadrupole response of a range of even-even, spherically-expected medium and heavy-mass nuclei. We obtained in the large majority of the considered nuclei an improved reproduction of the experimental centroid energies compared to RPA, and verified the enhancement of the widths when going from RPA to SSRPA. In addition, we showed that the SSRPA allows for a better description of the fine structure of the excitations, as provided by high-resolution experiments.

A third study involving the SSRPA model was dedicated to the analysis of beyond-mean-field effects in ^{48}Ca and ^{90}Zr. We proposed a method to extract beyond-mean-field effective masses from axial breathing modes in these nuclei, and we highlighted the compression of single-particle spectra which is observed by going beyond the mean-field approximation.

As a second step in our studies, we tackled the possible ways of enriching our models.

Firstly, we extended the method to nuclei with partially-filled orbitals, by using the equal-filling approximation. This provided us with a convenient way of reaching most even-even open-shell nuclei. An approach was introduced to estimate in part the pairing effects in nuclei, by calculating the occupation numbers in a BCS model, which are in turn used in the equal-filling factors. We concluded, by calculating the low-lying states of neutron-rich Argon isotopes, that such an inclusion of pairing correlations allows for a better agreement with recent experimental values than the original SSRPA model. The SSRPA model, on the other side, already improved the agreement with experimental results, compared to the RPA case, owing to the mixing with 2p2h configurations.

Secondly, we investigated the inclusion of beyond-QBA correlations in SRPA, through the iterative computation of occupation numbers carried out using RPA X and Y amplitudes. This allowed us to introduce a correlated ground state. However, the obtained renormalization of SRPA matrix elements revealed to be too weak to correct the problems of standard SRPA, but showed the expected trend towards such correction.

We therefore opened means to improve the description of both low-lying and higher energy excitations of nuclei. Several ways of development could

be followed from this study.

Given the promising results obtained in our estimate inclusion of pairing correlations, a step towards a more complete account of these correlations could be made. A quasiparticle SSRPA approach could be considered.

Alternatively, an estimate approach to pairing effects, similar to that which we introduced in the equal-filling approximation, could be made within the beyond-QBA models, still by computation of occupation numbers in BCS or HFB calculations.

Yet another possible extension along the inclusion of correlations through occupation numbers would be to take into account effects of a non-zero temperature, by introducing a temperature dependence in the one-body density matrix (Fermi distribution), thereby authorizing the study of giant resonances in hot nuclei.

On the other side, reducing the set of approximations (*e.g.* diagonal one-body density matrix) used in the SRPA renormalized beyond the QBA may be beneficial to further extensions. This could allow us to generate stronger correlations in the ground state by the use of X and Y amplitudes and could lead to an alternative method to the subtraction procedure. Such a method could correct the energy-dependent self-energy in such a way to cure the anomalous shift of the excitation spectra which characterises the standard SRPA. Of course, the double counting of correlations and the cutoff dependence of the results would remain in this way open problems if Skyrme interactions are still used.

CHAPTER 7

Appendices

Contents

Appendix 1. Computation of renormalized matrix elements 95
Appendix 2. Expression for the occupation numbers 102

Appendix 1. Computation of renormalized matrix elements

In this section, we present the main derivation steps of the elements of the A_{12} matrix.

Let us start by introducing the following shortcut notations:

$$\left\langle 0\middle|\left[a_k^\dagger a_p,[\hat{V},a_m^\dagger a_n^\dagger a_j a_i]\right]\middle|0\right\rangle = \frac{1}{4}\sum_{\mu,\nu,\mu',\nu'} v_{\mu\nu\mu'\nu'}\left\langle 0\middle|c_{1,22}\middle|0\right\rangle \tag{A1}$$

where we define

$$\begin{aligned} c_{1,22} &:= \left[a_k^\dagger a_p,[a_\mu^\dagger a_\nu^\dagger a_{\nu'} a_{\mu'},a_m^\dagger a_n^\dagger a_j a_i]\right] = \left[a_k^\dagger a_p,c_{22}\right] \\ c_{22} &:= \left[a_\mu^\dagger a_\nu^\dagger a_{\nu'} a_{\mu'},a_m^\dagger a_n^\dagger a_j a_i\right] \end{aligned}$$

We derive

$$c_{22} = a_\mu^\dagger a_\nu^\dagger\left[a_{\nu'}a_{\mu'},a_m^\dagger a_n^\dagger\right]a_j a_i + a_m^\dagger a_n^\dagger\left[a_\mu^\dagger a_\nu^\dagger,a_j a_i\right]a_{\nu'}a_{\mu'}$$

As one always has

$$\left[a_\alpha^\dagger a_\beta^\dagger,a_\epsilon a_\zeta\right] = \mathscr{A}(\alpha,\beta)\,\mathscr{A}(\epsilon,\zeta)\,\delta_{\epsilon\beta}\left(a_\alpha^\dagger a_\zeta - \frac{1}{2}\delta_{\zeta\alpha}\right)$$

one obtains

$$\begin{aligned} c_{22} = \quad & \mathscr{A}(\mu,\nu)\,\mathscr{A}(i,j)\,\delta_{\nu j}\left(a_m^\dagger a_n^\dagger a_\mu^\dagger a_i a_{\nu'}a_{\mu'} - \frac{1}{2}\delta_{\mu i}a_m^\dagger a_n^\dagger a_{\nu'}a_{\mu'}\right) \\ & - \mathscr{A}(\mu',\nu')\,\mathscr{A}(m,n)\,\delta_{\nu' n}\left(a_\mu^\dagger a_\nu^\dagger a_m^\dagger a_{\mu'}a_j a_i - \frac{1}{2}\delta_{\mu' m}a_\mu^\dagger a_\nu^\dagger a_j a_i\right) \end{aligned}$$

and

$$c_{1,22} = \mathscr{A}(\mu,\nu)\,\mathscr{A}(i,j)\,\delta_{\nu j}\left(\left[a_k^\dagger a_p, a_m^\dagger a_n^\dagger a_\mu^\dagger a_i a_{\nu'} a_{\mu'}\right] - \frac{1}{2}\delta_{\mu i}\left[a_k^\dagger a_p, a_m^\dagger a_n^\dagger a_{\nu'} a_{\mu'}\right]\right) - \mathscr{A}(\mu',\nu')\,\mathscr{A}(m,n)\,\delta_{\nu' n}\left(\left[a_k^\dagger a_p, a_\mu^\dagger a_\nu^\dagger a_m^\dagger a_{\mu'} a_j a_i\right] - \frac{1}{2}\delta_{\mu' m}\left[a_k^\dagger a_p, a_\mu^\dagger a_\nu^\dagger a_j a_i\right]\right)$$

By shuffling the indices to get commutators which are as much similar as possible, one may obtain

$$c_{1,22} = \mathscr{A}(\mu,\nu)\,\mathscr{A}(i,j)\,\delta_{\nu j}\left(\left[a_k^\dagger a_p, a_m^\dagger a_n^\dagger a_\mu^\dagger a_i a_{\nu'} a_{\mu'}\right] - \frac{1}{2}\delta_{\mu i}\left[a_k^\dagger a_p, a_m^\dagger a_n^\dagger a_{\nu'} a_{\mu'}\right]\right) - \mathscr{A}(\mu',\nu')\,\mathscr{A}(m,n)\,\delta_{\nu' n}\left(\left[a_k^\dagger a_p, a_m^\dagger a_\nu^\dagger a_\mu^\dagger a_i a_j a_{\mu'}\right] - \frac{1}{2}\delta_{\mu' m}\left[a_k^\dagger a_p, a_\nu^\dagger a_\mu^\dagger a_i a_j\right]\right)$$

We introduce further shortcut notations to ease the later derivations:

$$c_{1,22} = \mathscr{A}(\mu,\nu)\,\mathscr{A}(i,j)\,\delta_{\nu j}\left(c_{13} - \frac{1}{2}\delta_{\mu i} c_{12}\right) - \mathscr{A}(\mu',\nu')\,\mathscr{A}(m,n)\,\delta_{\nu' n}\left(c'_{13} - \frac{1}{2}\delta_{\mu' m} c'_{12}\right)$$

Let us denote by $\tau_{\alpha\to\beta}$ is the operator that changes α into β. Then:

$$\begin{aligned} c_{13} &:= \left[a_k^\dagger a_p, a_m^\dagger a_n^\dagger a_\mu^\dagger a_i a_{\nu'} a_{\mu'}\right] \\ c'_{13} &:= \left[a_k^\dagger a_p, a_m^\dagger a_\nu^\dagger a_\mu^\dagger a_i a_j a_{\mu'}\right] = \tau_{n\to\nu}\tau_{\nu'\to j} c_{13} \\ c_{12} &:= \left[a_k^\dagger a_p, a_m^\dagger a_n^\dagger a_{\nu'} a_{\mu'}\right] \\ c'_{12} &:= \left[a_k^\dagger a_p, a_\nu^\dagger a_\mu^\dagger a_i a_j\right] = \tau_{m\to\nu}\tau_{n\to\mu}\tau_{\nu'\to i}\tau_{\mu'\to j} c_{12} \end{aligned}$$

One derives the first commutator as follows:

$$\begin{aligned} c_{13} = {} & \mathscr{A}(m,n)\,\delta_{pm} a_k^\dagger a_n^\dagger a_\mu^\dagger a_i a_{\nu'} a_{\mu'} \\ & + \mathscr{A}(\mu',\nu')\,\delta_{\nu' k} a_m^\dagger a_n^\dagger a_\mu^\dagger a_i a_{\mu'} a_p \\ & + \delta_{\mu p} a_m^\dagger a_n^\dagger a_k^\dagger a_i a_{\nu'} a_{\mu'} \\ & + \delta_{ki} a_m^\dagger a_n^\dagger a_\mu^\dagger a_p a_{\mu'} a_{\nu'} \end{aligned}$$

Hence

$$\begin{aligned} c'_{13} = {} & \mathscr{A}(m,\nu)\,\delta_{pm} a_k^\dagger a_\nu^\dagger a_\mu^\dagger a_i a_j a_{\mu'} \\ & + \mathscr{A}(\mu',j)\,\delta_{jk} a_m^\dagger a_\nu^\dagger a_\mu^\dagger a_i a_{\mu'} a_p \\ & + \delta_{\mu p} a_m^\dagger a_\nu^\dagger a_k^\dagger a_i a_j a_{\mu'} \\ & + \delta_{ki} a_m^\dagger a_\nu^\dagger a_\mu^\dagger a_p a_{\mu'} a_j \end{aligned}$$

We now take the ground-state expectation value of the commutators:

$$\begin{aligned}\langle 0|c_{13}|0\rangle = \quad & \mathscr{A}(m,n)\,\delta_{pm}e_1 \\ & + \mathscr{A}(\mu',\nu')\,\delta_{\nu' k}e_2 \\ & + \delta_{\mu p}e_3 \\ & + \delta_{ki}e_4\end{aligned}$$

where

$$\begin{aligned}e_1 &:= \langle 0|a_k^\dagger a_n^\dagger a_\mu^\dagger a_i a_{\nu'} a_{\mu'}|0\rangle \\ e_2 &:= \langle 0|a_m^\dagger a_n^\dagger a_\mu^\dagger a_i a_{\mu'} a_p|0\rangle = -\tau_{k\to m}\tau_{\nu'\to p}e_1 \\ e_3 &:= \langle 0|a_m^\dagger a_n^\dagger a_k^\dagger a_i a_{\nu'} a_{\mu'}|0\rangle = -\tau_{\mu\to m}e_1 \\ e_4 &:= \langle 0|a_m^\dagger a_n^\dagger a_\mu^\dagger a_p a_{\mu'} a_{\nu'}|0\rangle = -\tau_{k\to m}\tau_{i\to p}e_1\end{aligned}$$

Applying the two approximations (3.25) and (3.26), one has

$$\begin{aligned}e_1 \simeq \quad & \delta_{\mu i}n_i n_k n_n \mathscr{A}(k,n)\,\delta_{\mu' k}\delta_{\nu' n} \\ & + n_\mu n_k n_n \mathscr{A}(\mu',\nu')\,\delta_{\nu'\mu}\mathscr{A}(k,n)\,\delta_{ik}\delta_{\mu' n}\end{aligned}$$

Hence

$$\begin{aligned}e_2 \simeq\ & -\delta_{\mu i}n_i n_m n_n \mathscr{A}(m,n)\,\delta_{\mu' m}\delta_{pn} \\ & - n_\mu n_m n_n \mathscr{A}(\mu',p)\,\delta_{p\mu}\mathscr{A}(m,n)\,\delta_{im}\delta_{\mu' n} \\ e_3 \simeq\ & -\delta_{mi}n_i n_k n_n \mathscr{A}(k,n)\,\delta_{\mu' k}\delta_{\nu' n} \\ & - n_m n_k n_n \mathscr{A}(\mu',\nu')\,\delta_{\nu' m}\mathscr{A}(k,n)\,\delta_{ik}\delta_{\mu' n} \\ e_4 \simeq\ & -\delta_{\mu p}n_p n_m n_n \mathscr{A}(m,n)\,\delta_{\mu' m}\delta_{\nu' n} \\ & - n_\mu n_m n_n \mathscr{A}(m,n)\,\delta_{pm}\mathscr{A}(\mu',\nu')\,\delta_{\nu'\mu}\delta_{\mu' n}\end{aligned}$$

Therefore, one finally gets

$$\begin{aligned}\langle 0|c_{13}|0\rangle = \quad & \mathscr{A}(m,n)\,\delta_{pm}\delta_{\mu i}n_i n_k n_n \mathscr{A}(k,n)\,\delta_{\mu' k}\delta_{\nu' n} \\ & + \mathscr{A}(m,n)\,\delta_{pm}n_\mu n_k n_n \mathscr{A}(\mu',\nu')\,\delta_{\nu'\mu}\mathscr{A}(k,n)\,\delta_{ik}\delta_{\mu' n} \\ & - \mathscr{A}(\mu',\nu')\,\delta_{\nu' k}\delta_{\mu i}n_i n_m n_n \mathscr{A}(m,n)\,\delta_{\mu' m}\delta_{pn} \\ & - \mathscr{A}(\mu',\nu')\,\delta_{\nu' k}n_\mu n_m n_n \mathscr{A}(\mu',p)\,\delta_{p\mu}\mathscr{A}(m,n)\,\delta_{im}\delta_{\mu' n} \\ & - \delta_{\mu p}\delta_{mi}n_i n_k n_n \mathscr{A}(k,n)\,\delta_{\mu' k}\delta_{\nu' n} \\ & - \delta_{\mu p}n_m n_k n_n \mathscr{A}(\mu',\nu')\,\delta_{\nu' m}\mathscr{A}(k,n)\,\delta_{ik}\delta_{\mu' n} \\ & - \delta_{ki}\delta_{\mu p}n_p n_m n_n \mathscr{A}(m,n)\,\delta_{\mu' m}\delta_{\nu' n} \\ & - \delta_{ki}n_\mu n_m n_n \mathscr{A}(m,n)\,\delta_{pm}\mathscr{A}(\mu',\nu')\,\delta_{\nu'\mu}\delta_{\mu' n}\end{aligned}$$

With further factorizing, one has

$$\begin{aligned}\langle 0|c_{13}|0\rangle = \quad & n_i n_k \mathscr{A}(m,n)\,\delta_{pm} n_n \delta_{\mu i}\mathscr{A}(k,n)\,\delta_{\mu' k}\delta_{\nu' n}\\ & + n_k \mathscr{A}(m,n)\,\delta_{pm} n_n \mathscr{A}(k,n)\,\delta_{ik} n_\mu \mathscr{A}(\mu',\nu')\,\delta_{\nu'\mu}\delta_{\mu' n}\\ & - n_i n_m n_n \mathscr{A}(m,n)\,\delta_{pn}\delta_{\mu i}\mathscr{A}(\mu',\nu')\,\delta_{\nu' k}\delta_{\mu' m}\\ & - n_m n_n \mathscr{A}(m,n)\,\delta_{im} n_\mu \mathscr{A}(\mu',\nu')\,\delta_{\nu' k}\mathscr{A}(\mu',p)\,\delta_{p\mu}\delta_{\mu' n}\\ & - \delta_{mi} n_i n_k n_n \mathscr{A}(k,n)\,\delta_{\mu p}\delta_{\mu' k}\delta_{\nu' n}\\ & - n_m n_k n_n \mathscr{A}(k,n)\,\delta_{ik}\delta_{\mu p}\mathscr{A}(\mu',\nu')\,\delta_{\nu' m}\delta_{\mu' n}\\ & - \delta_{ki} n_p n_m n_n \mathscr{A}(m,n)\,\delta_{\mu p}\delta_{\mu' m}\delta_{\nu' n}\\ & - \delta_{ki} n_m n_n \mathscr{A}(m,n)\,\delta_{pm} n_\mu \mathscr{A}(\mu',\nu')\,\delta_{\nu'\mu}\delta_{\mu' n}\end{aligned}$$

Similarly:

$$\begin{aligned}\left\langle 0\left|c'_{13}\right|0\right\rangle = \quad & n_i n_k \mathscr{A}(m,\nu)\,\delta_{pm}\delta_{\mu i} n_\nu \mathscr{A}(k,\nu)\,\delta_{\mu' k}\delta_{j\nu}\\ & + n_k \mathscr{A}(m,\nu)\,\delta_{pm} n_\mu n_\nu \mathscr{A}(\mu',j)\,\delta_{j\mu}\mathscr{A}(k,\nu)\,\delta_{ik}\delta_{\mu'\nu}\\ & - n_i n_m \mathscr{A}(\mu',j)\,\delta_{jk}\delta_{\mu i} n_\nu \mathscr{A}(m,\nu)\,\delta_{\mu' m}\delta_{p\nu}\\ & - n_m n_\nu \mathscr{A}(m,\nu)\,\delta_{im}\mathscr{A}(\mu',j)\,\delta_{jk} n_\mu \mathscr{A}(\mu',p)\,\delta_{p\mu}\delta_{\mu'\nu}\\ & - n_i n_k \delta_{mi}\delta_{\mu p} n_\nu \mathscr{A}(k,\nu)\,\delta_{\mu' k}\delta_{j\nu}\\ & - n_m n_k \delta_{\mu p} n_\nu \mathscr{A}(\mu',j)\,\delta_{jm}\mathscr{A}(k,\nu)\,\delta_{ik}\delta_{\mu'\nu}\\ & - n_p n_m \delta_{ki}\delta_{\mu p} n_\nu \mathscr{A}(m,\nu)\,\delta_{\mu' m}\delta_{j\nu}\\ & - \delta_{ki} n_m n_\mu n_\nu \mathscr{A}(m,\nu)\,\delta_{pm}\mathscr{A}(\mu',j)\,\delta_{j\mu}\delta_{\mu'\nu}\end{aligned}$$

Let us now evaluate the remaining commutators:

$$\begin{aligned}c_{12} = \quad & \mathscr{A}(m,n)\,\delta_{pm} a_k^\dagger a_n^\dagger a_{\nu'} a_{\mu'}\\ & + \mathscr{A}(\mu',\nu')\,\delta_{\nu' k} a_m^\dagger a_n^\dagger a_{\mu'} a_p\end{aligned}$$

and

$$\begin{aligned}\left\langle 0\left|c_{12}\right|0\right\rangle = \quad & \mathscr{A}(m,n)\,\delta_{pm} f_1\\ & + \mathscr{A}(\mu',\nu')\,\delta_{\nu' k} f_2\end{aligned}$$

where

$$\begin{aligned}f_1 &:= \left\langle 0\left|a_k^\dagger a_n^\dagger a_{\nu'} a_{\mu'}\right|0\right\rangle\\ f_2 &:= \left\langle 0\left|a_m^\dagger a_n^\dagger a_{\mu'} a_p\right|0\right\rangle = -\tau_{k\to m}\tau_{\nu'\to p} f_1\end{aligned}$$

By applying the two approximations, one obtains

$$\begin{aligned}f_1 &\simeq n_k n_n \mathscr{A}(k,n)\,\delta_{\mu' k}\delta_{\nu' n}\\ f_2 &\simeq -n_m n_n \mathscr{A}(m,n)\,\delta_{\mu' m}\delta_{pn}\end{aligned}$$

Hence

$$\begin{aligned}\langle 0|c_{12}|0\rangle \;=\;& n_k \mathscr{A}(m,n)\,\delta_{pm} n_n \mathscr{A}(k,n)\,\delta_{\mu' k}\delta_{\nu' n} \\ & - n_m n_n \mathscr{A}(m,n)\,\mathscr{A}(\mu',\nu')\,\delta_{\nu' k}\delta_{\mu' m}\delta_{pn}\end{aligned}$$

Similarly:

$$\begin{aligned}\left\langle 0\left|c'_{12}\right|0\right\rangle \;=\;& \mathscr{A}(\nu,\mu)\,\delta_{p\nu} n_k n_\mu \mathscr{A}(k,\mu)\,\delta_{jk}\delta_{i\mu} \\ & - \mathscr{A}(j,i)\,\delta_{ik} n_\nu n_\mu \mathscr{A}(\nu,\mu)\,\delta_{j\nu}\delta_{p\mu}\end{aligned}$$

We now regroup the above results in the overall sum:

$$\begin{aligned}\sum_{\mu,\nu,\mu',\nu'} v_{\mu\nu\mu'\nu'}\left\langle 0\left|c_{1,22}\right|0\right\rangle \;=\; \sum_{\mu,\nu,\mu',\nu'} v_{\mu\nu\mu'\nu'}\Bigg(\;& \mathscr{A}(\mu,\nu)\,\mathscr{A}(i,j)\,\delta_{\nu j} \\ & \times\left(\langle 0|c_{13}|0\rangle - \frac{1}{2}\delta_{\mu i}\langle 0|c_{12}|0\rangle\right) \\ & - \mathscr{A}(\mu',\nu')\,\mathscr{A}(m,n)\,\delta_{\nu' n} \\ & \times\left(\left\langle 0\left|c'_{13}\right|0\right\rangle - \frac{1}{2}\delta_{\mu' m}\left\langle 0\left|c'_{12}\right|0\right\rangle\right)\Bigg)\end{aligned}$$

$$\begin{aligned}\sum_{\mu,\nu,\mu',\nu'} v_{\mu\nu\mu'\nu'}\left\langle 0\left|c_{1,22}\right|0\right\rangle \;=\; \sum_{\mu,\nu,\mu',\nu'} v_{\mu\nu\mu'\nu'}\Bigg(\;& \mathscr{A}(i,j)\,\delta_{\nu j} \\ & \times\left(\langle 0|c_{13}|0\rangle - \frac{1}{2}\delta_{\mu i}\langle 0|c_{12}|0\rangle\right) \\ & - \mathscr{A}(i,j)\,\delta_{\mu j} \\ & \times\left(\left\langle 0\left|\tau_{\mu\to\nu}c_{13}\right|0\right\rangle - \frac{1}{2}\delta_{\nu i}\langle 0|c_{12}|0\rangle\right) \\ & - \mathscr{A}(m,n)\,\delta_{\nu' n} \\ & \times\left(\left\langle 0\left|c'_{13}\right|0\right\rangle - \frac{1}{2}\delta_{\mu' m}\left\langle 0\left|c'_{12}\right|0\right\rangle\right) \\ & + \mathscr{A}(m,n)\,\delta_{\mu' n} \\ & \times\left(\left\langle 0\left|\tau_{\mu\to\nu}c'_{13}\right|0\right\rangle - \frac{1}{2}\delta_{\nu' m}\left\langle 0\left|c'_{12}\right|0\right\rangle\right)\Bigg)\end{aligned}$$

$$\begin{aligned}\sum_{\mu,\nu,\mu',\nu'} v_{\mu\nu\mu'\nu'} \left\langle 0 \left| c_{1,22} \right| 0 \right\rangle = \quad & \mathscr{A}(i,j) \Bigg(\sum_{\mu,\mu',\nu'} v_{\mu j\mu'\nu'} \langle 0 | c_{13} | 0 \rangle \\ & - \frac{1}{2} \sum_{\mu',\nu'} v_{ij\mu'\nu'} \langle 0 | c_{12} | 0 \rangle \Bigg) \\ & - \mathscr{A}(i,j) \Bigg(\sum_{\nu,\mu',\nu'} v_{j\nu\mu'\nu'} \left\langle 0 \left| \tau_{\mu\to\nu} c_{13} \right| 0 \right\rangle \\ & - \frac{1}{2} \sum_{\mu',\nu'} v_{ji\mu'\nu'} \langle 0 | c_{12} | 0 \rangle \Bigg) \\ & - \mathscr{A}(m,n) \Bigg(\sum_{\mu,\nu,\mu'} v_{\mu\nu\mu' n} \left\langle 0 \left| c'_{13} \right| 0 \right\rangle \\ & - \frac{1}{2} \sum_{\mu,\nu} v_{\mu\nu mn} \left\langle 0 \left| c'_{12} \right| 0 \right\rangle \Bigg) \\ & + \mathscr{A}(m,n) \Bigg(\sum_{\mu,\nu,\nu'} v_{\mu\nu n\nu'} \left\langle 0 \left| \tau_{\mu'\to\nu'} c'_{13} \right| 0 \right\rangle \\ & - \frac{1}{2} \sum_{\mu,\nu} v_{\mu\nu nm} \left\langle 0 \left| c'_{12} \right| 0 \right\rangle \Bigg)\end{aligned}$$

Now

$$\begin{aligned}\sum_{\nu,\mu',\nu'} v_{j\nu\mu'\nu'} \left\langle 0 \left| \tau_{\mu\to\nu} c_{13} \right| 0 \right\rangle &= - \sum_{\mu,\mu',\nu'} v_{\mu j\mu'\nu'} \langle 0 | c_{13} | 0 \rangle \\ \sum_{\mu,\nu,\nu'} v_{\mu\nu n\nu'} \left\langle 0 \left| \tau_{\mu'\to\nu'} c'_{13} \right| 0 \right\rangle &= - \sum_{\mu,\nu,\mu'} v_{\mu\nu\mu' n} \left\langle 0 \left| c'_{13} \right| 0 \right\rangle \\ \sum_{\mu',\nu'} v_{ji\mu'\nu'} \langle 0 | c_{12} | 0 \rangle &= - \sum_{\mu',\nu'} v_{ij\mu'\nu'} \langle 0 | c_{12} | 0 \rangle \\ \sum_{\mu,\nu} v_{\mu\nu nm} \left\langle 0 \left| c'_{12} \right| 0 \right\rangle &= - \sum_{\mu,\nu} v_{\mu\nu mn} \left\langle 0 \left| c'_{12} \right| 0 \right\rangle\end{aligned}$$

Thus finally

$$\begin{aligned}\sum_{\mu,\nu,\mu',\nu'} v_{\mu\nu\mu'\nu'} \left\langle 0 \left| c_{1,22} \right| 0 \right\rangle = \quad & \mathscr{A}(i,j) \Bigg(2 \sum_{\mu,\mu',\nu'} v_{\mu j\mu'\nu'} \langle 0 | c_{13} | 0 \rangle \\ & - \sum_{\mu',\nu'} v_{ij\mu'\nu'} \langle 0 | c_{12} | 0 \rangle \Bigg) \\ & - \mathscr{A}(m,n) \Bigg(2 \sum_{\mu,\nu,\mu'} v_{\mu\nu\mu' n} \left\langle 0 \left| c'_{13} \right| 0 \right\rangle \\ & - \sum_{\mu,\nu} v_{\mu\nu mn} \left\langle 0 \left| c'_{12} \right| 0 \right\rangle \Bigg)\end{aligned}$$

After evaluation of the sums and gathering all the terms, on obtains

$$\begin{aligned}\left\langle 0\middle|\left[a_k^\dagger a_p,[\hat{V},a_m^\dagger a_n^\dagger a_j a_i]\right]\middle|0\right\rangle \simeq\quad & \frac{1}{2}\mathscr{A}(m,n)\,\mathscr{A}(i,j)\,\delta_{pm}v_{ijnk}\\ & \times(n_k-n_p)\big[n_i(n_j-n_n)-n_n(n_i-1)\big]\\ & +\frac{1}{2}\mathscr{A}(m,n)\,\mathscr{A}(i,j)\,\delta_{ki}v_{pjmn}\\ & \times(n_k-n_p)\big[n_j(1-n_m)-n_m(n_j-n_n)\big]\\ & +\mathscr{A}(m,n)\,\mathscr{A}(i,j)\,\delta_{pm}\delta_{ki}\\ & \times(n_k-n_p)(n_j-n_n)\sum_\mu v_{j\mu\mu n}n_\mu\end{aligned}$$

Using the fact that the interaction is antisymmetrized to simplify some antisymmetrizers:

$$\begin{aligned}\left\langle 0\middle|\left[a_k^\dagger a_p,[\hat{V},a_m^\dagger a_n^\dagger a_j a_i]\right]\middle|0\right\rangle \simeq\quad & \mathscr{A}(m,n)\,\delta_{pn}v_{ijkm}\\ & \times(n_k-n_p)\big[n_m(1-n_i-n_j)+n_in_j\big]\\ & +\mathscr{A}(i,j)\,\delta_{kj}v_{ipmn}\\ & \times(n_k-n_p)\big[n_i(1-n_m-n_n)+n_mn_n\big]\\ & +\mathscr{A}(m,n)\,\mathscr{A}(i,j)\,\delta_{pn}\delta_{kj}\\ & \times(n_k-n_p)(n_i-n_m)\sum_\mu v_{i\mu\mu m}n_\mu\end{aligned}\tag{A2}$$

Appendix 2. Expression for the occupation numbers

In this Appendix, we derive the main equations of the number operator method [193]. The main goal here is to obtain an expression for the diagonal elements n_α of the one-body density matrix $\rho_{\alpha\beta} := \langle 0| a^\dagger_\beta a_\alpha |0\rangle$, as functions of the amplitudes X and Y of the RPA excitation operators. Indeed, as we use the approximation (3.25) in our models, the two-body elements appearing in the (S)RPA matrix elements are just combinations of one-body elements.

In the following notations, we do not display the couplings to quantum numbers for simplicity.

We start with a general property of the number operator $\hat{N} = \sum_\alpha a^\dagger_\alpha a_\alpha$ (where α labels here a single-particle state) that can be readily proven: with P_n a product of any n annihilation operators $P_n = \prod_{q=1}^n a_{\alpha_q}$, and with $\left|\xi\right\rangle$ any state of A fermions, one has:

$$\hat{N}\, P_n \left|\xi\right\rangle = (A-n)\, P_n \left|\xi\right\rangle . \tag{A3}$$

We then use this property to derive the following equation for a particle-state m:

$$\begin{aligned} n_m &= \frac{1}{A-1} \sum_\alpha \langle 0| a^\dagger_m a^\dagger_\alpha a_\alpha a_m |0\rangle \\ &= \frac{1}{A-1} \Big(\sum_i \langle 0| a^\dagger_m a^\dagger_i a_i a_m |0\rangle + \sum_n \langle 0| a^\dagger_m a^\dagger_n a_n a_m |0\rangle \Big), \end{aligned} \tag{A4}$$

where, as usual, i and n label hole-states and particle-states respectively.

By rearranging the hole-state indices, on gets

$$n_m = \sum_i \langle 0| a^\dagger_m a_i a^\dagger_i a_m |0\rangle - \sum_n \langle 0| a^\dagger_m a^\dagger_n a_n a_m |0\rangle \ , \tag{A5}$$

and using the completeness of the RPA excited states (labeled by ν), one has

$$n_m = \sum_\nu \sum_i \left| \langle 0| a^\dagger_m a_i |\nu\rangle \right|^2 - \sum_n \langle 0| a^\dagger_m a^\dagger_n a_n a_m |0\rangle \ . \tag{A6}$$

Now employing the expression of the RPA excitation operator (2.21), one can derive the following relation between the first term of Eq. (A6) and the Y amplitudes, by assuming that creation and annihilation operators satisfy boson commutation relations (as in the QBA):

$$\sum_\nu \sum_i \left| \langle 0| a^\dagger_m a_i |\nu\rangle \right|^2 \simeq \sum_\nu \sum_i |Y_{mi}(\nu)|^2 \ . \tag{A7}$$

The second term can be evaluated by inserting twice the number operator in the expectation value and using again the property (A3):

$$\langle 0|\, a_m^\dagger a_n^\dagger a_n a_m \,|0\rangle \;=\; \frac{1}{(A-2)(A-3)} \sum_{\alpha,\beta} \langle 0|\, a_m^\dagger a_n^\dagger a_\alpha^\dagger a_\beta^\dagger a_\beta a_\alpha a_n a_m \,|0\rangle \;.$$

It is then possible to apply a similar treatment as that applied to $\sum_\alpha \langle 0|\, a_m^\dagger a_\alpha^\dagger a_\alpha a_m \,|0\rangle$ in Eq. (A4), and use again the completeness of the RPA excited states, as we did previously. Explicitly displaying only terms of quadratic order in the amplitudes, one finally gets

$$\sum_n \langle 0|\, a_m^\dagger a_n^\dagger a_n a_m \,|0\rangle \;=\; \frac{1}{2} \sum_\nu \sum_i |Y_{mi}(\nu)|^2 + O(|Y^4|)\,. \tag{A8}$$

Gathering the two terms (A7) and (A8), Eq. (A6) simply becomes

$$n_m \;\simeq\; \frac{1}{2} \sum_\nu \sum_i |Y_{mi}(\nu)|^2 + O(|Y^4|)\,. \tag{A9}$$

A similar derivation applied to the occupation number of a hole-state i yields:

$$n_i \;\simeq\; 1 - \frac{1}{2} \sum_\nu \sum_m |Y_{mi}(\nu)|^2 + O(|Y^4|)\,. \tag{A10}$$

Equations (A9) and (A10) are the expressions used in our applications of SRPA renormalized with RPA occupation numbers calculated iteratively.

Résumé en français

Contents

1 Introduction 105
2 Méthodes de champ moyen en théorie des fonctionnelles de la densité 106
2.1 Fonctionnelles de la densité 106
2.2 La méthode de Hartree-Fock 107
2.3 RPA basée sur l'état de HF 108
3 Une approche au-delà du champ moyen comme point de départ: SRPA 110
3.1 Formalisme 110
3.2 Inconvénients de la SRPA standard 112
4 Une correction de la SRPA: SRPA avec soustraction 112
4.1 Principe de la SRPA avec soustraction 112
4.2 Résultats: Polarisabilité et réponse dipolaire de ^{48}Ca 113
4.3 Résultats: Réponse quadrupolaire: systématiques sur une sélection de noyaux 114
4.4 Résultats: Effets au-delà du champ moyen sur les masses effectives 115
5 Extensions du modèle 116
5.1 Noyaux à orbitales partiellement occupées et appariement 116
5.2 Extension au-delà de la QBA 118
6 Conclusion générale et perspectives 119

1 Introduction

Les noyaux atomiques sont généralement qualifiés de systèmes complexes. Cette complexité ressort d'une part du fait qu'ils constituent des systèmes quantiques à N corps, d'autre part de la grande diversité des phénomènes qu'ils engendrent.

La présente étude se place à des échelles d'énergie basse, auxquelles on considère les noyaux comme étant constitués de protons et de neutrons. Ces particules sont supposées ponctuelles et sans structure interne, et sont considérées comme les degrés de liberté pertinents des noyaux.

Nous étudions les noyaux en utilisant des techniques pour les systèmes à N corps, où N est ici le nombre de nucléons (A neutrons et Z protons). Ces

techniques sont également utilisées dans d'autres domaines de la physique, tels que la physique atomique, la physique de la matière condensée, la chimie, ou l'astrophysique nucléaire.

L'étude des noyaux atomiques fait également souvent appel à des concepts et méthodes utilisés pour décrire la matière nucléaire. Cette dernière est un système nucléaire idéalisé, infini, dont les propriétés peuvent être reliées à celles des noyaux.

Les développements théoriques et les applications de la présente étude sont basés sur le modèle de second random-phase approximation (SRPA), qui est appliqué dans le cadre des fonctionnelles de la densité (EDF). Nous supposons que les noyaux sont à symétrie sphérique et ne traitons que le cas des noyaux pair-pair (A et Z pairs).

L'objectif de notre étude est d'obtenir une description microscopique la plus précise possible des excitations nucléaires collectives, en particulier les excitations de basse énergie et les résonances géantes.

Une attention particulière est portée est la description de la largeur des résonances géantes. Cette dernière peut être divisée de manière conceptuelle en trois contributions: la largeur de damping Landau — provenant de la présence d'états non collectifs dans la région de l'état collectif —, la largeur de spreading — provenant du couplage des configurations 1 particule-1 trou (1p1h) avec des configurations d'ordre supérieur (2 particules-2 trous (2p2h), etc.) — et la largeur d'escape — provenant du couplage avec des états du continuum. Cette dernière contribution n'est pas prise en compte dans notre étude, du fait de l'absence de couplage avec le continuum.

2 Méthodes de champ moyen en théorie des fonctionnelles de la densité

2.1 Fonctionnelles de la densité

De façon analogue aux théories de la fonctionnelle de la densité (DFT), l'énergie d'un système nucléaire peut être écrite comme une fonctionnelle de sa densité. À la différence des application usuelles de la DFTs, où la cohérence des systèmes est assurée par un potentiel externe, les noyaux atomiques sont liés par l'action de leurs propres constituants. Il est possible d'obtenir des équations de champ moyen pour les noyaux atomiques qui sont similaires aux équations de Kohn-Sham, qui dérivent des théorèmes de

Hohenberg-Kohn sur lesquels sont fondés les DFTs. Cependant, les EDFs nucléaires ont été développées sur des bases empiriques et non sur de tels théorèmes.

Les EDFs nucléaires sont généralement dérivées d'interactions effectives phénoménologiques. Ces interactions contiennent des paramètres ajustés sur une sélection d'observables des noyaux et sur des propriétés de la matière nucléaire. Les modèles microscopiques utilisant des EDFs ont été employés depuis les années 1970, et on généralement permis une description satisfaisante des propriétés globales des noyaux. Ces modèles s'appliquent en principe à toute la carte des noyaux.

Les deux types d'interactions effectives les plus couramment utilisées sont les interactions de Skyrme [13–15] et de Gogny [16, 17]. Toutes les applications de notre étude emploient l'interaction de Skyrme.

Notons que certaines propriétés des EDFs nucléaires (portée nulle; dépendance en densité) peuvent engendrer, au-delà de l'approximation de champ moyen, des problèmes tels que le double comptage de corrélations, des instabilités et des divergences.

2.2 La méthode de Hartree-Fock

Le formalisme utilisé dans nos développements est celui de la seconde quantification. L'état du système vide de particules est noté $|-\rangle$, sauf indication contraire.

L'expression générale du hamiltonien employé est la suivante:

$$\hat{H} = \hat{T} + \hat{V} = \sum_{\mu,\mu'} T_{\mu\mu'} a^\dagger_\mu a_{\mu'} + \frac{1}{4} \sum_{\mu,\nu,\mu',\nu'} v_{\mu\nu\mu'\nu'} a^\dagger_\mu a^\dagger_\nu a_{\nu'} a_{\mu'} , \qquad \text{(i)}$$

où $T_{\mu\mu'}$ un élément de matrice de l'opérateur d'énergie cinétique dans l'espace d'états de simple-particule, et $v_{\mu\nu\mu'\nu'}$ est un élément de matrice antisymétrisé du potentiel à deux corps:

$$\begin{aligned} T_{\alpha\beta} &:= \langle\alpha|\,\hat{T}\,|\beta\rangle\,, \\ v_{\alpha\beta\gamma\delta} &:= \langle\alpha\beta|\,\hat{V}\,|\gamma\delta\rangle - \langle\alpha\beta|\,\hat{V}\,|\delta\gamma\rangle = -v_{\beta\alpha\gamma\delta} = -v_{\alpha\beta\delta\gamma}\,. \end{aligned}$$

En supposant un état fondamental où les états de plus basse énergie sont occupés par des nucléons, les états inoccupés sont appelés état de particule et les états occupés sont appelés état de trou. Sauf indication contraire, nous utilisons conventionnellement les indices i, j, k, l pour faire référence à des états de trou, et les indices m, n, p, q pour faire référence à des états de

particule, tandis que des lettres grecques sont utilisées lorsque la distinction entre les deux n'est pas faite.

La méthode de Hartree-Fock (HF) permet dans notre cas d'obtenir l'état fondamental sur lequel nos applications de la random-phase approximation (RPA) sont initialement basées. La détermination de cet état consiste en une méthode variationnelle, où l'énergie du système

$$E(\Psi) := \frac{\left\langle \Psi \left| \hat{H} \right| \Psi \right\rangle}{\langle \Psi | \Psi \rangle} \tag{ii}$$

doit être minimisée par l'état $|\Psi\rangle$ que l'on cherche, et qui est supposé être un déterminant de Slater.

Au terme d'une dérivation utilisant ces hypothèses, les équations de HF sont obtenues:

$$\sum_{\nu} \left(T_{\alpha\nu} + \sum_{k=1}^{A} \sum_{\mu,\mu'} v_{\alpha\mu\beta\mu'} D_{\mu' k} D^{*}_{\mu k} \right) D_{\nu\beta} = \epsilon^{\mathrm{HF}}_{\alpha} D_{\alpha\beta} \,. \tag{iii}$$

Dans ces équations, D est une transformation unitaire permettant le passage de la base d'états simple-particule initiale à la base HF, et $\epsilon^{\mathrm{HF}}_{\alpha}$ est l'énergie de l'état simple-particule α.

2.3 RPA basée sur l'état de HF

Les excitations d'un système à N corps dont la dynamique est caractérisée par un hamiltonien $\hat{H}$ sont décrites par les équations du mouvement [41]:

$$\forall R,\ \forall \lambda \in \mathscr{H},\ \left\langle 0 \left| \left[R, [\hat{H}, Q^{\dagger}_{\lambda}] \right] \right| 0 \right\rangle = \hbar\omega_{\lambda} \left\langle 0 \left| \left[R, Q^{\dagger}_{\lambda} \right] \right| 0 \right\rangle, \tag{iv}$$

où $|0\rangle$ est l'état fondamental du système, R un opérateur sur l'espace de Hilbert $\mathscr{H}$, $|\lambda\rangle$ un état propre (état excité) du hamiltonien associé à l'énergie d'excitation ω_{λ}, et $Q^{\dagger}_{\lambda}$ l'opérateur d'excitation, dont l'application à $|0\rangle$ donne $|\lambda\rangle$:

$$\begin{cases} Q^{\dagger}_{\lambda} |0\rangle = |\lambda\rangle & \text{(v)} \\ Q_{\lambda} |0\rangle = 0 \,. & \text{(vi)} \end{cases}$$

L'objectif général de la méthode est de déterminer l'ensemble des états excités $|\lambda\rangle$ et des énergies ω_{λ} du noyau en résolvant les équations (iv).

L'hypothèse de départ de la RPA est la forme de l'opérateur d'excitation, où seules des configurations 1p1h interviennent:

$$Q^{\dagger}_{\nu} := \sum_{m,i} \left(X_{mi}(\nu)\, \alpha^{\dagger}_{mi} - Y_{mi}(\nu)\, \alpha_{mi} \right), \tag{vii}$$

avec

$$\alpha^{\dagger}_{mi} := a^{\dagger}_{m} a_{i} \,. \tag{viii}$$

Les amplitudes "X" and "Y" de l'opérateur d'excitation sont des inconnues du problème.

Les équations du mouvement (iv) peuvent alors être réécrites sous la forme matricielle suivante (équations RPA):

$$\begin{pmatrix} A & B \\ B^* & A^* \end{pmatrix} \begin{pmatrix} X(\nu) \\ Y(\nu) \end{pmatrix} = \hbar\omega_{\nu} \begin{pmatrix} G & 0 \\ 0 & -G^* \end{pmatrix} \begin{pmatrix} X(\nu) \\ Y(\nu) \end{pmatrix}, \tag{ix}$$

où A, B et G sont des blocs matriciels.
Dans ces équations, les matrices

$$\mathscr{S} := \begin{pmatrix} A & B \\ B^* & A^* \end{pmatrix} \tag{x}$$

et

$$\mathscr{M} := \begin{pmatrix} G & 0 \\ 0 & -G^* \end{pmatrix} \tag{xi}$$

sont respectivement appelées matrice de stabilité et métrique, et sont hermitiennes.

Un état propre $|\nu\rangle$ est dit stable si son énergie $\hbar\omega_{\nu}$, telle que calculée en résolvant l'Eq. (2.29), est réelle. Le théorème de Thouless [42] établit l'équivalence entre la minimisation de la valeur moyenne du hamiltonien $\left\langle \psi \left| \hat{H} \right| \psi \right\rangle$ par un déterminant de Slater $|\psi\rangle$ et la stabilité des solutions des équations RPA, lorsque $|\psi\rangle$ est pris comme étant l'état fondamental dans ces équations. Pour satisfaire cette condition de minimisation, il est nécessaire que la matrice de stabilité $\mathscr{S}$ de la RPA soit positive.

Une relation de normalisation des amplitudes X et Y de la RPA peut être obtenue en imposant l'orthonormalité des états excités:

$$\langle \lambda' | \lambda \rangle = \delta_{\lambda\lambda'} \,. \tag{xii}$$

On obtient finalement

$$\delta_{\lambda\lambda'} = \sum_{m,i,n,j} \left(X^*_{mi}(\lambda') X_{nj}(\lambda) G_{mi,nj} - Y^*_{mi}(\lambda') Y_{nj}(\lambda) G^*_{mi,nj} \right) \tag{xiii}$$

$$= \begin{pmatrix} X^{\dagger}(\nu) & Y^{\dagger}(\nu) \end{pmatrix} \mathscr{M} \begin{pmatrix} X(\nu) \\ Y(\nu) \end{pmatrix}. \tag{xiv}$$

Enfin, étant donné un opérateur à 1 corps

$$\hat{F} = \sum_{\alpha,\beta} \langle \alpha | \hat{F} | \beta \rangle a^{\dagger}_{\alpha} a_{\beta} ,$$

on établit l'expression de son amplitude de transition $\langle \lambda | \hat{F} | 0 \rangle$ en fonction des amplitudes RPA:

$$\langle \lambda | \hat{F} | 0 \rangle = \sum_{m,i,n,j} \left(X^{*}_{mi}(\lambda) \langle n | \hat{F} | j \rangle - Y^{*}_{mi}(\lambda) \langle j | \hat{F} | n \rangle \right) G^{*}_{mi,nj} . \tag{xv}$$

Notons que la RPA standard repose sur l'approximation de quasiboson (QBA), selon laquelle l'état fondamental corrélé (exact) $|0\rangle$ est approximé par l'état de HF $|\mathrm{HF}\rangle$ dans la construction des blocs matriciels A, B et G:

$$\begin{aligned} \left\langle 0 \left| \left[a^{\dagger}_{i} a_{m}, a^{\dagger}_{n} a_{j} \right] \right| 0 \right\rangle &= \delta_{mn}\delta_{ij} - \delta_{mn} \left\langle 0 \left| a_{j} a^{\dagger}_{i} \right| 0 \right\rangle - \delta_{ij} \left\langle 0 \left| a_{n} a^{\dagger}_{m} \right| 0 \right\rangle \\ &\simeq \delta_{mn}\delta_{ij} = \left\langle \mathrm{HF} \left| \left[a^{\dagger}_{i} a_{m}, a^{\dagger}_{n} a_{j} \right] \right| \mathrm{HF} \right\rangle . \end{aligned} \tag{xvi}$$

Cette approximation constitue une incohérence dans le formalisme et ne respecte pas le principe de Pauli.

3 Une approche au-delà du champ moyen comme point de départ: SRPA

3.1 Formalisme

La RPA a été employée avec succès dans le passé pour décrire les états de basse énergie des noyaux et les résonances géantes. Cependant, ce modèle ne permet pas de fournir une description réaliste de la largeur de spreading et de la fragmentation des excitation. Il est en effet nécessaire d'inclure des configurations plus complexes que les configurations 1p1h.

Une possibilité est l'inclusion de configurations 2p2h, ce qui est le cas de la SRPA. L'espace des configurations est ainsi considérablement étendu, limitant les applications de la SRPA à des calculs à fortes approximations par le passé [50–54].

Récemment, des applications de la SRPA ont pu être réalisée en réduisant de manière importante l'usage d'approximations [55–60].

Comme dans le cas de la RPA, nous dérivons les équations de la SRPA à partir des équations du mouvement (iv). L'opérateur d'excitation s'écrit désormais

$$Q^\dagger_\nu := \sum_{m,i} \left(X_{mi}(\nu)\, \alpha^\dagger_{mi} - Y_{mi}(\nu)\, \alpha_{mi} \right) + \sum_{\substack{m,n>m \\ i,j>i}} \left(X_{mnij}(\nu)\, \alpha^\dagger_{mnij} - Y_{mnij}(\nu)\, \alpha_{mnij} \right), \tag{xvii}$$

avec

$$\alpha^\dagger_{mi} := a^\dagger_m a_i\,, \tag{xviii}$$

$$\alpha^\dagger_{mnij} := a^\dagger_m a^\dagger_n a_j a_i\,. \tag{xix}$$

Avec cette hypothèse, la réécriture des équations du mouvement sous forme matricielle aboutit à des équations de la même forme que celles de la RPA (Eq. (ix)), où les blocs matriciels sont cependant de taille bien supérieure du fait de l'inclusion des configurations 2p2h.

La relation de normalisation s'écrit alors

$$\delta_{\lambda\lambda'} \simeq \sum_{m,i,n,j} \left(X^*_{mi}(\lambda') X_{nj}(\lambda)\, G_{mi,nj} - Y^*_{mi}(\lambda')\, Y_{nj}(\lambda)\, G^*_{mi,nj} \right) + \sum_{\substack{p,m,k,i, \\ q>p,n>m, \\ l>k,j>i}} \left(X^*_{pqkl}(\lambda') X_{mnij}(\lambda)\, G_{pqkl,mnij} - Y^*_{pqkl}(\lambda')\, Y_{mnij}(\lambda)\, G^*_{pqkl,mnij} \right). \tag{xx}$$

Afin d'établir l'Eq. (xx), les deux approximations suivantes ont été utilisées:

1. $$\forall(\alpha,\beta,\gamma,\delta),\ \rho_{\alpha\beta\gamma\delta} = \rho_{\alpha\gamma}\rho_{\beta\delta} - \rho_{\alpha\delta}\rho_{\beta\gamma}\,, \tag{xxi}$$

   où les éléments de matrices de densité à 1 et 2 corps sont respectivement définis par

   $$\rho_{\alpha\beta} := \langle 0|\, a^\dagger_\beta a_\alpha\, |0\rangle\,, \tag{xxii}$$

   et

   $$\rho_{\alpha\beta\gamma\delta} := \langle 0|\, a^\dagger_\gamma a^\dagger_\delta a_\beta a_\alpha\, |0\rangle\,. \tag{xxiii}$$

2. $$\forall(\alpha,\beta),\ \rho_{\alpha\beta} = \delta_{\alpha\beta}\, n_\alpha\,, \tag{xxiv}$$

   où n_α est le nombre d'occupation de l'état simple-particule α.

Avec ces approximation, l'expression de l'amplitude de transition $\langle\lambda|\,\hat{F}\,|0\rangle$ d'un opérateur $\hat{F}$ est identique à celle de la RPA (Eq. (xv)).

3.2 Inconvénients de la SRPA standard

La forme standard de la SRPA présente d'importants problèmes, qui peuvent être liés aux possibles instabilités ainsi qu'à l'usage d'EDFs.

Problèmes liés aux instabilités

Des instabilités peuvent survenir en SRPA, provenant du fait que la condition garantissant la positivité de la matrice de stabilité de la SRPA est plus complexe qu'en RPA, en raison de la présence des configurations 2p2h [67]. En effet, le fait de choisir l'état fondamental comme étant l'état de HF ne garantit pas que la matrice de stabilité est positive, contrairement au cas de la RPA (théorème de Thouless).

La présence d'instabilités en SRPA est possible également avec des interactions sortant du cadre des EDFs.

Les instabilités sont notamment visibles par un décalage des spectres d'excitation de plusieurs MeVs vers les basses énergies, comparé aux spectres obtenus en RPA.

Problèmes liés aux EDFs

Les paramètres des interactions effectives, dont les EDFs dérivent le plus souvent, sont ajustées sur des grandeurs mesurées des noyaux, en général à l'aide de modèle de champ moyen. Par conséquent, ils tiennent compte implicitement de corrélations, qui sont également inclues de façon explicite par l'inclusion des configurations 2p2h en SRPA. Ainsi, il y a un risque de double comptage de corrélations.

De plus, certaines interactions largement utilisées, telles que les interactions de Skyrme et de Gogny, contiennent des termes de portée nulle, qui peuvent être à l'origine de divergences ultraviolettes (dépendance des résultats en le cutoff sur les configurations 2p2h).

4 Une correction de la SRPA: SRPA avec soustraction

4.1 Principe de la SRPA avec soustraction

La procédure de soustraction a été introduite par Tselyaev [79] dans le modèle de quasi-particle-time-blocking approximation (QTBA), comme moyen de résoudre le problème posé par les états fallacieux (*spurious states*). Il a

montré par la suite [68] que cette procédure permettait d'éviter le problème de double comptage des corrélations dans une catégorie de modèles au-delà de la RPA utilisant des EDFs. Ces modèles, dont la SRPA fait partie, peuvent être exprimés formellement comme des problèmes de type RPA où la matrice de stabilité dépend de l'énergie d'excitation.

La même étude montre que les problèmes d'instabilités dans ces modèles sont aussi résolus par la soustraction. Les EDFs sont construites dans un esprit de DFT, selon lequel la réponse RPA est considérée comme la réponse statique exacte. Par conséquent, la polarisabilité statique en RPA (qui est proportionnelle au moment inverse pondéré en masse m_{-1}^{RPA}) est considérée comme la polarisabilité statique exacte. Dans cet esprit, étant donné un problème au-delà de la RPA, noté RPA', tel que mentionné *supra*, la soustraction consiste à imposer l'égalité du moment inverse du modèle RPA' à celui de la RPA:

$$m_{-1}^{\mathrm{RPA}'} = m_{-1}^{\mathrm{RPA}}, \tag{xxv}$$

ce qui se traduit également par l'égalité suivante des matrices de stabilité:

$$\mathscr{S}^{\mathrm{RPA}'}(0) = \mathscr{S}^{\mathrm{RPA}}. \tag{xxvi}$$

Pour satisfaire cette condition, il suffit en pratique d'imposer que les blocs A_{11} et B_{11} (relatifs au couplage des configurations 1p1h entre elles) de la SRPA soient soustraits de la self-energy à énergie nulle, de sorte que ces blocs en SRPA soustraite (SSRPA) s'écrivent

$$A_{11}^{\mathrm{S}} := A_{11} - W_A(0), \tag{xxvii}$$

$$B_{11}^{\mathrm{S}} := B_{11} - W_B(0). \tag{xxviii}$$

4.2 Résultats: Polarisabilité et réponse dipolaire de ^{48}Ca

Ce travail [82] a constitué la première application de la SSRPA à l'étude de la réponse et de la polarisabilité dipolaire de ^{48}Ca. Cette dernière grandeur a d'importantes implications, notamment dans la description de l'épaisseur de peau neutronique pour les noyaux riches en neutrons, ou dans l'étude des étoiles à neutrons.

Des analyses expérimentales de la réponse dipolaire de ^{48}Ca ont suggéré l'importance de modèles au-delà du champ moyen pour décrire la région de basse énergie du spectre [91, 92], et de récentes mesures ont été effectuée également dans la région des résonances géantes [95, 96], motivant la présente étude.

Les calculs effectués au cours de cette étude ont employé deux paramétrisations de l'interaction de Skyrme: SLy4 [99–101] et SGII [16, 17]. Comme les autres applications présentées dans ce manuscrit, les termes J^2, où J est la densité spin-orbit, n'ont pas été inclus.

L'analyse des résultats a montré que les états d'énergie inférieure à 10 MeV ont une position en énergie et une magnitude correspondant mieux aux valeurs expérimentales en SSRPA qu'en SRPA sans soustraction. Ces résultats étaient davantage satisfaisants avec SGII qu'avec SLy4. La strength intégrée et la strength intégrée pondérée en énergie sont également améliorées dans cette région d'énergie par l'usage de la soustraction.

Concernant la région d'énergie de la résonance géante, une largeur et fragmentation bien plus réaliste en SSRPA qu'en RPA a été obtenue, ainsi qu'une correction, bien que partielle, du décalage énergétique lié aux instabilités en SRPA standard. Nous avons observé également une reproduction réaliste de la pente de la polarisabilité dipolaire dans la région de la résonance géante, obtenue avec la SSRPA, comparée à la pente trop forte obtenue en RPA et avec un ensemble de calculs de type coupled-cluster.

En conclusion, la méthode de soustraction permis d'améliorer la description des états de basse énergie et de la résonance géante dipolaire de ^{48}Ca, par rapport à la RPA et la SRPA. La reproduction réaliste de la pente de la polarisabilité est également une indication de la description satisfaisante du spreading.

4.3 Résultats: Réponse quadrupolaire: systématiques sur une sélection de noyaux

Cette deuxième étude [107] a consisté à appliquer notre modèle de SRPA avec soustraction de manière systématique à une sélection de noyaux de masse moyenne et lourds (^{30}Si, ^{34}Si, ^{36}S, ^{40}Ca, ^{48}Ca, ^{56}Ni, ^{68}Ni, ^{90}Zr, ^{114}Sn, ^{116}Sn, ^{120}Sn, ^{132}Sn et ^{208}Pb), de manière à analyser le centroïde et la largeur de leur résonance géante quadrupolaire isoscalaire.

De nombreux travaux expérimentaux ont été conduits concernant cette résonance géante, pour différents noyaux [112–118]. De plus, de récentes expériences à haute résolution ont permis d'obtenir sa structure fine dans ^{40}Ca, ^{58}Ni, ^{90}Zr, ^{120}Sn et ^{208}Pb [119, 120].

Nous avons effectué des calculs de RPA et SSRPA avec la paramétrisation SLy4 de l'interaction de Skyrme.

Tout d'abord, les valeurs obtenues des centroïdes en SSRPA ont montré

une tendance systématique à la diminution par rapport à la RPA, et ainsi une amélioration de la reproduction des données expérimentales disponibles dans la majorité des cas.

Ensuite, les calculs de largeurs de résonance ont montré que les valeurs obtenues en SSRPA étaient systématiquement plus élevées qu'en RPA, témoignant de l'effet du couplage des configurations 1p1h et 2p2h. Ces largeurs ont été calculées en remplaçant chaque pic des spectres discrets par une lorentzienne, puis en ajustant une lorentzienne globale sur le spectre continu qui en résultait.

Enfin, la comparaison aux données expérimentales de structure fine de résonance quadrupolaire a montré en général un bien meilleure reproduction dans le cas de la SSRPA que dans le cas de la RPA.

4.4 Résultats: Effets au-delà du champ moyen sur les masses effectives

La résonance géante quadrupolaire isoscalaire est liée à la masse effective m^* de la matière nucléaire: d'après la théorie de Landau des liquides de Fermi, il existe une relation linéaire entre le centroïde de cette résonance et la quantité $\sqrt{m/m^*}$. Nous avons proposé dans cette étude [133] une méthode pour la description microscopique des effets au-delà du champ moyen sur les masses effectives de la matière nucléaire. Deux noyaux ont été étudiés: ^{48}Ca et ^{90}Zr.

Pour une particule d'impulsion k et d'énergie $E = \frac{\hbar^2 k^2}{2m} + \Sigma_k + \Sigma_{k,E}$, avec $\Sigma_k + \Sigma_{k,E}$ est la self-energy, nous avons:

$$\frac{1}{m^*} = \frac{\mathrm{d}E}{\mathrm{d}k}\frac{1}{\hbar^2 k}, \tag{xxix}$$

$$\frac{m^*}{m} = \underbrace{\left(1 - \frac{\partial \Sigma_{k,E}}{\partial E}\right)}_{E\text{-mass}} \cdot \underbrace{\left(1 + \frac{m}{\hbar^2 k}\frac{\partial \Sigma_k}{\partial k}\right)^{-1}}_{k\text{-mass}}. \tag{xxx}$$

où la k-mass est la seule contribution au ratio $\frac{m^*}{m}$ en champ moyen, et la E-mass n'est supérieure à 1 qu'en présence de corrélations au-delà du champ moyen.

La méthode consiste à:

1. Calculer les centroïdes et la valeur $\sqrt{m/m^*}$ en RPA, pour plusieurs paramétrisations de l'interaction de Skyrme;

2. Calculer les centroïdes en SSRPA (deux paramétrisations: SLy4 et SGII);

3. Effectuer une régression linéaire des centroïdes RPA et reporter les centroïdes SSRPA sur les droites obtenues;

4. Déduire la valeur de m^* et en extraire celle de la E-mass, qui renseigne sur la magnitude des effets au-delà du champ moyen.

Pour les deux paramétrisation utilisée en SSRPA, nous observons une augmentation des masses effectives m^* par rapport aux valeurs obtenues en RPA, ce qui est cohérent avec l'inclusion de corrélations propre à la SSRPA. Nous avons également évalué les erreurs théoriques de nos calculs de masses effectives. Ces erreurs proviennent, pour le cas du champ moyen, du fait que différentes paramétrisation de l'interaction sont utilisées. Au-delà du champ moyen, celles-ci proviennent non seulement de l'usage de différentes paramétrisations, mais également du fait que les résultats changent d'un noyau à l'autre. Nous avons pu montré que les erreurs théoriques au-delà du champ moyen n'étaient cependant pas plus importantes que celles en champ moyen.

Nous avons complété nos résultats en mettant en évidence la compression des spectres simple-particule par l'effet des corrélations au-delà du champ moyen, comme suggéré par de précédents travaux [75, 153].

Enfin, nous avons vérifié nos résultats précédents en calculant les valeurs de E-mass à partir des valeurs de self-energy pour des éléments de matrices SSRPA près de l'énergie du centroïde.

5 Extensions du modèle

5.1 Noyaux à orbitales partiellement occupées et appariement

Dans toutes nos applications précédentes des modèles de RPA et de SSRPA, seuls des noyaux dont les orbitales sont totalement occupées ont été considérés. En effets, nos outils numériques ne permettaient pas le traitement de noyaux à orbitales partiellement occupées.

Pour ce faire, nous avons eu recours à l'approximation d'equal-filling (EFA) en symétrie sphérique, selon laquelle, sur une orbitale de moment cinétique total j de dégénérescence $(2j+1)$, la probabilité d'occupation de chaque état simple-particule est égale à $\frac{1}{2j+1}$. Dans le cas où l'état fondamental est l'état de HF, cette approximation se traduit par la renormalisation des

fonctions d'onde de simple-particules par un facteur $\sqrt{n_\alpha}$ ou $\sqrt{1-n_\alpha}$, où n_α est le nombre d'occupation de l'état α, selon que l'état α joue le rôle, dans un élément de matrice donné, d'état de trou ou de particule, respectivement[1].

Dans nos applications pratiques de RPA et de SSRPA, l'EFA est mise en place par l'application de tels facteurs aux éléments de matrices A et B, ainsi que dans la relation Eq. (xv). Nous désignons par "HF-based EFA" cette méthode de renormalisation.

Pour aller plus loin dans cette extension, nous avons entrepris d'estimer les effets d'appariement, en incluant ces corrélations via les nombres d'occupation apparaissant dans les expressions renormalisées par l'EFA. Nous avons choisi pour cela de calculer les nombres d'occupation avec un modèle de Bardeen-Cooper-Schrieffer (BCS). Dans ce modèle, la probabilité pour un état α d'être occupé ou inoccupé est donnée par la quantité v_α ou u_α respectivement:

$$v_\alpha^2 = \frac{1}{2}\left(1 - \frac{\tilde{\epsilon}_\alpha}{\sqrt{\tilde{\epsilon}_\alpha^2 - \Delta_\alpha^2}}\right), \tag{xxxi}$$

$$u_\alpha^2 = \frac{1}{2}\left(1 + \frac{\tilde{\epsilon}_\alpha}{\sqrt{\tilde{\epsilon}_\alpha^2 - \Delta_\alpha^2}}\right). \tag{xxxii}$$

Les relations $v_\alpha^2 = n_\alpha$ et $u_\alpha^2 = 1 - n_\alpha$ permettent ainsi, en utilisant les expression EFA des éléments de matrices, d'obtenir des facteurs de renormalisation incluant des corrélations d'appariement ("BCS-based EFA"). Dans le cas de la RPA ainsi renormalisée, les expressions des éléments de matrice sont analogues à certains termes qui sont présents dans les expressions correspondantes de la QRPA, mais d'autres termes de la QRPA ne sont pas retrouvés. Dans le cas de la SSRPA, certains termes sont cette fois présents en SSRPA renormalisée et non en QRPA.

Il est important de noter que cette méthode de renormalisation ne tient pas compte de l'appariement dans l'interaction résiduelle.

Une étude expérimentale récente [156] a rapporté la première spectroscopie γ du noyau ^{52}Ar, ainsi qu'une analyse des états 2^+ les plus bas en énergie sur une plage d'isotopes de l'argon pour lesquels $N > 20$. L'objectif principal était de déterminer l'évolution, en dessous de $Z = 20$, de la fermeture de couche $N = 34$ auparavant suggérée uniquement pour ^{54}Ca.

[1] Voir aussi Ref. [155].

Nous nous sommes intéressés à la comparaison de ces résultats avec ceux de nos modèles HF-based et BCS-based EFA. En nous concentrant sur les quatre noyaux ^{46}Ar, ^{48}Ar, ^{50}Ar et ^{52}Ar, nous avons calculé les énergie des états 2^+ les plus bas en RPA et en SSRPA avec les renormalisations HF-based et BCS-based EFA.

Nos résultats, montrant l'énergie en fonction du nombre de masse, ont montré en RPA une tendance semblable pour les deux types de renormalisation, qui était en désaccord avec la tendance des points expérimentaux. En effectuant les calculs correspondant en SSRPA, nous avons montré premièrement que l'inclusion des configurations 2p2h permettait d'atténuer l'écart de tendance par rapport aux valeurs expérimentales. Deuxièmement, l'ajout des corrélations d'appariement a engendré une augmentation de l'énergie pour $N = 34$, vers un meilleur accord avec la valeur expérimentale récemment mesurée.

5.2 Extension au-delà de la QBA

Ce second type d'extension a concerné la SRPA sans soustraction. La SRPA standard fait usage de la QBA qui, comme indiqué précédemment, constitue notamment une incohérence dans le formalisme. Certaines études ont suggéré le choix d'un état fondamental corrélé pour aller au-delà de cette approximation, et ainsi obtenir une alternative à la méthode de soustraction [67, 194, 195].

En suivant un modèle de SRPA étendue développé précédemment à cette thèse et appliqué à l'étude des agrégats métalliques [153], nous nous affranchissons de la QBA en utilisant des expressions des éléments de matrices RPA et SRPA qui dépendent de la matrice de densité à 1 corps.

En supposant la matrice de densité à 1 corps diagonale, les éléments de matrices contiennent des facteurs faisant intervenir les nombres d'occupation, que nous autorisons à prendre des valeurs comprises entre 0 et 1 — contrairement au cas de la QBA, où seules les valeurs 1 et 0 sont autorisées. Puis, l'utilisation de la number operator method [193] permet d'établir une expression de ces nombres d'occupation en fonction des amplitudes "Y" de la RPA, ce qui implique une procédure itérative. En effet, nous avons calculé de manière itérative les nombres d'occupation à l'aide d'une RPA au-delà de la QBA, jusqu'à convergence, puis nous avons utilisé ces nombres d'occupation pour construire les éléments de matrice d'une SRPA au-delà de la QBA.

Nous avons appliqué ce modèle aux réponses monopolaire et quadrupo-

laire de ^{16}O. Nos résultats ont montré que la SRPA ainsi renormalisée conduit à un décalage des spectres vers les plus hautes énergies, par rapport à la SRPA standard, ce qui va dans le sens d'une correction du décalage énergétique dû aux instabilités. Cependant, cet effet est trop faible pour pouvoir corriger adéquatement le décalage (effet de l'ordre de 0.5 MeV, contre un décalage de plusieurs MeVs en général).

Ainsi cette méthode au-delà de la QBA est insuffisante pour corriger les problèmes de la SRPA.

6 Conclusion générale et perspectives

Notre objectif initial d'améliorer la description des excitations collectives a été atteint: nous avons mis en évidence l'importance de modèles au-delà du champ moyen, comme la SSRPA, pour décrire de manière satisfaisante la fragmentation et la largeur de spreading des excitations.

Nous avons montré la capacité de la SRPA avec soustraction à corriger dans une large mesure les problèmes de la SRPA standard. Ainsi, la reproduction des largeurs et des centroïdes des résonances géantes, ainsi que leur structure fine, s'en trouvent améliorées. Nous avons également pu estimer les effets au-delà du champ moyen sur les masses effectives de la matière nucléaire.

En second lieu, nous avons étendu nos modèles. L'usage de l'approximation d'equal-filling en SRPA avec soustraction nous a permis d'étudier des noyaux à orbitales partiellement occupées, puis d'effectuer une estimation des effets d'appariement. Enfin, le développement d'un modèle de SRPA s'affranchissant de l'approximation de quasiboson a montré que les corrélations obtenues par des calculs de RPA au-delà de cette approximation sont insuffisantes pour corriger les problèmes de la SRPA standard.

Plusieurs directions de développement ultérieur pourraient être suivies. Premièrement, une prise en compte complète des corrélations d'appariement pourrait être entreprise en SRPA avec soustraction, pour vérifier l'importance de ces effets dans l'amélioration des résultats. Deuxièmement, le jeu d'approximations utilisé dans notre approche au-delà de l'approximation de quasiboson, afin d'observer la mesure dans laquelle ce type d'approche peut corriger les problèmes de la SRPA. L'inclusion de corrélations d'appariement pourrait aussi être envisagée dans cette approche. Enfin, les effets d'une température non nulle pourraient être analysés.

Bibliography

[1] C. Drischler, A. Carbone, K. Hebeler, A. Schwenk, *Phys. Rev. C* **94**, 054307 [2016] [cit. on p. 6].

[2] J. W. Holt, N. Kaiser, *Phys. Rev. C* **95**, 034326 [2017] [cit. on p. 6].

[3] A. Ekström *et al.*, *Phys. Rev. C* **91**, 051301(R) [2015] [cit. on pp. 6, 73, 74].

[4] B.-A. Li, B.-J. Cai, L.-W. Chen, J. Xu, *Prog. Part. Nucl. Phys.* **99**, 29–119, ISSN: 0146-6410 [2018] [cit. on pp. 6, 59].

[5] X. Roca-Maza, N. Paar, *Prog. Part. Nucl. Phys.* **101**, 96–176, ISSN: 0146-6410 [2018] [cit. on p. 6].

[6] U. Garg, G. Colò, *Prog. Part. Nucl. Phys.* **101**, 55–95, ISSN: 0146-6410 [2018] [cit. on p. 6].

[7] A. Bracco, E. Lanza, A. Tamii, *Prog. Part. Nucl. Phys.* **106**, 360–433, ISSN: 0146-6410 [2019] [cit. on p. 6].

[8] J. Speth, A. van der Woude, *Rep. Prog. Phys.* **44**, 719–786 [1981] [cit. on p. 8].

[9] K. Goeke, J. Speth, *Annual Review of Nuclear and Particle Science* **32**, 65–115 [1982] [cit. on p. 8].

[10] J. Wambach, *Rep. Prog. Phys.* **51**, 989–1046 [1988] [cit. on p. 8].

[11] J. Speth, *Electric and Magnetic Giant Resonances in Nuclei*, Vol. 7 of *International Review of Nucl. Phys.* [World Scientific, Singapore, 1991] [cit. on p. 8].

[12] M. N. Harakeh, A. van der Woude, *Giant Resonances: Fundamental High-Frequency Modes of Nuclear Excitation*, ed. by P. E. Hodgson [Oxford University Press, Oxford, UK, 2001] [cit. on pp. 8, 24].

[13] T. H. R. Skyrme, *Phil. Mag.* **1**, 1043–1054 [1956] [cit. on pp. 12, 107].

[14] T. Skyrme, *Nucl. Phys.* **9**, 615–634, ISSN: 0029-5582 [1958] [cit. on pp. 12, 107].

[15] D. Vautherin, D. M. Brink, *Phys. Rev. C* **5**, 626–647 [1972] [cit. on pp. 12, 107].

[16] D. Gogny, *in Proceedings of the International Conference on Nuclear Self-Consistent Fields, Trieste 1975, North Holland, Amsterdam, 1975* [Edited by Ripka G., Porneuf M., published for the International Atomic Energy Agency by North-Holland Pub. Co., American Elsevier Pub. Co. Amsterdam, 1975], ISBN: 0444109625 [cit. on pp. 12, 107, 114].

[17] D. Gogny, *Nucl. Phys. A* **237**, 399–418, ISSN: 0375-9474 [1975] [cit. on pp. 12, 107, 114].

[18] J. W. Negele, *Rev. Mod. Phys.* **54**, 913–1015 [1982] [cit. on p. 12].

[19] J. W. Negele, D. Vautherin, *Phys. Rev. C* **5**, 1472–1493 [1972] [cit. on p. 12].

[20] J. W. Negele, D. Vautherin, *Phys. Rev. C* **11**, 1031–1041 [1975] [cit. on p. 12].

[21] M. Bender, P.-H. Heenen, P.-G. Reinhard, *Rev. Mod. Phys.* **75**, 121–180 [2003] [cit. on p. 12].

[22] P. Hohenberg, W. Kohn, *Phys. Rev.* **136**, B864–B871 [1964] [cit. on p. 12].

[23] W. Kohn, *Rev. Mod. Phys.* **71**, 1253–1266 [1999] [cit. on p. 12].

[24] W. Kohn, L. J. Sham, *Phys. Rev.* **140**, A1133–A1138 [1965] [cit. on p. 12].

[25] M. Grasso, *Prog. Part. Nucl. Phys.* **106**, 256–311, ISSN: 0146-6410 [2019] [cit. on pp. 13, 32].

[26] J. E. Drut, R. J. Furnstahl, L. Platter, *Prog. Part. Nucl. Phys.* **64**, 120–168, ISSN: 0146-6410 [2010] [cit. on p. 13].

[27] C. J. Yang, M. Grasso, D. Lacroix, *Phys. Rev. C* **94**, 031301(R) [2016] [cit. on p. 13].

[28] M. Grasso, D. Lacroix, C. J. Yang, *Phys. Rev. C* **95**, 054327 [2017] [cit. on p. 13].

[29] J. Bonnard, M. Grasso, D. Lacroix, *Phys. Rev. C* **98**, 034319 [2018] [cit. on p. 13].

[30] P. Papakonstantinou, T.-S. Park, Y. Lim, C. H. Hyun, *Phys. Rev. C* **97**, 014312 [2018] [cit. on p. 13].

[31] H. Gil, P. Papakonstantinou, C. H. Hyun, Y. Oh, *arXiv [nucl-th]* **1805.11321** [2018] [cit. on p. 13].

[32] A. Boulet, D. Lacroix, *Phys. Rev. C* **97**, 014301 [2018] [cit. on p. 13].

[33] A. Roggero, A. Mukherjee, F. Pederiva, *Phys. Rev. C* **92**, 054303 [2015] [cit. on pp. 13, 59].

[34] D. Lacroix, *Phys. Rev. A* **94**, 043614 [2016] [cit. on p. 13].

[35] D. Lacroix, A. Boulet, M. Grasso, C.-J. Yang, *Phys. Rev. C* **95**, 054306 [2017] [cit. on p. 13].

[36] J. Dobaczewski, *J. Phys. G* **43**, 04LT01 [2016] [cit. on p. 13].

[37] A. L. Fetter, J. D. Walecka, *Quantum Theory of Many-Particle Systems* [Dover Publications, New York, 2003] [cit. on pp. 13, 59].

[38] P. Ring, P. Schuck, *The Nuclear Many-Body Problem* [Springer-Verlag, 1980] [cit. on pp. 14–16, 36, 69].

[39] G. C. Wick, *Phys. Rev.* **80**, 268–272 [1950] [cit. on pp. 15, 27].

[40] D. J. Rowe, *Rev. Mod. Phys.* **40**, 153–166 [1968] [cit. on pp. 17, 19, 24, 78].

[41] D. J. Rowe, *Nuclear Collective Motion* [World Scientific, 2010] [cit. on pp. 17, 71, 108].

[42] D. Thouless, *Nucl. Phys.* **21**, 225–232, ISSN: 0029-5582 [1960] [cit. on pp. 19, 21, 29, 36, 109].

[43] D. Thouless, *Nucl. Phys.* **22**, 78–95, ISSN: 0029-5582 [1961] [cit. on p. 19].

[44] M. Tohyama, P. Schuck, *Eur. Phys. J. A* **45**, 257–266 [2010] [cit. on p. 19].

[45] J. Dukelsky, P. Schuck, *Phys. Lett. B* **387**, 233–238, ISSN: 0370-2693 [1996] [cit. on pp. 21, 79].

[46] S. Schäfer, P. Schuck, *Phys. Rev. B* **59**, 1712–1733 [1999] [cit. on pp. 21, 79].

[47] M. Grasso, F. Catara, *Phys. Rev. C* **63**, 014317 [2000] [cit. on pp. 21, 79].

[48] N. Paar, D. Vretenar, E. Khan, G. Colò, *Rep. Prog. Phys.* **70**, 691–793 [2007] [cit. on p. 23].

[49] G. Colò, N. Van Giai, P. F. Bortignon, R. A. Broglia, *Phys. Rev. C* **50**, 1496–1508 [1994] [cit. on pp. 24, 52].

[50] B. Schwesinger, J. Wambach, *Nucl. Phys. A* **426**, 253–275, ISSN: 0375-9474 [1984] [cit. on pp. 24, 110].

[51] D. Cha, B. Schwesinger, J. Wambach, J. Speth, *Nucl. Phys. A* **430**, 321–348, ISSN: 0375-9474 [1984] [cit. on pp. 24, 110].

[52] S. Drożdż, J. L. Tain, J. Wambach, *Phys. Rev. C* **34**, 345–347 [1986] [cit. on pp. 24, 110].

[53] S. Drożdż, V. Klemt, J. Speth, J. Wambach, *Phys. Lett. B* **166**, 18–22, ISSN: 0370-2693 [1986] [cit. on pp. 24, 110].

[54] S. Drożdż, V. Klemt, J. Speth, J. Wambach, *Nucl. Phys. A* **451**, 11–20, ISSN: 0375-9474 [1986] [cit. on pp. 24, 110].

[55] P. Papakonstantinou, R. Roth, *Phys. Lett. B* **671**, 356–360, ISSN: 0370-2693 [2009] [cit. on pp. 24, 110].

[56] P. Papakonstantinou, R. Roth, *Phys. Rev. C* **81**, 024317 [2010] [cit. on pp. 24, 29–31, 110].

[57] D. Gambacurta, M. Grasso, F. Catara, *Phys. Rev. C* **81**, 054312 [2010] [cit. on pp. 24, 29, 30, 41, 44, 110].

[58] D. Gambacurta, M. Grasso, F. Catara, *Phys. Rev. C* **84**, 034301 [2011] [cit. on pp. 24, 41, 45, 110].

[59] D. Gambacurta, M. Grasso, V. De Donno, G. Co', F. Catara, *Phys. Rev. C* **86**, 021304(R) [2012] [cit. on pp. 24, 110].

[60] D. Gambacurta, M. Grasso, F. Catara, *J. Phys. G* **38**, 035103 [2011] [cit. on pp. 24, 41, 43, 110].

[61] C. Yannouleas, M. Dworzecka, J. Griffin, *Nucl. Phys. A* **397**, 239–295, ISSN: 0375-9474 [1983] [cit. on p. 24].

[62] J. D. Providência, *Nucl. Phys.* **61**, 87–96, ISSN: 0029-5582 [1965] [cit. on pp. 24, 29, 41, 42].

[63] M. G. M. Tohyama, *Z. Phys. A* **332**, 269–274 [1989] [cit. on p. 24].

[64] D. Lacroix, S. Ayik, P. Chomaz, *Prog. Part. Nucl. Phys.* **52**, 497–563, ISSN: 0146-6410 [2004] [cit. on p. 24].

[65] C. Yannouleas, *Phys. Rev. C* **35**, 1159–1161 [1987] [cit. on p. 24].

[66] L. G. Molinari, *arXiv* **1710** [2017] [cit. on p. 27].

[67] P. Papakonstantinou, *Phys. Rev. C* **90**, 024305 [2014] [cit. on pp. 29, 36, 80, 84, 112, 118].

[68] V. I. Tselyaev, *Phys. Rev. C* **88**, 054301 [2013] [cit. on pp. 29, 32, 35, 36, 113].

[69] N. V. Giai, H. Sagawa, *Phys. Lett. B* **106**, 379–382, ISSN: 0370-2693 [1981] [cit. on p. 29].

[70] N. V. Giai, H. Sagawa, *Nucl. Phys. A* **371**, 1–18, ISSN: 0375-9474 [1981] [cit. on p. 29].

[71] R. B. Wiringa, V. G. J. Stoks, R. Schiavilla, *Phys. Rev. C* **51**, 38–51 [1995] [cit. on p. 30].

[72] R. Roth, T. Neff, H. Hergert, H. Feldmeier, *Nucl. Phys. A* **745**, 3–33, ISSN: 0375-9474 [2004] [cit. on p. 30].

[73] R. Roth, H. Hergert, P. Papakonstantinou, T. Neff, H. Feldmeier, *Phys. Rev. C* **72**, 034002 [2005] [cit. on p. 30].

[74] D. Brink, E. Boeker, *Nucl. Phys. A* **91**, 1–26, ISSN: 0375-9474 [1967] [cit. on p. 30].

[75] D. Gambacurta, F. Catara, *Phys. Rev. B* **79**, 085403 [2009] [cit. on pp. 30, 31, 63, 116].

[76] M. Brack, *Rev. Mod. Phys.* **65**, 677–732 [1993] [cit. on p. 30].

[77] J. Borggreen *et al.*, *Phys. Rev. B* **48**, 17507–17516 [1993] [cit. on p. 31].

[78] C. J. Yang, M. Grasso, X. Roca-Maza, G. Colò, K. Moghrabi, *Phys. Rev. C* **94**, 034311 [2016] [cit. on p. 32].

[79] V. I. Tselyaev, *Phys. Rev. C* **75**, 024306 [2007] [cit. on pp. 35, 52, 112].

[80] P. Nozieres, D. Pines, *Theory Of Quantum Liquids* [Avalon Publishing, 1999], ISBN: 9780813346533 [cit. on p. 36].

[81] D. Gambacurta, M. Grasso, J. Engel, *Phys. Rev. C* **92**, 034303 [2015] [cit. on pp. 38–41, 58].

[82] D. Gambacurta, M. Grasso, O. Vasseur, *Phys. Lett. B* **777**, 163–168, ISSN: 0370-2693 [2018] [cit. on pp. 41, 43, 44, 113].

[83] M. Waroquier *et al.*, *Phys. Rep.* **148**, 249–306, ISSN: 0370-1573 [1987] [cit. on p. 41].

[84] S. Adachi, S. Yoshida, *Phys. Lett. B* **81**, 98–102, ISSN: 0370-2693 [1979] [cit. on p. 41].

[85] X. Roca-Maza *et al.*, *Phys. Rev. C* **92**, 064304 [2015] [cit. on p. 43].

[86] M. Warda, X. Viñas, X. Roca-Maza, M. Centelles, *Phys. Rev. C* **80**, 024316 [2009] [cit. on p. 44].

[87] M. Centelles, X. Roca-Maza, X. Viñas, M. Warda, *Phys. Rev. Lett.* **102**, 122502 [2009] [cit. on p. 44].

[88] J. M. Lattimer, M. Prakash, *The Astrophysical Journal* **550**, 426–442 [2001] [cit. on p. 44].

[89] J. M. Lattimer, *Nucl. Phys. A* **928**, Special Issue Dedicated to the Memory of Gerald E Brown (1926-2013), 276–295, ISSN: 0375-9474 [2014] [cit. on p. 44].

[90] M. Baldo, G. Burgio, *Prog. Part. Nucl. Phys.* **91**, 203–258, ISSN: 0146-6410 [2016] [cit. on p. 44].

[91] T. Hartmann *et al.*, *Phys. Rev. C* **65**, 034301 [2002] [cit. on pp. 44, 46, 113].

[92] T. Hartmann *et al.*, *Phys. Rev. Lett.* **93**, 192501 [2004] [cit. on pp. 44–46, 113].

[93] G. Tertychny *et al.*, *Nucl. Phys. A* **788**, Proceedings of the 2nd International Conference on Collective Motion in Nuclei under Extreme Conditions, 159–164, ISSN: 0375-9474 [2007] [cit. on p. 44].

[94] N. N. Arsenyev, A. P. Severyukhin, V. V. Voronov, N. Van Giai, *Phys. Rev. C* **95**, 054312 [2017] [cit. on p. 44].

[95] A. Tamii *et al.*, *Phys. Rev. Lett.* **107**, 062502 [2011] [cit. on pp. 44, 113].

[96] J. Birkhan *et al.*, *Phys. Rev. Lett.* **118**, 252501 [2017] [cit. on pp. 44, 46–50, 113].

[97] C. Ur, *Rom. Rep. Phys.* **68**, S483–S538 [2016] [cit. on p. 44].

[98] F. Camera *et al.*, *Rom. Rep. Phys.* **68**, S539–S619 [2016] [cit. on p. 44].

[99] E. Chabanat, P. Bonche, P. Haensel, J. Meyer, R. Schaeffer, *Nucl. Phys. A* **627**, 710–746, ISSN: 0375-9474 [1997] [cit. on pp. 44, 114].

[100] E. Chabanat, P. Bonche, P. Haensel, J. Meyer, R. Schaeffer, *Nucl. Phys. A* **635**, 231–256, ISSN: 0375-9474 [1998] [cit. on pp. 44, 114].

[101] E. Chabanat, P. Bonche, P. Haensel, J. Meyer, R. Schaeffer, *Nucl. Phys. A* **643**, 441, ISSN: 0375-9474 [1998] [cit. on pp. 44, 114].

[102] P.-G. Reinhard, *Nucl. Phys. A* **649**, Giant Resonances, 305–314, ISSN: 0375-9474 [1999] [cit. on p. 47].

[103] I. A. Egorova, E. Litvinova, *Phys. Rev. C* **94**, 034322 [2016] [cit. on pp. 49, 52].

[104] M. Miorelli *et al.*, *Phys. Rev. C* **94**, 034317 [2016] [cit. on p. 50].

[105] S. Bacca *et al.*, *Phys. Rev. C* **90**, 064619 [2014] [cit. on p. 50].

[106] G. Hagen *et al.*, *Nature Physics* **12**, Article, 186 EP - [2015] [cit. on p. 50].

[107] O. Vasseur, D. Gambacurta, M. Grasso, *Phys. Rev. C* **98**, 044313 [2018] [cit. on pp. 51, 52, 114].

[108] R. Pitthan, T. Walcher, *Phys. Lett. B* **36**, 563–564, ISSN: 0370-2693 [1971] [cit. on p. 51].

[109] S. Fukuda, Y. Torizuka, *Phys. Rev. Lett.* **29**, 1109–1111 [1972] [cit. on p. 51].

[110] M. Lewis, F. Bertrand, *Nucl. Phys. A* **196**, 337–346, ISSN: 0375-9474 [1972] [cit. on p. 51].

[111] F. E. Bertrand, *Nucl. Phys. A* **354**, 129–156, ISSN: 0375-9474 [1981] [cit. on p. 51].

[112] D. H. Youngblood *et al.*, *Phys. Rev. C* **23**, 1997–2007 [1981] [cit. on pp. 51–53, 114].

[113] Y.-W. Lui *et al.*, *Phys. Rev. C* **83**, 044327 [2011] [cit. on pp. 51–53, 114].

[114] W. Borghols *et al.*, *Nucl. Phys. A* **504**, 231–268, ISSN: 0375-9474 [1989] [cit. on pp. 51, 114].

[115] M. M. Sharma *et al.*, *Phys. Rev. C* **38**, 2562–2572 [1988] [cit. on pp. 51–53, 114].

[116] T. Li *et al.*, *Phys. Rev. C* **81**, 034309 [2010] [cit. on pp. 51, 52, 114].

[117] C. Monrozeau *et al.*, *Phys. Rev. Lett.* **100**, 042501 [2008] [cit. on pp. 51, 53, 114].

[118] M. Vandebrouck *et al.*, *Phys. Rev. C* **92**, 024316 [2015] [cit. on pp. 51, 114].

[119] I. Usman *et al.*, *Phys. Lett. B* **698**, 191–195, ISSN: 0370-2693 [2011] [cit. on pp. 51, 54, 55, 57, 114].

[120] A. Shevchenko *et al.*, *Phys. Rev. Lett.* **93**, 122501 [2004] [cit. on pp. 51, 56, 114].

[121] V. G. Soloviev, *Theory of Atomic Nuclei: Quasiparticles and Phonons* [Institute of Physics, Bristol, 1992] [cit. on p. 52].

[122] N. Van Giai, C. Stoyanov, V. V. Voronov, *Phys. Rev. C* **57**, 1204–1209 [1998] [cit. on p. 52].

[123] A. P. Severyukhin, S. Åberg, N. N. Arsenyev, R. G. Nazmitdinov, *Phys. Rev. C* **95**, 061305 [2017] [cit. on p. 52].

[124] G. Colò, H. Sagawa, N. Van Giai, P. F. Bortignon, T. Suzuki, *Phys. Rev. C* **57**, 3049–3054 [1998] [cit. on p. 52].

[125] Y. F. Niu, G. Colò, E. Vigezzi, C. L. Bai, H. Sagawa, *Phys. Rev. C* **94**, 064328 [2016] [cit. on p. 52].

[126] G. F. Bertsch, P. F. Bortignon, R. A. Broglia, *Rev. Mod. Phys.* **55**, 287–314 [1983] [cit. on p. 52].

[127] G. Colò, P. Bortignon, *Nucl. Phys. A* **696**, 427–441, ISSN: 0375-9474 [2001] [cit. on p. 52].

[128] S. P. Kamerdzhiev, G. Y. Tertychny, V. I. Tselyaev, *Fiz. Elem. Chastits At. Yadra (Phys. Part. Nucl.)*, 333 (134) [1997] [cit. on p. 52].

[129] E. Litvinova, P. Ring, V. Tselyaev, *Phys. Rev. C* **78**, 014312 [2008] [cit. on p. 52].

[130] G. Scamps, D. Lacroix, *Phys. Rev. C* **88**, 044310 [2013] [cit. on p. 52].

[131] H. Aiba, M. Matsuo, S. Nishizaki, T. Suzuki, *Phys. Rev. C* **68**, 054316 [2003] [cit. on p. 54].

[132] H. Aiba, M. Matsuo, S. Nishizaki, T. Suzuki, *Phys. Rev. C* **83**, 024314 [2011] [cit. on p. 54].

[133] M. Grasso, D. Gambacurta, O. Vasseur, *Phys. Rev. C* **98**, 051303(R) [2018] [cit. on pp. 59, 115].

[134] D. Pines, *The Many-Body Problem: A Lecture Note and Reprint Volume* [Frontiers in Physics, Benjamin, San Francisco, 1961] [cit. on p. 59].

[135] A. A. Abrikosov, I. M. Khalatnikov, *Rep. Prog. Phys.* **22**, 329–367 [1959] [cit. on p. 59].

[136] S. Nascimbène *et al.*, *Phys. Rev. Lett.* **103**, 170402 [2009] [cit. on p. 59].

[137] J. Blaizot, *Phys. Rep.* **64**, 171–248, ISSN: 0370-1573 [1980] [cit. on pp. 59, 60].

[138] O. Bohigas, A. Lane, J. Martorell, *Phys. Rep.* **51**, 267–316, ISSN: 0370-1573 [1979] [cit. on p. 59].

[139] N. K. Glendenning, *Compact Stars: Nucl. Phys., Particle Physics, and General Relativity* [Springer, New York, 2000] [cit. on p. 59].

[140] L. Hedin, S. Lundqvist, in *Solid State Physics*, ed. by F. Seitz, D. Turnbull, H. Ehrenreich [Academic Press, 1970], vol. 23, pp. 1–181 [cit. on p. 59].

[141] C. Lobo, A. Recati, S. Giorgini, S. Stringari, *Phys. Rev. Lett.* **97**, 200403 [2006] [cit. on p. 59].

[142] S. Pilati, S. Giorgini, *Phys. Rev. Lett.* **100**, 030401 [2008] [cit. on p. 59].

[143] M. M. Forbes, A. Gezerlis, K. Hebeler, T. Lesinski, A. Schwenk, *Phys. Rev. C* **89**, 041301 [2014] [cit. on p. 59].

[144] J. Jeukenne, A. Lejeune, C. Mahaux, *Phys. Rep.* **25**, 83–174, ISSN: 0370-1573 [1976] [cit. on p. 60].

[145] C. Mahaux, P. Bortignon, R. Broglia, C. Dasso, *Phys. Rep.* **120**, 1–274, ISSN: 0370-1573 [1985] [cit. on p. 60].

[146] J. Blaizot, B. Friman, *Nucl. Phys. A* **372**, 69–89, ISSN: 0375-9474 [1981] [cit. on p. 60].

[147] V. Bernard, N. V. Giai, *Nucl. Phys. A* **348**, 75–92, ISSN: 0375-9474 [1980] [cit. on pp. 60, 62].

[148] J. Dobaczewski, H. Flocard, J. Treiner, *Nucl. Phys. A* **422**, 103–139, ISSN: 0375-9474 [1984] [cit. on p. 60].

[149] H. Köhler, *Nucl. Phys. A* **258**, 301–316, ISSN: 0375-9474 [1976] [cit. on p. 60].

[150] J. Erler, P. Klüpfel, P.-G. Reinhard, *J. Phys. G* **38**, 033101 [2011] [cit. on p. 62].

[151] G. Colò, H. Sagawa, P. F. Bortignon, *Phys. Rev. C* **82**, 064307 [2010] [cit. on p. 62].

[152] D. Gambacurta, F. Catara, *Phys. Rev. B* **77**, 205434 [2008] [cit. on pp. 62, 79–82].

[153] D. Gambacurta, F. Catara, *Phys. Rev. B* **81**, 085418 [2010] [cit. on pp. 63, 80, 82, 84, 116, 118].

[154] S. Perez-Martin, L. M. Robledo, *Phys. Rev. C* **78**, 014304 [2008] [cit. on p. 68].

[155] G. Pozzi, *A Microscopic Model for the Collective Response in Odd Nuclei*, Tesi di Laurea, Matricola n.772405 [Università Degli Studi di Milano, 2010-2011] [cit. on pp. 68, 117].

[156] H. N. Liu *et al.*, *Phys. Rev. Lett.* **122**, 072502 [2019] [cit. on pp. 73, 74, 76, 117].

[157] [http://www.nndc.bnl.gov/.] [cit. on pp. 73, 74].

[158] K. Nowak *et al.*, *Phys. Rev. C* **93**, 044335 [2016] [cit. on pp. 73, 74].

[159] F. Nowacki, A. Poves, *Phys. Rev. C* **79**, 014310 [2009] [cit. on pp. 73, 74].

[160] Y. Utsuno *et al.*, in *Proceedings of the Conference on Advances in Radioactive Isotope Science (ARIS2014)* [cit. on pp. 73, 74].

[161] Y. Utsuno *et al.*, *Phys. Rev. C* **86**, 051301 [2012] [cit. on pp. 73, 74].

[162] J. Simonis, S. R. Stroberg, K. Hebeler, J. D. Holt, A. Schwenk, *Phys. Rev. C* **96**, 014303 [2017] [cit. on pp. 73, 74].

[163] K. Hebeler, S. K. Bogner, R. J. Furnstahl, A. Nogga, A. Schwenk, *Phys. Rev. C* **83**, 031301 [2011] [cit. on pp. 73, 74].

[164] J. Simonis, K. Hebeler, J. D. Holt, J. Menéndez, A. Schwenk, *Phys. Rev. C* **93**, 011302 [2016] [cit. on pp. 73, 74].

[165] K.-J. Hara, *Prog. Theor. Phys.* **32**, 88–105, ISSN: 0033-068X [1964] [cit. on p. 78].

[166] D. Karadjov, V. Voronov, F. Catara, *Phys. Lett. B* **306**, 197–200, ISSN: 0370-2693 [1993] [cit. on pp. 78, 79].

[167] D. Karadjov, V. V. Voronov, F. Catara, *J. Phys. G* **20**, 1431–1440 [1994] [cit. on p. 78].

[168] J. Toivanen, J. Suhonen, *Phys. Rev. Lett.* **75**, 410–413 [1995] [cit. on p. 78].

[169] J. Suhonen *et al.*, *Z. Phys. A* **358**, 297–301, ISSN: 1431-5831 [1997] [cit. on p. 78].

[170] A. Raduta, C. Raduta, A. Faessler, W. Kamiński, *Nucl. Phys. A* **634**, 497–524, ISSN: 0375-9474 [1998] [cit. on p. 78].

[171] J. Dukelsky, G. Röpke, P. Schuck, *Nucl. Phys. A* **628**, 17–40, ISSN: 0375-9474 [1998] [cit. on p. 78].

[172] D. S. Delion, P. Schuck, J. Dukelsky, *Phys. Rev. C* **72**, 064305 [2005] [cit. on p. 78].

[173] M. Jemaï, D. S. Delion, P. Schuck, *Phys. Rev. C* **88**, 044004 [2013] [cit. on p. 78].

[174] P. Schuck, M. Tohyama, *Phys. Rev. B* **93**, 165117 [2016] [cit. on p. 78].

[175] F. Catara, P. Chomaz, N. V. Giai, *Phys. Lett. B* **233**, 6–10, ISSN: 0370-2693 [1989] [cit. on p. 79].

[176] D. Beaumel, P. Chomaz, *Annals of Physics* **213**, 405–428, ISSN: 0003-4916 [1992] [cit. on p. 79].

[177] M. Sambataro, F. Catara, *Phys. Rev. C* **51**, 3066–3077 [1995] [cit. on p. 79].

[178] M. Sambataro, J. Suhonen, *Phys. Rev. C* **56**, 782–790 [1997] [cit. on p. 79].

[179] E. Lanza, M. Andrés, F. Catara, P. Chomaz, C. Volpe, *Nucl. Phys. A* **613**, 445–471, ISSN: 0375-9474 [1997] [cit. on p. 79].

[180] C. Volpe, P. Chomaz, M. Andrés, F. Catara, E. Lanza, *Nucl. Phys. A* **647**, 246–256, ISSN: 0375-9474 [1999] [cit. on p. 79].

[181] M. Sambataro, N. Dinh Dang, *Phys. Rev. C* **59**, 1422–1431 [1999] [cit. on p. 79].

[182] M. Grasso, F. Catara, M. Sambataro, *Phys. Rev. C* **66**, 064303 [2002] [cit. on p. 79].

[183] D. Gambacurta, M. Sambataro, F. Catara, *Phys. Rev. C* **73**, 014310 [2006] [cit. on p. 79].

[184] J. Dukelsky, P. Schuck, *Nucl. Phys. A* **512**, 466–482, ISSN: 0375-9474 [1990] [cit. on p. 79].

[185] D. Janssen, P. Schuck, *Z. Phys. A* **339**, 43–50, ISSN: 0939-7922 [1991] [cit. on p. 79].

[186] F. Catara, N. D. Dang, M. Sambataro, *Nucl. Phys. A* **579**, 1–12, ISSN: 0375-9474 [1994] [cit. on p. 79].

[187] F. Catara, G. Piccitto, M. Sambataro, N. Van Giai, *Phys. Rev. B* **54**, 17536–17546 [1996] [cit. on pp. 79–81, 84].

[188] F. Catara, M. Grasso, G. Piccitto, M. Sambataro, *Phys. Rev. B* **58**, 16070–16075 [1998] [cit. on pp. 79–81].

[189] F. Krmpotić, E. de Passos, D. Delion, J. Dukelsky, P. Schuck, *Nucl. Phys. A* **637**, 295–324, ISSN: 0375-9474 [1998] [cit. on p. 79].

[190] F. Šimkovic, A. A. Raduta, M. Veselský, A. Faessler, *Phys. Rev. C* **61**, 044319 [2000] [cit. on p. 79].

[191] D. Gambacurta, M. Grasso, F. Catara, M. Sambataro, *Phys. Rev. C* **73**, 024319 [2006] [cit. on p. 79].

[192] D. Gambacurta, F. Catara, M. Grasso, *Phys. Rev. C* **80**, 014303 [2009] [cit. on p. 79].

[193] D. J. Rowe, *Phys. Rev.* **175**, 1283–1292 [1968] [cit. on pp. 79, 83, 102, 118].

[194] K. Takayanagi, K. Shimizu, A. Arima, *Nucl. Phys. A* **477**, 205–230, ISSN: 0375-9474 [1988] [cit. on pp. 84, 118].

[195] K. Takayanagi, K. Shimizu, A. Arima, *Nucl. Phys. A* **481**, 313–332, ISSN: 0375-9474 [1988] [cit. on pp. 84, 118].

[196] G. Colò, L. Cao, N. V. Giai, L. Capelli, *Comp. Phys. Comm.* **184**, 142–161, ISSN: 0010-4655 [2013] [cit. on p. 85].

List of Figures

1.1 Illustration of degrees of freedom 4
1.2 Domains of physics applying many-body techniques 5
1.3 Schematic view of a neutron star. 6
1.4 Examples of EOS of infinite matter 7
1.5 Collective modes of GRs 8

3.1 ISM and IVM response of ^{16}O in RPA and SRPA. 30
3.2 ISQ response of ^{48}Ca, IVD response of ^{16}O. 31
3.3 Multipole strength distributions for the Na_9^+ metal cluster. . . . 31

4.1 ISM response of ^{16}O for several cutoffs in the subtracted terms 39
4.2 Ratios of moments of the quadrupole strength (RPA, SRPA, SSRPA) 40
4.3 ^{48}Ca low-energy spectrum against experimental data 46
4.4 ^{48}Ca low-energy spectrum against experimental data 47
4.5 ^{48}Ca dipole strength distributions in RPA, SRPA and SSRPA (SGII) compared with experiments 48
4.6 ^{48}Ca dipole strength distributions in RPA, SRPA and SSRPA (SLy4) compared with experiments 48
4.7 ^{48}Ca GDR responses in SSRPA, shifted 49
4.8 Electric dipole polarizability as a function of the excitation energy 50
4.9 SSRPA systematic study: centroids 53
4.10 SSRPA systematic study: widths 54
4.11 SSRPA systematic study: ^{40}Ca 55
4.12 SSRPA systematic study: ^{90}Zr 56
4.13 SSRPA systematic study: ^{120}Sn 56
4.14 SSRPA systematic study: ^{208}Pb 57
4.15 SSRPA systematic study: Cutoff independence 58
4.16 IS GQR centroids of ^{48}Ca and ^{90}Zr versus $\sqrt{m/m^*}$ 61
4.17 MF and BMF theoretical errors due to different parametrizations 63
4.18 BMF effects on the A_{11} matrix elements: ^{48}Ca 64

4.19 BMF effects on the A_{11} matrix elements: ^{90}Zr 65

5.1 Experimental and theoretical 2_1^+ energies of even-even Ar isotopes 74
5.2 2_1^+ energies in $N = 28$ to $N = 34$ Argon isotopes, RPA with EFA 76
5.3 2_1^+ energies in $N = 28$ to $N = 34$ Argon isotopes, SSRPA with EFA 77
5.4 2_1^+ energies in $N = 28$ to $N = 34$ Argon isotopes, BCS-based RPA and SSRPA with EFA 78
5.5 Occupation numbers calculated iteratively in RPA: ^{16}O 86
5.6 Occupation numbers calculated iteratively in RPA: ^{16}O 87
5.7 SRPA renormalized with occupation numbers: ^{16}O 88
5.8 SRPA renormalized with occupation numbers: ^{16}O 89

Index

Bardeen-Cooper-Schrieffer (BCS), 2, 71
Beyond mean field (BMF), 58–60, 62

Correlated ground state, 20, 21

Density matrix, 16, 24, 27, 28, 42
Diagonal approximation, 24
Dipole giant resonance (GDR), 2
Double counting of correlations, 32, 36

Energy-density functional (EDF), 2, 7, 28, 32
Energy-weighted moment, 36, 45
Energy-weighted sum rule (EWSR), 21
Equal-filling approximation (EFA), 67
Equations of motion, 17, 18, 25
Escape width, 9, 23
Extended RPA (ERPA), 80
Extended SRPA (ESRPA), 80

Giant dipole resonance (GDR), 46
Giant monopole resonance (GMR), 51
Giant quadrupole resonance (GQR), 51, 59

Hartree-Fock (HF), 1, 14, 57

Isoscalar (IS), 29, 51
Isovector (IV), 29, 30

Landau damping, 9, 23

Mean field (MF), 1, 12, 14, 32
Metric matrix, 19, 20, 27, 36

Number operator method, 79

Occupation number, 3, 28, 78, 79

Polarizability, 36

Quasiboson approximation (QBA), 3, 22, 24, 29, 77
Quasiparticle RPA (QRPA), 23, 68

Random-phase approximation (RPA), 1, 4, 14, 17
Rearrangement terms, 41
Response function, 35, 36
RPA matrix, 36

Second RPA (SRPA), 1, 2, 6, 23
Slater determinant, 15, 16, 21
Spreading width, 9, 23
Spurious state, 35
Stability, 19, 29, 33, 36
Stability matrix, 19, 36
Subtracted SRPA (SSRPA), 2, 38
Subtraction, 33, 35

Thouless theorem, 19, 21, 29, 36

Ultraviolet divergence, 32

université PARIS-SACLAY | ÉCOLE DOCTORALE PHENIICS

Titre : Description microscopique de nucléons corrélés : Propriétés collectives dans les noyaux stables et exotiques

Mots clés : Modèles pour les systèmes à N corps, Nucléons corrélés, Propriétés collectives dans les noyaux, Théories au-delà du champ moyen, Second random-phase approximation

Résumé : Ce travail de doctorat s'inscrit dans le cadre des techniques adaptées à la résolution du problème à N corps nucléaire. Il a été motivé par la perspective d'utiliser des méthodes allant au-delà de l'approximation de champ moyen pour améliorer la description des spectres d'excitation des noyaux stables et exotiques, notamment les états de basse énergie et les résonances géantes. À cette fin, l'approche choisie est le développement de modèles basés sur la second random-phase approximation (SRPA) utilisée avec une procédure de soustraction. Ces développements ont pour but d'étendre le champ d'applicabilité du modèle initial et d'inclure des corrélations dans l'état fondamental.

Une première partie consiste en l'application de la SRPA avec une méthode de soustraction à l'étude de la réponse dipolaire (comprenant la polarisabilité électrique dipolaire) et quadrupolaire de noyaux de masse moyenne à lourds. Nous vérifions que la SRPA avec soustraction corrige les problèmes observés avec la SRPA standard et améliore la description des spectres d'excitation, comparativement à la random-phase approximation (RPA). Nous étudions également les effets au-delà du champ moyen dûs à la SSRPA avec soustraction, en exploitant la relation entre les modes de respiration axiaux des noyaux et la masse effective de la matière nucléaire.

Une seconde partie est dédiée à des extensions.
Premièrement, nous étendons les outils numérique initiaux en utilisant l'approximation equal-filling (EFA) afin de permettre les applications aux noyaux ayant une orbitale partiellement occupée. Nous proposons ensuite une méthode d'estimation partielle des effets d'appariement en utilisant des nombres d'occupation corrélés.
Une étude des moyens de renormaliser la SRPA avec soustraction est menée en employant un modèle allant au-delà de l'approximation de quasiboson. Cette extension est également basée sur l'utilisation de nombres d'occupation comme moyen d'inclure des corrélations dans l'état fondamental. Nous montrons que les corrélations obtenues par le calcul itératif en RPA des nombres d'occupation ne sont pas suffisantes pour corriger les problèmes de la SRPA standard.

Title : A microscopic treatment of correlated nucleons: Collective properties in stable and exotic nuclei

Keywords : Many-body theories, Correlations between nucleons, Collective behavior in nuclei, Modern beyond-mean-field models, Second random-phase approximation

Abstract : This Ph.D. work falls within the scope of theoretical techniques tailored to the solution of the nuclear many-body problem. It was motivated by the perspective of using beyond-mean-field methods to improve the description of excitation spectra of stable and exotic nuclei, especially the low-energy states and the giant resonances. The chosen path in this direction is the development of models based on the second random-phase approximation (SRPA) used with a subtraction procedure. These developments aim to extend the range of applicability of the initial model and to include correlations in the ground state.

A first part consists in applying the SRPA used with a subtraction method to the study of the dipole and quadrupole response in medium to heavy-mass nuclei, including the electric dipole polarizability. We verify that the subtracted SRPA corrects the problems observed with the standard SRPA model and improves the description of excitation spectra compared to the random-phase approximation (RPA). We also study beyond-mean-field effects that arise in the subtracted SRPA by exploiting the relation between the axial breathing modes in nuclei and the effective mass in nuclear matter.

A second part is dedicated to extensions.
As a first step, we extend the initial numerical tools by employing the equal-filling approximation (EFA), to enable applications to nuclei with partially-occupied orbitals. We next propose a method to estimate part of the pairing effects using correlated occupation numbers.
A study of possible ways to renormalize the SRPA is carried out by employing a model which goes beyond the quasiboson approximation. This extension also relies on the use of occupation numbers as a means to include ground-state correlations. We show that correlations obtained from the computation of occupation numbers in iterative RPA calculations are not sufficient to address the standard SRPA drawbacks.

Université Paris-Saclay
Espace Technologique / Immeuble Discovery
Route de l'Orme aux Merisiers RD 128 / 91190 Saint-Aubin, France